CR-132496

REPORT NO. GDCA-DBG73-002
CONTRACT NAS9-12326

DETECTION OF FATIGUE CRACKS BY NONDESTRUCTIVE TESTING METHODS

GENERAL DYNAMICS
Convair Aerospace Division

REPORT NO. GDCA-DBG73-002

DETECTION OF FATIGUE CRACKS BY NONDESTRUCTIVE TESTING METHODS

March 1973

R. T. Anderson
T. J. DeLacy
R. C. Stewart

Submitted to
National Aeronautics and Space Administration
LYNDON B. JOHNSON SPACE CENTER
Houston, Texas

Prepared by
CONVAIR AEROSPACE DIVISION OF GENERAL DYNAMICS
San Diego, California

FOREWORD

This is the final report on a study of detection of fatigue cracks in 2219-T87 aluminum sheet and plate by nondestructive testing methods. The study was performed by the Convair Aerospace Division of General Dynamics Corporation under Contract NAS 9-12326. Mr. W. L. Castner was the technical monitor.

The study was conducted by the Research and Engineering Department with R. T. Anderson of the San Diego operation of Convair Aerospace Division as Program Manager. The major effort at the San Diego operation was performed by T. J. DeLacy, R. C. Stewart, and W. M. Thomas. Gratefully acknowledged is the technical assistance of C. R. Maikish, C. J. Kropp, and E. Wehrhan for specimen preparation and V. H. David fo statistical analysis, all of the San Diego operation. At the Fort Worth operation, Messrs. B. G. W. Yee, J. Romanko, A. H. Gardner and H. J. Weltman contributed invaluable assistance in ultrasonic, holographic and replication methods optimization. The technical guidance and consultation of W. L. Castner of NASA-MSC is also gratefully acknowledged.

TABLE OF CONTENTS

TABLE OF CONTENTS, Contd

LIST OF FIGURES

LIST OF FIGURES, Contd

LIST OF TABLES

SUMMARY

This program assessed the effectiveness of various NDT methods to detect small tight cracks by randomly introducing fatigue cracks into aluminum sheets, optimizing NDT methods and calibrating NDT equipment with fatigue cracked standards, and evaluating a number of cracked specimens by the optimized NDT methods. The evaluations were conducted by highly trained personnel, provided with detailed procedures, in order to minimize the effects of human variability. These personnel performed the NDT on the test specimens without knowledge of the flaw locations and reported on the flaws detected. The performance of these tests was measured by comparing the flaws detected against the flaws present. The specimens were etched and evaluated again by the original personnel to assess the effects of etching on flaw detectability. Finally, the specimens were proof loaded and evaluated again.

The principal NDT methods utilized were radiographic, ultrasonic, penetrant, and eddy current. Holographic interferometry, acoustic emission monitoring, and replication methods were also applied on a reduced number of specimens.

Generally, the best performance was shown by eddy current, ultrasonic, penetrant and holographic tests. Etching provided no measurable improvement, while proof loading improved flaw detectability. Data are shown that quantify the performances of the NDT methods applied.

SECTION 1

INTRODUCTION

NDT has proved to be an important element of fracture control designs. The application of fracture control to space vehicle and aircraft design makes recognition of the fact that materials and structures contain flaws. Whether or not these flaws are defects detrimental to the intended functional performance of the structure or component in question depends upon several inter-related factors:

a. The fracture toughness characteristics of the structural material must be known or determined.

b. Flaw sizes determined to be critical must be large enough to exceed the threshold sensitivities of available inspection methods.

c. The inspection methods must be capable of reliably detecting critical flaws when applied under production inspection conditions.

d. The structural design should reflect the combined effects of the first three factors.

One of the major shortcomings of the fracture control design philosophy is the inability to quantify the reliability of NDT to detect flaws of specific sizes. This program is specifically directed toward the objective of defining the reliability of NDT methods to detect fatigue cracks of various sizes in 2219-T87 aluminum plate and sheet. This provides the most simple configuration and, hence, is an ideal starting point to assess the capability of the nondestructive tests, with the least influence from human variations and complex configurations. These factors should be studied in the future with the foundation provided by studies such as this one.

SECTION 2

SPECIMEN PREPARATION

2.1 FATIGUE CRACK INTRODUCTION

In previous fracture mechanics test programs conducted at Convair Aerospace, surface flaw test specimens were made with a single flaw located in the center of the specimen. As is common in the industry, this surface flaw is made by first notching the surface and then subjecting the specimen to cyclic load precracking. The surface notch is made by drilling a hole or cutting a slot by either conventional machining or by electric discharge machining (EDM). Since fracture mechanics analyses are based upon flaws which have very small crack tip radii, the machined notch or hole requires precracking by low stress cyclic loading. Cyclic loading is usually performed in a standard fatigue testing machine by loading the notched specimen in three-point bending. Tension loading may or may not follow.

Cyclic loading a surface notch in three-point bending results in initiating a surface crack at the notch which propagates at a faster rate at the surface, the 2c dimension, as compared to the depth of this crack, the a dimension. If fatigue precracking is allowed to continue, the depth of the surface crack approaches a point approximately 60% of the specimen thickness while the surface crack length increases until failure occurs. Additional crack growth in the depth direction with little or no growth at the surface can only be achieved by cyclic loading in the tension direction.

The present program was more complex than previous fracture mechanics programs due to the many requirements imposed on specific flaws required in each test specimen. The requirements are:

a. One to five surface flaws required per test specimen.

b. Various combinations of long, shallow as well as short, deep surface flaws required per specimen.

c. Surface flaws of specific aspect ratios, a/2c.

d. Surface flaws of specific depth ratios, a/t, based on a final specimen thickness that is less than the original thickness; surface hole or notch is completely removed to obtain the final thickness.

e. Back surface dimpling caused by the growing crack is not allowed.

f. Back surface crack break-through of the surface crack is not allowed.

g. Flaws located only at intersections of 1/2-inch square grid pattern drawn on the test specimen.

In making surface-cracked specimens it is common practice to precrack a surface notch or hole to a desired crack length which can be measured on the surface. The depth of the precrack is controlled by predetermined combinations of cyclic bending and/or tension loading. The present program required surface flaws of specific size at a final thickness less than the original thickness at precracking. Due to this requirement, it was necessary to develop a method of precracking in which the method of cyclic loading, load level, load ratio, and number of load cycles were held to specific values or very close tolerance. Since cyclic load precracking involves the initiation and propagation of a crack, the usual scatter band observed in standard fatigue tests was experienced with the present program of precracking. This observation, unfortunately, manifested itself in some specimens which either fractured or were discarded due to unsuitable surface cracks.

Many experimental samples of 0.125-inch thick 2219-T87 were prepared to develop a scheme of precracking the required sizes and shapes of surface flaws in each specimen. The following surface flaws were required in a final specimen thickness of 0.060-inch.

① a = 0.380 mm (0.015 in.), 2c = 1.53 mm (0.06 in.); a/2c = 0.25, a/t = 0.25

② a = 0.761 mm (0.03 in.), 2c = 1.53 mm (0.06 in.); a/2c = 0.5, a/t = 0.5

③ a = 0.761 mm (0.03 in.), 2c = 7.64 mm (0.30 in.); a/2c = 0.1, a/t = 0.5

It was found that surface flaw numbers ① and ② could be made by cyclically loading a hole made with 0.25 mm (0.010 in.) diameter tungsten wire using the EDM process The depth of the hole was held to a range of 0.25 mm (0.060 in.) to 0.25 mm (0.[illegible]). To ensure the initiation of a surface crack at the EDM hole, the sample was first cyclically loaded in three-point bending. A span of 45.6 mm (1.8 in.) or 66.0 mm (2.6 in.) was used with a fixture attached to a standard fatigue machine operating at a frequency of 1800 Hz and a load ratio, R, of +0.1. Loading was continued until a crack with a surface trace of 1.19 mm (0.04 in.) to 1.78 mm (0.07 in.) was achieved. The samples were then cyclically loaded in tension until a crack length of 2.28 mm (0.09 in.) was obtained for the number one flaw and a 3.56 mm (0.14 in.) length for the number two flaw.

A two-step cyclic loading procedure was also used with the number three (③) flaw. A 1.02 mm (0.040 in.) to 1.09 mm (0.043 in.) deep EDM notch was made in the specimen surface using a 0.127 mm (0.005 in.) thick by 5.06 mm (0.200 in.) wide strip of either tungsten or cold rolled stainless steel. The notch was cracked to a length of about 11.47 mm (0.45 in.) in a three-point bending fatigue fixture. The specimen was then cyclically loaded in tension until the surface crack measured a maximum of 11.96 mm (0.47 in.)

The procedure developed for all the required surface flaws was entirely dependent on examining the fracture surface of a surface flaw. It was found that the best method of measuring surface flaws required a crack photograph at either a 5 × or 10 × magnification. In addition, an adaptation of a polarized light technique[4] was used to enhance

the cyclic load crack growth area and thus delineate the exact crack front. These special photomacrographs permitted very precise measurements of the crack depth and length at the planned reduced thickness.

Specimens requiring multiple surface flaws also required a stepped procedure of initiating the flaws in groups. As an example, specimen A-24 required not only number one and number two size flaws, but also two number three size flaws. Experimentation showed that the numbers one and two flaws were first initiated to full size. One number three size flaw was then initiated; however, to prevent further growth of this flaw the area surrounding it was reinforced with doubler plates. The doublers consisted of 6.35 mm (0.25 in.) thick 7075-T651 aluminum alloy plate which was adhesively bonded to both faces. After reinforcement, the second number three size flaw was initiated in the specimen. As the program continued, it became prudent to reinforce the areas surrounding the smaller size surface flaws.

The surface flaw precracking scheme for the 6.35 mm (0.25 in.) thick 2219-T87 test specimens is similar to the one described above for the 3.16 mm (0.125 in.) thickness. The following surface flaws were required in a final plate thickness of 5.70 mm (0.225 in.):

① a = 1.42 mm (0.056 in.), 2c = 2.87 mm (0.113 in.); a/2c = 0.50, a/t = 0.25

② a = 1.14 mm (0.045 in.), 2c = 11.4 mm (0.45 in.); a/2c = 0.10, a/t = 0.20

③ a = 2.87 mm (0.113 in.), 2c = 11.4 mm (0.45 in.); a/2c = 0.25, a/t = 0.50

Initiating a size one flaw in the 6.35 mm (0.25 in.) thick material required a surface hole made with a 0.254 mm (0.010 in.) diameter tungsten wire in an EDM machine. This hole was made 0.508 mm (0.020 in.) deep. This surface hole was cracked to a length of 0.254 mm (0.010 in.) to 0.304 mm (0.12 in.) in a three-point bending fatigue fixture. Cyclic tension load was then used to increase the crack length of 0.380 mm (0.15 in.) to 0.406 mm (0.16 in.) long. The size two flaw was initiated from an EDM surface notch made with a 0.127 mm (0.005 in.) by 10.2 mm (0.40 in.) stainless steel or tungsten electrode. The notch depth was held to 0.508 mm (0.020 in.). Three-point cyclic loading was used to precrack this notch to a range of 11.4 to 11.7 mm (0.45 to 0.46 in.) long. Cyclic tension loading was then used to increase the crack length to 11.9 mm (0.47 in.). The size three flaw was started from a 0.508 mm (0.020 in.) deep EDM surface notch made with a 0.127 mm (0.005 in.) by 5.08 mm (0.020 in.) stainless steel or tungsten foil electrode. Only three-point cyclic loading was necessary to precrack this notch to a length of 13.2 mm (0.52 in.).

It was also found necessary to develop the surface flaws in the 6.35 mm (0.250 in.) thick plate in a stepwise procedure as was used with the 3.16 mm (0.125 in.) thick sheet specimens. To prevent additional crack growth of completed surface flaws, it was also necessary to reinforce the area surrounding the fully grown flaws with adhesively bonded doublers.

Although these techniques produced desired crack geometries on preliminary specimens with at least one replication, it is apparent from post-mortem examination of cracks produced in the final specimens that considerable scatter in crack shapes resulted. For example, Table 2.1-1 gives the average dimensions obtained as compared with those desired.

Table 2.1-1. Average and Desired Dimensions

Flaw Size	Desired Geometry				Attained Geometry							
	a		2c		$\bar{a}$		R_a		$\overline{2c}$		R_{2c}	
	in.	mm	in.	mm	in.	mm	in.	mm	in.	mm	in.	mm
A-1	0.015	0.38	0.060	1.52	0.016	0.41	0.005	0.13	0.063	1.60	0.022	0.56
							0.029	0.74			0.104	2.64
A-2	0.030	0.76	0.060	1.52	0.026	0.66	0.019	0.48	0.091	2.31	0.069	1.75
							0.040	1.02			0.129	3.28
A-3	0.030	0.76	0.300	7.62	0.040	1.02	0.012	0.30	0.336	8.54	0.197	5.00
							0.054	1.37			0.384	9.75
B-1	0.056	1.42	0.113	2.88	0.044	1.12	0.027	0.69	0.137	3.48	0.109	2.77
							0.064	1.63			0.190	4.83
B-2	0.045	1.14	0.450	11.42	0.102	2.59	0.054	1.37	0.472	12.00	0.426	10.82
							0.144	3.66			0.520	13.21
B-3	0.113	2.88	0.450	11.42	0.101	2.56	0.088	2.24	0.521	13.23	0.498	12.65
							0.112	2.84			0.550	13.97

2.2 SURFACE FINISH MACHINING

Final machining of the test specimen surfaces was accomplished by face milling. The milling operation was performed on a No. 2 Cincinnati vertical milling machine. Figure 2.2-1 shows a close-up view of the milling operation. A vacuum chuck was used as the holding fixture for the test specimen during the operation. Edge clamps were also used in addition to the vacuum chuck to further ensure positive clamping of the cut.

The four types of surface finishes required for the program were:

a. Coarse: 5.7 to 5.9 μm (225 to 230 μin.) average roughness

b. Rough: 3.0 to 3.3 μm (120 to 130 μin.) average roughness

c. Fine: 1.27 to 1.52 μm (50 to 60 μin.) average roughness

d. Extra Fine: 0.69 to 0.81 μm (27 to 32 μin.) average roughness

The basic depth of cut was:

a. 0.63 mm (0.025 in.) for the thick specimens

b. 1.65 mm (0.065 in.) for the thin specimens

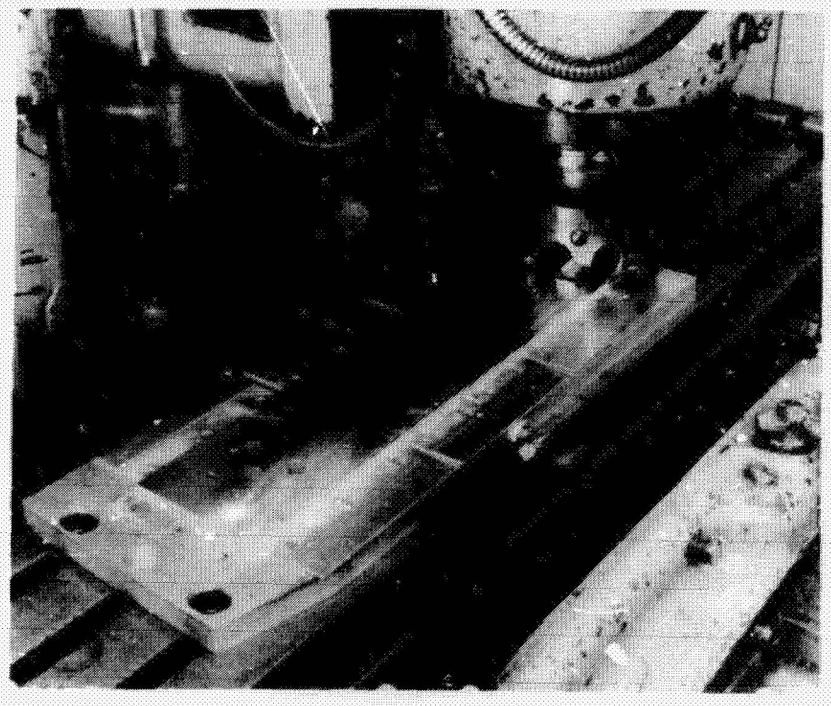

Figure 2.2-1. Closeup View of the Face Milling Operation Performed on the Test Specimen Surface

A Shearjoy type of face mill (manufactured by Lovejoy Tool Co.) 12.7 cm (5.0 in.) diameter with ten teeth was used as the cutter for all of the cutting performed on the test specimen. The basic geometry of the cutter comprises a 0.51 radian (29-1/2 degree) axial rake, 0 radian (0 degree) radial rake and a 0.79 radian (45 degree) lead angle. High speed steel (M-2) was used as the tool material. The spindle speed remained constant for all cuts and the feed rate was varied as follows:

Surface Finish — μm (μ in.)	Feed Rate — mm/s (in/sec)
0.69 - 0.81 (27 - 32)	0.76 (0.030)
1.27 - 1.52 (50 - 60)	1.62 (0.064)
3.0 - 3.3 (120 - 130)	3.22 (0.127)
5.7 - 5.9 (225 - 230)	5.23 (0.206)

At the completion of milling each specimen, a Surfindicator was used to measure the surface finish. Figure 2.2-2 shows the setup used.

2.3 ACOUSTIC EMISSION MONITORING

Fatigue crack growth during specimen preparation was monitored with acoustic emission monitoring (AEM) equipment on 16 specimens. This preliminary work was done to aid

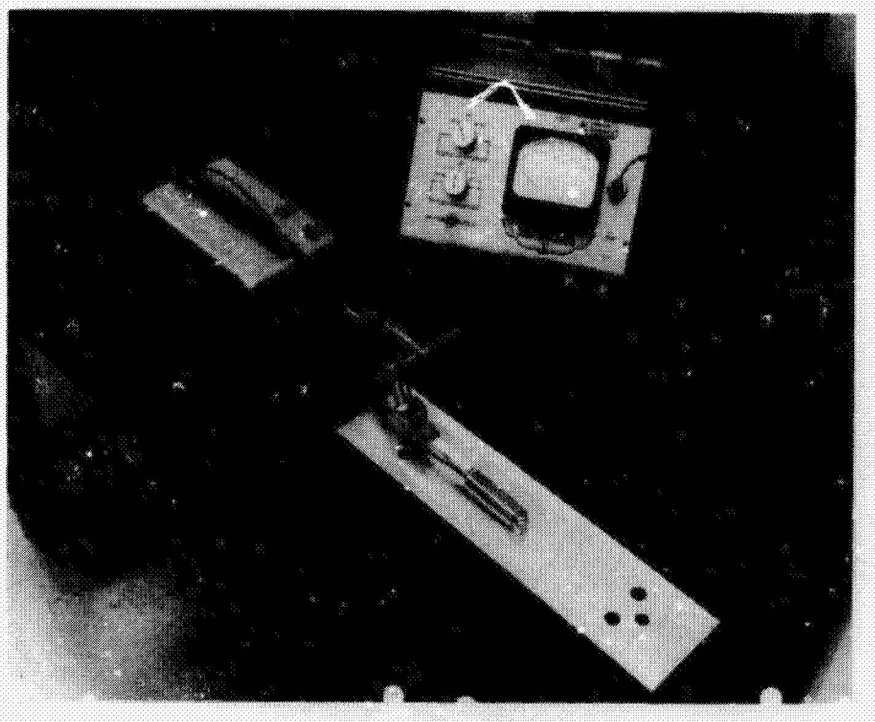

Figure 2.2-2. Measuring the Surface Finish of a Completed Test Specimen With a Surfindicator

in choice of equipment and sensitivity settings; transducer types, locations, and spacings; and determination of suitability of proposed recorders.

AEM is based on the understanding that any growth of a fatigue crack results in a release of energy. Part of this energy is in the form of a stress wave that travels through the material. This stress or acoustic wave can excite a suitably matched and coupled transducer whose output can be displayed in some real-time analog form or recorded for later analysis.

These transducers must be very sensitive to faithfully present such low level inputs as those from a fatigue crack. Extraneous emissions arising from sources other than propagating cracks will also be recorded unless some form of spatial filtration or source location is incorporated into the test equipment.

Since fatigue test machines and test specimen grips, attach bolts, etc., produce significant extraneous emissions from frictional rubbing, band pass filters are a help. In this case 50 kHz high-pass filtering was used. The greatest aid in separating true acoustic emission signals from background noise has been the use of multiple transducers in a master-slave array with a guard ring concept. With the master(s) (1 or 2) in the center, near the expected source of emissions from propagating cracks, and the slaves (up to six) in a ring around the master(s), the time of arrival of the signal at each transducer can be measured. Outside noise will arrive at one or more of the slaves before it reaches a master. True acoustic emissions from propagating cracks will arrive at one or both of the masters before any slave sees it. An "event converter" has been incorporated to perform this spatial filtering.

The AEM unit has a logic circuit that outputs a pulse (to a separate counter) whenever a master sensor signal is received earlier (plus one-microsecond) than any signal from a slave sensor. The accumulated total in this counter is the acoustic emission (AE) count. The AEM unit also outputs a pulse (to another separate counter) when any signal is received above the threshold level. This accumulated total is the noise or background count.

The threshold sensitivity of each of these circuits as input to the spatial filtering logic is adjustable. These adjustments are set with reference to the output voltage from the preamplifier.

The general test setup is shown in Figure 2.3-1 with a specimen mounted in a tensile fatigue test machine. Figure 2.3-2 shows the construction of the transducer. The active element is lead-zirconate-titanate Glennite HDT-31 plate 0.51 mm (0.02 in.) thick by 5.1 mm (0.2 in.) square. A whisker wire is spot soldered to the back for connection to the coaxial lead wire. A compression spring (not visible) is used to provide steady intimate contact of the crystal face and the test specimen. A soft rubber pad insulates the spring from the crystal and whisker wire. A silicone base grease is used as a couplant on the crystal face. The brass case is clamped to the specimen holding the

Figure 2.3-1. Acoustic Emission Monitoring Setup for Detecting Fatigue Crack Growth

Figure 2.3-2. Sensor for Acoustic Emission Monitoring

spring-loaded crystal in the desired location. The rim of the case and the clamp provide electrical ground paths to the specimen. The tube on the side of the transducer case is threaded for a grounding screw if one is necessary. Positive grounding is required for adequate shielding from electrical noise. The coaxial cable shield is soldered to the outside of the brass transducer case.

Each transducer lead goes to its own preamplifier. These are fixed gain units; 50-500 kHz bandpass with 100 X amplification. A dc power supply is set at 15.0 volts to feed the preamplifier units.

The amplified outputs are connected to the input jacks of the AEM unit designed and assembled by the Research and Engineering Department of Convair Aerospace Division - Fort Worth operation. The output jacks are connected to two counters.

A two-channel recorder takes the scaler outputs from the counters for a visual record of the count accumulation as a function of the number of fatigue cycles.

The pulse generator and CRT scope seen in Figure 2.3-1 were used for setup calibration.

Figure 2.3 shows a test specimen mounted in the fatigue machine with a typical arrangement of transducer locations. The two center units are the masters, located astride and as close as possible to the expected AE source (starter notch), and the two outer units are the slaves. In all cases the arrangement is similar with the master(s) (one or two) close to the AE source and a slave between the master(s) and the nearest source of unwanted noise. The background count is from the fatigue test machine and its grips, bolts, pins, etc.

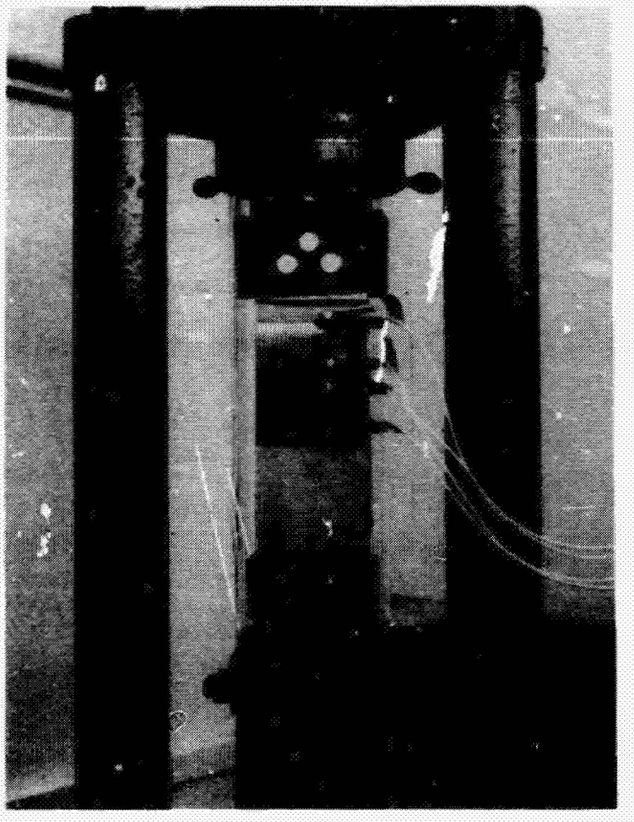

Figure 2.3-3. Specimen in Fatigue Machine With Four AEM Transducers

This arrangement was used to monitor the fatigue crack growth on 16 specimens. Different ranges of sensitivity settings of the master-slave logic circuits were used. The data have been plotted in terms of AE count and background count versus number of loading cycles. Analysis of the data can be found in Section 5.2 of this report.

SECTION 3

NDT TECHNIQUE OPTIMIZATION

3.1 X-RAY TECHNIQUE OPTIMIZATION

Aluminum test plates 1.58 mm (0.062 in.) and 5.7 mm (0.225 in.) thick were radiographed to establish a baseline approach for examining flawed specimens. A wire penetrameter was used to determine the relative information value of each radiograph; the penetrameter consisted of an array of aluminum wires ranging from 0.018 mm (0.071 in.) to 0.51 mm (0.020 in.) diameter. Figure 3.1-1 shows the penetrameter.

The relatively low X-ray absorption cross-section of aluminum, the high directional sensitivity of radiography, and practical considerations such as inspection time and cost are limiting factors when developing a highly sensitive radiographic technique suitable for service inspection. Accordingly, to prevent the evaluation of a "purely laboratory tool" a maximum exposure limit of 9000 milliampere seconds was established for radiography on the basis of known limitations of commercial X-ray equipment. An optimum energy level was experimentally determined below which significant improvement in the visibility of a threshold-level signal (smallest detectable wire) was not observed.

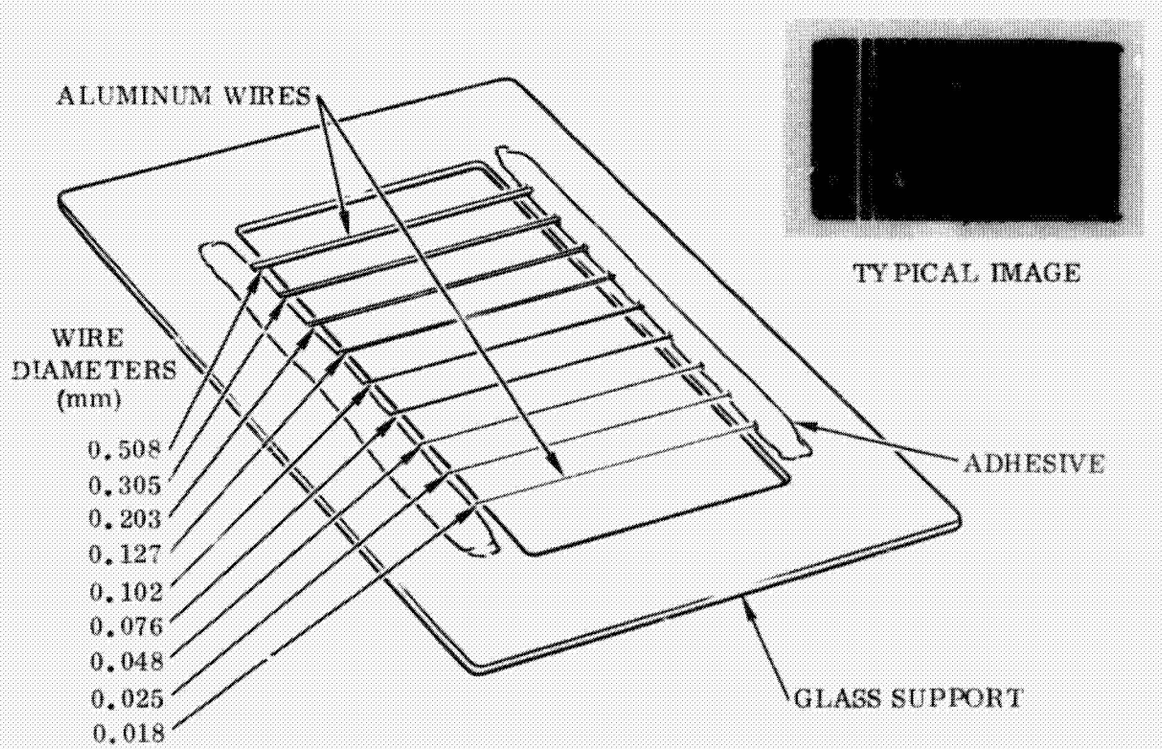

Figure 3.1-1. Penetrameter

Figure 3.1-2 shows exposure versus energy data for 1.58 mm (0.062 in.) and 5.7 mm (0 225 in.) aluminum plate exposed to an average film density of 2.5 H&D units. The exposures were made at a source to film distance of 56 cm (22 in.) using a 0.25 mm (0.010 in.) thick beryllium window tube X-ray unit. Based on these data, energy levels of 32 and 47 keV were selected for radiography of the 1.58 mm and 5.7 mm specimens, respectively. The corresponding wire penetrameter sensitivity was shown to be about 1.5% for the 1.58 mm plate and less than 1% for the 5.7 mm plate. Higher sensitivity in the thicker plate was desired because of the relatively high aspect ratios of the defects to be evaluated.

While radiography was not considered a candidate for inspecting fatigue cracks, every effort was made to develop an optimum radiographic technique which would accurately report its limitations. Accordingly, throughout the development and application of radiography, controls were used to prevent variations in film processing, line voltage, etc., which might have affected the repeatability and/or sensitivity of the test. Density versus exposure strips (grey scales) were processed regularly to observe the consistency of the developer solution. A digital voltmeter was used to reproduce kilovolt settings and to measure X-ray tube current; variations in tube current were corrected by an exposure integrator (capacitor-relay system) which was incorporated into the X-ray unit.

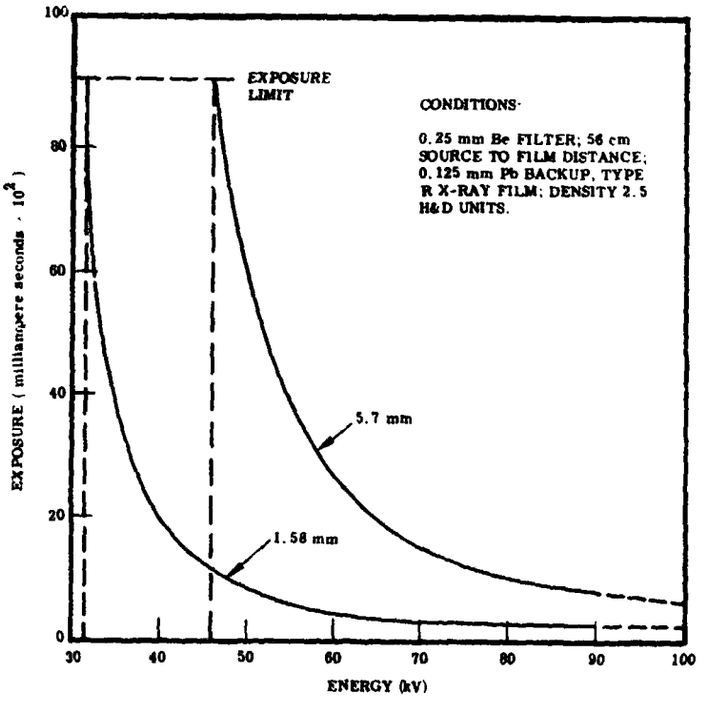

Figure 3.1-2. Energy versus Exposure Time

Based on 50% threshold visibility (marginal detection) of typical flaws, i.e., No. 2 fatigue cracks, defect angulation and source to detector distance were studied to observe the effects of image penumbra (halo distortion) and wide angle coverage of the specimens. For the X-ray equipment used (0.5 mm focal spot), marked deterioration in the projected image of the defect was detectable at ±4.5 degrees from the centerline axis of the X-ray beam and/or at a source to film distance of 25 cm (0.98 in.) or less. A source-to-film distance of 1.20 meters (3.94 feet) was subsequently established to obtain coverage of two test plates with a single X-ray exposure.

The following technique was developed for evaluation of the flawed specimens.

X-ray source:	0.5 mm focal spot, 0.25 mm Be window
Energy level:	32 keV, 1.58 mm specimens; 47 keV, 5.7 mm specimens
Film:	Eastman Kodak Type R, single emulsion
Cassette:	Paper; 0.13 mm lead backup
Source-to-film distance:	1.2 meters
Exposure:	9000 milliampere seconds
Processing:	HC110; 294°K (70°F), 360 seconds; nitrogen burst. Stop bath, 10 seconds; fixer/hardener 360 seconds; eliminator 180 seconds; wash 296°K (68°F), 1200 seconds; forced air dry 322°K (120°F).

Radiography was performed on all specimens in accordance with the above technique; the resulting films were viewed using 7 × magnification. A ruled template (overlay) was used to assure complete coverage of the film and for correlating defect location.

3.2 PENETRANT TECHNIQUE OPTIMIZATION

Development of a suitable penetrant technique began with the evaluation of eight penetrant materials ranging from Group V to Group VII sensitivity. Seven out of the eight were of the water washable fluorescent type; one post emulsified fluorescent penetrant was evaluated in the Group VII sensitivity class. Visible dye penetrants were not evaluated because of their relatively poor sensitivity and lack of dimensional stability.

Two aluminum test blocks with an anodic coating 20 micrometers (0.5 microinch) thick were used for the initial screening. The coating contained a network of cracks that averaged between 6 and 8 micrometers in width. The transparency of the coating enabled one to observe washing and removal of the penetrant materials thus reducing the chance for sensitivity loss through repeated applications of penetrant to a single test block. The block is shown in Figure 3.2-1.

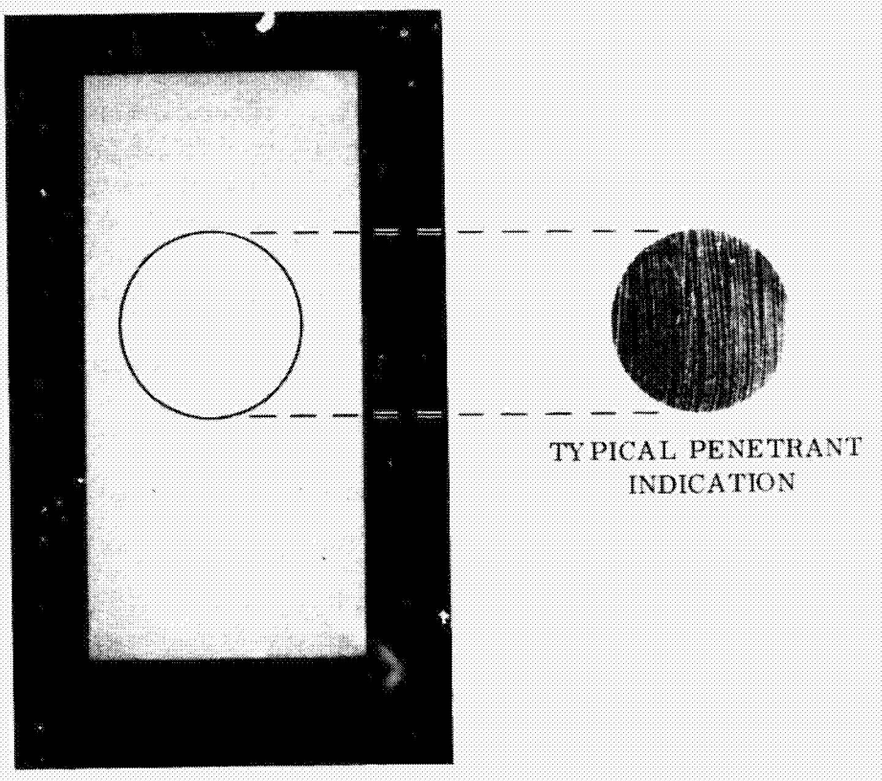

Figure 3.2-1. Sensitivity Block for Evaluating Penetrant Response

It was clear from early experiments with the fluorescent penetrants that sensitivity is as dependent upon operator technique as it is on the material itself; brightness loss during removal or washing of excess penetrant (background) was a major consideration in determining equivalence between penetrant systems. Since under optimum conditions parameters affecting washability and dilution of penetrant indications (such as water pressure, water temperature, and time) may differ significantly for each penetrant material and type of defect, no attempt was made to rank the performance of penetrants within any given class. The selection of a single penetrant material was based on a specific application technique intended to reduce the operator variables that might influence the sensitivity and repeatability of the test.

An air-assist hydrowash comprised of a sprayer head and air input manifold with pressure regulation was used. The system applied penetrant removers and enabled forced-air water wash in instances where the high dimensional threshold stability of super-sensitive penetrants would otherwise increase the presence of background fluorescence thereby inhibiting defect detection and/or accurate measurement of defect size.

The penetrant materials evaluated included special formulations containing known degrees of stabilization to reduce brightness loss; production as well as laboratory type materials were studied. Figure 3.2-2 shows the penetrants and apparatus used. Post emulsified and water-washable types of penetrants were selected from among the most common used in the industry.

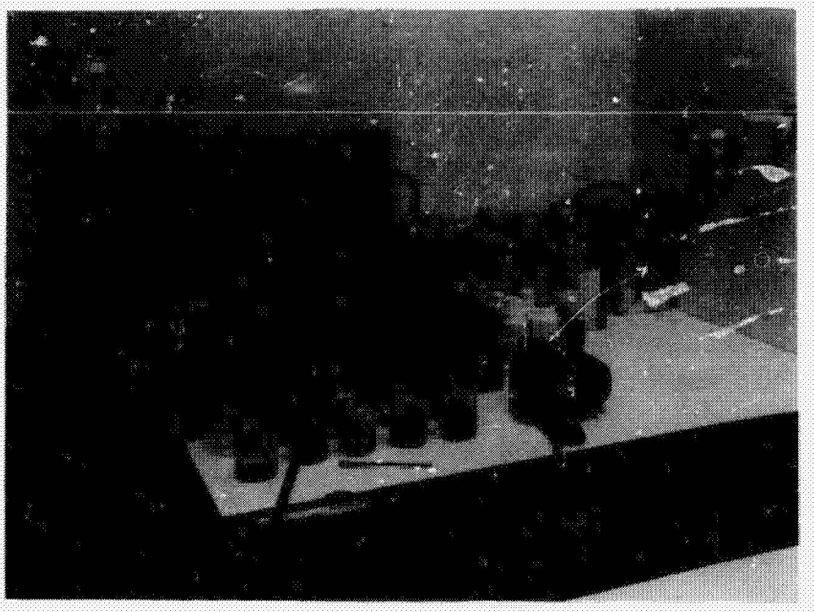

Figure 3.2-2. Fluorescent Penetrants and Hydrowash Apparatus

Tests were performed using both the anodized aluminum test blocks and fatigue cracked specimens. It was found that with careful penetrant removal procedures the more sensitive penetrant materials (Group VI and above) were superior over the range of surface finishes encountered in the specimens. However, in several instances indications were discontinuous apparently because of surface smearing during machining; a microetchant was subsequently specified for use prior to the application of the penetrant. Post-cleaning procedures involved ultrasonic cleaning in dichloromethane (Cl_2CH_2) to assure complete removal of penetrant residue entrapped by flaws.

Based on the specific conditions of the test (such as the nature of the flaws, surface condition, influence of the operator) a Group VII water washable fluorescent penetrant was selected for the evaluation phase. The technique used with the material was 600 seconds dwell, 90 seconds wash (ambient temperature), air dry, and 600 seconds development in nonaqueous solvent suspendable developer.

3.3 EDDY CURRENT TECHNIQUE OPTIMIZATION

Commercially available equipment designed specifically for eddy current flaw detection was used. Two specimens, A-2 and A-9, were selected for comparison of different instruments and techniques. A-2 contained a single size 1 crack, estimated to be 1.90 mm (0.075 in.) long and A-9 had two size 2 flaws estimated to be 2.03 mm (0.080 in.) and 2.28 mm (0.090 in.) long.

Within the capabilities of the instruments and probe coils available, it was desired to evaluate and select optimum characteristics for:

a. Frequency

b. Coil size and type

c. Liftoff suppression

d. Indicator response

e. Simplicity and ease of operation and standardization

Table 3.3-1 lists the types of equipment evaluated and their prominent characteristics. It is apparent that instruments A, B, D, and F had quite similar response characteristics at less than full gain and with a single coil. The instrument selected for use during the subsequent evaluations was B, on the basis that it was more simple to operate than A or F and was more available than D.

During these comparisons it became apparent that unaided manual scanning would be far from optimum. In previous studies at Convair and elsewhere[2], it was shown that fully automated eddy current scanning for large, fairly simple shapes could be managed with about the same ease as ultrasonic scanning. Contact contour following and X-Y scanning require design and fabrication of electro-mechanical positioning drives, but such devices are relatively simple to construct (although perhaps expensive). Since it is thus apparent that large areas of structural elements could not be optimally scanned, it was decided to utilize a simple fixture to facilitate scanning. Figure 3.3-1 shows the fixture, constructed from stock slides, with the spring-loaded probe coil mounted on the end of a micrometer slide.

In order to detect flaws smaller than those in A-1 and A-9, Specimen A-6 was selected since it contained a size 1 flaw estimated to be 1.52 mm (0.060 in.) long. It was found that with an index interval of 1.90 mm (0.075 in.), this size flaw would be reliably detected with the probe coil that was used throughout this program. The coil dimensions were 3.18 mm (0.125 in.) diameter, 1.78 mm (0.070 in.) high, with a ferrite core diameter of 1.02 mm (0.040 in.). It was later shown on the Martin specimens that this index interval was adequate to detect all flaws above the threshold capabilities of the test technique.

Table 3.3-1. Comparison of Representative Commercially Available Eddy Current Flaw Detectors

Instrument	Type-Description	Optimum Frequency (kHz)	Gain	Liftoff Compensation mm(in.)	Instrument Response, % Full-Scale of Meter: Crack Length, mm (in.) 1.90 (0.075)	2.03 (0.080)	2.28 (0.090)
A	Multi-frequency, vector point						
	Single coil	100	<max	0.076 (0.003)	44	64	96
	Differential coil	500	max	0	15		30
B	Impedance bridge, amplitude, multi-frequency, single coil	196	<max	0.076 (0.003)	44	60	97
C	Impedance bridge, amplitude, fixed frequency, single coil	1850	max	0.076 (0.003)	15		40
D	Impedance bridge, amplitude, multi-frequency, single coil	190	<max	0.076 (0.003)	40		96
E	Impedance bridge, amplitude, multi-frequency, single coil	130	max	0.076 (0.003)			30
F	Multi-frequency, vector point, single coil	100	<max	0.076 (0.003)	45		100
G	Multi-frequency, vector point, single coil	100	max	0.076 (0.003)	34	66	100

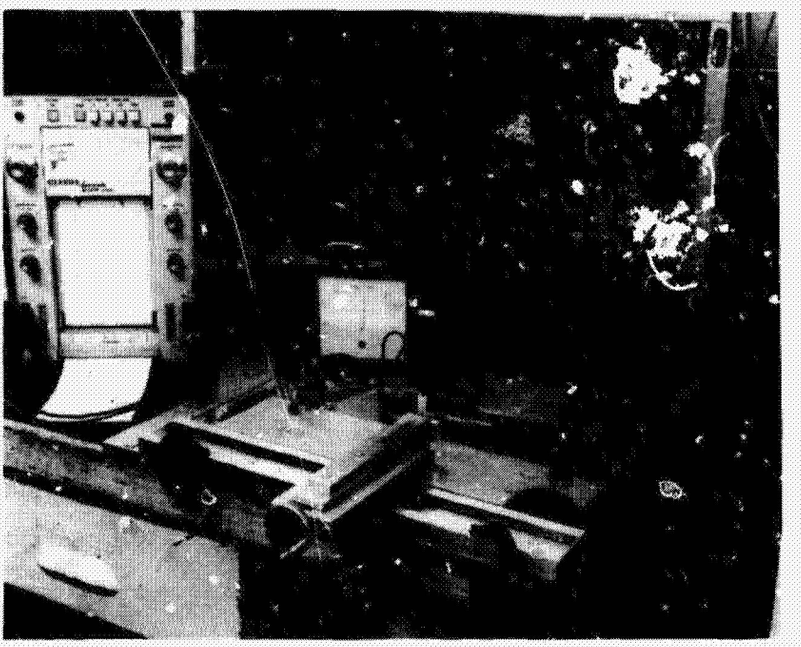

Figure 3.3-1. Eddy Current Setup for Detection of Fatigue Cracks in Aluminum Specimens

Figure 3.3-1 also shows a strip chart recorder. It was found that the scanning rate could be substantially increased if the output from the eddy current instrument amplifier was detected by the strip chart recorder. Although the meter movement supplied with the instrument is not highly damped, the frequency response of the meter is extremely low by comparison with the response of the pen-type galvanometer. In addition, the current-limiting diode in the meter circuit limits the current to approximately twice the meter range which in this case was 500 μA. In by-passing the meter and using the strip chart recorder, a much larger range of bridge unbalance can be displayed in addition to the benefit obtained from increased frequency response. A recorder with a frequency response of at least 60 to 100 Hz should be used.

With this arrangement, the 102 × 204 mm (4 × 8 in.) area of the test specimens could be scanned with assured 100 percent coverage very quickly. With the recorder it was possible to identify cracks as close as 12.7 mm (0.5 in.) together at a scan rate of approximately 45.7 cm/s (18 in./s).

All optimization tests included compensation for liftoff up to 0.076 mm (0.003 in.), and standard stock probe coils were used throughout since it was not anticipated that cracks shorter than 1.52 mm (0.060 in.) would be obtained. However, smaller cracks

were inadvertently produced in both the Convair and Martin specimens. Had it been realized at the time of the optimization tests that flaws smaller than those intended would, in fact, have been as prevalent as they were in the Martin specimens, it would have been necessary to further refine the eddy current optimization. Higher frequencies, smaller probe coils, and smaller index intervals would probably have been necessary to detect flaws much smaller than about 1 mm (0.39 in.). However, during the subsequent evaluations, none of these were changed from the original optimization.

The procedures used for all the evaluations, including the Martin specimens, can be found in Appendix I.

3.4 ULTRASONIC TECHNIQUE OPTIMIZATION

The ultrasonic technique optimization was predicated on the assumption that fatigue cracks were the only flaws being sought. In plate and sheet used in aircraft, missile, and spacecraft structure, fatigue cracks may originate from internal material discontinuities and may remain totally submerged during the life of the structure that contains them. However, the more general case is that, regardless of this source of origin, some component of a fatigue crack will be manifest in a principal surface of the structure. Furthermore, except for sectional changes and unusual loading conditions, fatigue cracks in sheet and plate tend to lie in planes perpendicular to the direction of applied stress and more or less normal to the principal surfaces of the material. These facts immediately suggest that, for ultrasonic testing, the principal sound beam be introduced at an angle to the surfaces and propagated parallel with the directions along which the applied stresses reacted.

By design, the fatigue cracks introduced into the specimens of this program were transverse to the direction of rolling of the raw material stocks, and although randomly located within the specimen test area, were produced by means that would result in their propagation in the short transverse direction. Knowledge of these conditions simplified the number of options that were necessary to consider in the development of optimum ultrasonic test techniques. For conditions in which little is known about the loads history, somewhat different techniques than those finally used would possibly have better application.

The techniques evaluated, exclusively shear wave, are:

a. Contact critical angle shear wave (Rayleigh or surface wave)

b. Contact shear wave

c. Immersion shear wave

d. Immersion critical angle shear wave

e. Delta

Since it was desired to produce a record of the ultrasonic tests, the contact methods were not intensively studied. However, data were developed to compare the relative merit of contact shear wave versus Delta as a function of off-axis alignment with the flaw plane. As expected, and as determined in previous investigations by Convair[3], the Delta technique proved superior in providing detectability through a greater angle of off-axis alignment than did conventional shear wave techniques.

It was decided to pursue optimization of immersion techniques. Considerable effort was spent in optimizing the Delta technique, which is summarized below.

3.4.1 DELTA CONFIGURATION TECHNIQUE. The physical parameters of the Delta configuration, such as angle of incidence, distance of separation (DOS) between transducers, DOS between the receiving transducer and the surface of the specimens, and transducer variations, grossly influence the sensitivity of the Delta technique to detect flaws.

Many transducer arrangements are possible to form a Delta method. The one that has been found to be most practical to apply consists of one transducer as transmitter and one as receiver.

A typical Delta-Scan configuration is shown in Figure 3.4-1. The ultrasonic transducer, T, injects compressional waves through a liquid coupling and into the test

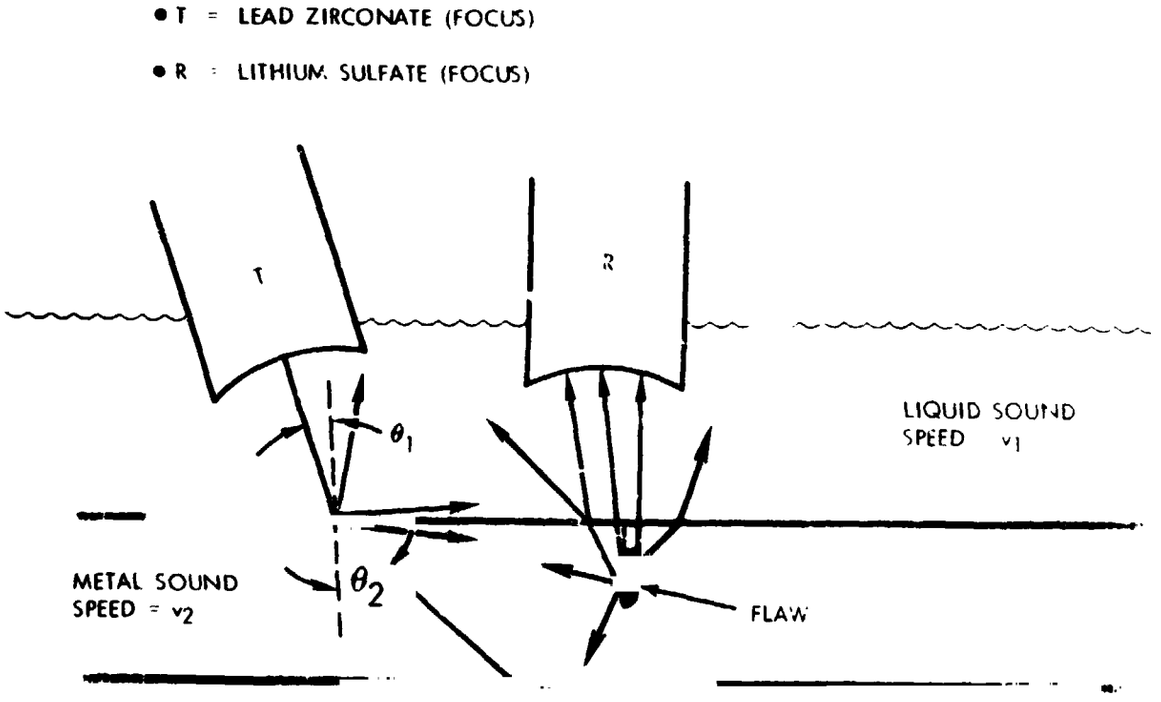

Figure 3.4-1. Typical Delta-Scan Configuration

components. These waves are incident upon the liquid-solid interface at an angle such that some of the energy is mode-converted into shear waves in the solid, some reflected at the interface, and some is propagated as surface waves in the proximity of the interface. When some of these sound energies strike the bottom of the solid-liquid (air) interface, they are re-directed according to Snell's law. When sound energy is incident on a discontinuity, it will be reflected, refracted, mode converted or scattered, depending on the shape and size of the discontinuity in relation to the wavelength of sound. Before any of these re-directed energies can reach the receiving transducer, they must be mode converted at the top solid-liquid interface into compressional waves. Depending on the incident angle and plate thickness, multiple reflection of the shear wave is possible. With the use of focused transducers, many angles of propagation are possible for the shear wave inside the plate. The picture is even more complicated when the dispersion and beam spread of the sound energy are taken into consideration. No known analytical expression describes the interaction and distribution of sound energy at the discontinuity for the Delta configuration.

The current practice in Delta-Scan operation is to use the shear mode peak as a flaw indicator by establishing an electronic gate at the location of the simple shear peak. For most applications, this mode gives the best signal-to-noise ratio for flaw detection. A shear mode peak whose amplitude is above a certain level triggers an audible and visible signal to alert the operator. Signals outside the gate are not used. It is apparent that other characteristics of the signal structure are dependent on the presence or absence of a flaw and are not being utilized. For example, the present Delta arrangement produces three prominent peaks which have been arbitrarily called Y, shear, and X mode. The exact characters of the X and Y modes are not well understood at this time. However, the X mode behaves very similarly to Stoneley waves which propagate at a liquid-solid interface with a velocity less than that of compressional or shear waves in either medium. This mode can be used rather effectively to detect surface flaws. The Y mode appears to be shear waves taking a direct path to the flaw versus a single reflection from the bottom surface designated above as the simple shear peak.

3.4.2 DELTA SIGNAL COUNTING TECHNIQUE. The signal counting technique operates by counting the number of oscillations in the received RF signal with excursions above and below a settable reference level, over a settable time span, or gating period. The reference level is set so that the background signal gives only one or two counts per gating period.

There are four amplitude sensors, each of which is set to a different amplitude level (A_3, A_2, A_1, A_0). Oscillations with amplitudes equal to or greater than level A_0 produce two counts each; equal to or greater than level A_2 produce four counts each; and equal to or greater than level A_3 produce eight counts each. That is, those with higher amplitudes produce higher counts and thus contribute more to the total count. More sensors with weighted factors of 16, 32, etc. can be added, but such circuits are complex and costly.

The gating period is set by the repetition rate of the transmitted pulses (a few hundred to a few thousand pulses per second). The present operation uses the n^{th} pulse to open the gate and $(n+1)^{th}$ pulse to close the gate. With a repetition rate of 1000 pulses per second, the gating period is one millisecond. The gating period can be lengthened to include many periods of the repetition rate, thereby increasing the total count. However, the gating period cannot be very long because the combined time of gating period plus the display time by the counter is inversely proportional to the scanning speed of the Delta head. That is, if the combined gate and display time is shorter, the scanning speed can be faster without losing the ability to resolve closely-spaced flaws. A block diagram showing the experimental hookup is shown in Figure 3.4-2. The use of commercial ultrasonic testing equipment as pulser-receiver permits parallel data taking with the amplitude-gate method and the signal-counting method for direct comparison.

3.4.3 CRITICAL ANGLE IMMERSION SHEAR WAVE TECHNIQUE. Immersion shear wave tests were conducted concurrent with the Delta experiments described above. Several specimens produced early in the program were used as reference and selected because they contained known undersize cracks. Two cracks measuring less than 1.52 mm (0.060 in.) long as verified by penetrant and visual measurement were reliably detected at incident angles between 0.51 rad (29.25°) and 0.53 rad (30.5°) with a 10 MHz, 12.7 mm (0.5 in.) diameter lithium sulfate transducer having a focal length

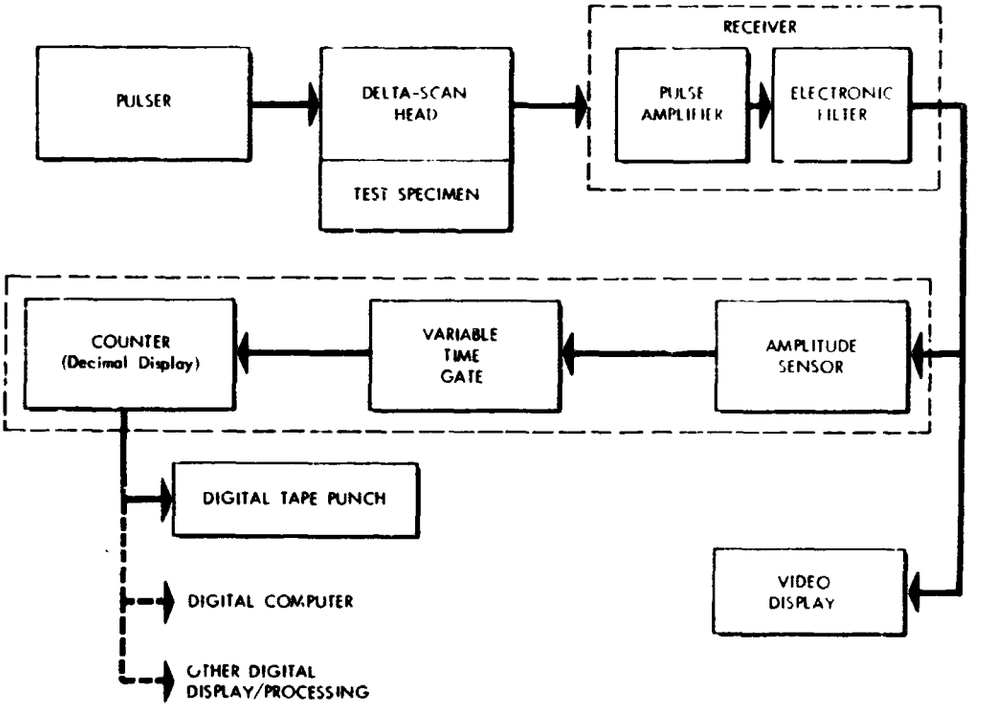

Figure 3.4-2. Signal Counting Technique

in water of 44.5 mm (1.75 in.). It was found that the variations in surface finish had a noticable effect as the transducer was scanned over the midline of the specimens. The lay of the surface roughness was along the long axis of the specimens and was produced by a rotory cutter that was centered about the long axis and transversed the long axis. Thus each surface cut left small "ridges" that were aligned normal to the incident ultrasonic beam within approximately ±3.3 mm (0.13 in.) of the specimen centerline. The instrument sensitivity had to be adjusted to exclude these ripples from being recorded.

The decrease in sensitivity required because of surface finish in a sense penalized the technique. With slow scanning, defect signals could be observed visually "walking" through the surface ripple. These signals were of the same order of amplitude as the surface ripple and, hence, could not be electronically recorded even though they could be readily seen. The sensitivity had to be compromised in order to produce a recording. This factor, however, does relate to "real world" problems of production inspection. That is, recognition of surface finish noise precluded the use of a technique that would detect smaller flaws in areas where surface finish lay was greater than approximately 0.087 rad (5°) off normal to the incident wave front.

The specimens had to be segregated into two groups according to surface finish: the two roughest finishes in one group, the smoother finishes into another. For the first evaluation, this requirement dictated that the surface finish be measured prior to testing.

Critical angle immersion shear wave testing was chosen for the evaluation since it only involved a single transducer and was at least as sensitive as any other technique investigated. It was quite simple to produce a C-scan recording with 1:1 characteristics since the critical angle shear wave was essentially a surface wave with very short range in the metal because of water dampening. Although the reflected signal could be seen within approximately 3.3 mm (0.13 in.) from the flaw, the amplitude increased exponentially with decreasing distance from the flaw. With the alarm level set high enough to exclude centerline surface finish noise, the longitudinal persistence of the flaw indication was as short as two scan indexes (1.27 mm or 0.050 in.) for the smallest flaws. However small, the indications were quite distinctive.

On the Martin-Marietta Corporation (MMC) specimens, the surface finish lay was transverse to the long axis of the specimen. This permitted testing at higher levels of receiver gain than on the Convair specimens since surface noise was at a lower level. C-scan results from the two MMC specimens chosen for reference are shown in Appendix I. The reference C-scans and procedures used for the Convair specimens are also shown in Appendix I.

3.5 REPLICATION TECHNIQUE OPTIMIZATION

When properly selected and applied to a solid surface, silicone rubber will faithfully conform to the contour of the solid and, upon cure, may be examined to reveal the condition of the surface. Very small irregularities, such as tight cracks, are detectable by this method only at high magnifications, such as 100 ×, which is not practical from an inspection standpoint. It is desirable, therefore, to increase the detectability of small cracks by producing a color contrast in the replica. Such a contrast is produced by first causing colored material to specifically concentrate or accumulate in the crack. Upon subsequent replication, the pigment is encapsulated and is detectable in the cured replica at magnifications of 10 × or less.

The basic requirements for the preparation of color-enhanced silicone rubber replicas are:

a. Penetration of colored material (pigment) in the crack.

b. Removal of excess pigment from adjacent areas without disturbing material in the crack.

c. Replication of the area and transfer of the pigment from the crack into the replica.

This technique was optimized in an independent research and development program conducted at General Dynamics in 1970. The experimentation and results of that study are summarized below.

Initial experimentation was based on efforts to utilize standard commercially available penetrant dyes in the initial step of the procedure. The following materials were included in these studies:

a. Fluoro Finder FL-50, Testing Systems Inc., Glenside, Pennsylvania.

b. Spotcheck Penetrant, Magnaflux Corp., Chicago, Illinois.

c. Met-L-Check Penetrant, Met-L-Check Co., Los Angeles, California.

d. Hy Rez Penetrant, Magnaflux Corp., Chicago, Illinois

The test specimen was a strip of aluminum containing drilled holes, with a large stress corrosion crack along the surface length and through the holes. Each of the penetrant fluids was applied to the surface of the metal, allowed to "soak in" for a period of 15 minutes, and the excess removed per manufacturer's recommendation. Then silicone rubber replicating fluid was applied. The replicating fluid was formulated of 35 grams RTV-11 silicone rubber (General Electric Corp., Waterford, New York) and 0.1 gram Nuocure 28 catalyst (Tenneco Chemical Co., Elizabeth, New Jersey).

Fluro Finder FL-50, Spotcheck, and Met-L-Check penetrants were non-volatile and remained in the liquid state up to the application of silicone rubber. Upon contact with the rubber, the liquid penetrant dispersed into the rubber resulting in a diffuse area of color unsuitable for flaw detection. Moreover, the penetrant retarded the cure of the rubber in the areas of contact.

Hi Rez dried to a solid residue and caused no problem with subsequent replication. However, its sensitivity was poor. The replica displayed the wider portion of the crack, but the tight part of the crack, including the area inside the holes, could not be detected.

Similar results were obtained using the penetrants in standard penetrant dye methods per manufacturers' instructions. In all cases sensitivity was lacking and none of the materials revealed the cracks inside the holes.

The performance of the commercial penetrants showed that improved formulations were needed before a successful inspection procedure could be developed. To improve sensitivity, fluids with greater penetrating ability were required and a penetrant was needed that would dry or volatilize and leave a solid colored residue. This could be accomplished by making a solution or dispersion of a non-volatile pigment in a volatile solvent with a low surface tension.

The candidate vehicles chosen for evaluation were:

Candidate	Surface Tension Value
Ethyl ether	17.0 dynes per centimeter
Methyl alcohol	22.6 dynes per centimeter
Trichloroethylene	Unknown
Dimethyl siloxane (Dow Corning 200 fluid, 0.65 centistoke)	15.9 dynes per centimeter

Two pigments were evaluated:

a. Molybdenum disulfide powder, sub-micron particles.

b. Carbon black ("Thermax," R. T. Vanderbilt Co., New York, N.Y.).

Each powder was dispersed into each fluid, and the mixture was applied to the specimen and allowed to evaporate to dryness. The excess dry powder was removed by two methods: wiping with a dry cloth and with a chloroform wipe. (Chloroform was chosen because its high surface tension, 27.1 dynes per centimeter, prevents it from washing away the pigment inside the crack.) The aluminum test specimen was then covered with the silicone rubber replicating material previously described. Following cure, the solid replicas were removed and examined under 10 × magnification.

The results revealed that the dimethyl silicone fluid was the best of the vehicles tested and that the carbon black was the better pigment. Dry cloth removal of excess pigment produced a better replica than the chloroform wipe did.

This method provides a permanent record and has the capability to provide an inspection of cavities in parts that would be difficult to inspect using other methods. Hence, the method should not be considered as a primary inspection method for fatigue crack detection. It should be reserved for complex configurations. Figure 3.5-1 shows a typical fatigue crack indication.

3.6 ACOUSTIC EMISSION MONITORING

The acoustic emission monitoring system used during this phase was the same as that described in Section 2.3. However, since it was desired to demonstrate the capability of the acoustic emission method to detect and locate the emission sources from crack growth during proof loading, the system was rearranged slightly. In addition to two slave sensors positioned near the specimen grip ends, two independent master sensors were used. These were positioned inboard from the slaves and connected through preamplifiers to the AE unit. The amplified signals were input to a dual-beam oscilloscope. The oscilloscope sweep was triggered by the arrival at either master of an emission signal with amplitude above a preset limit. The single sweep was photographed. The sweep was timed to display the emission as received by both masters. Since the emission sources were from one or more of the cracks, a small time difference between the two signals could be related, by sensor geometry and known acoustical velocity properties, to the location of the source relative to the master sensors.

The two specimens used had been scrapped during specimen preparation due to flaw growth beyond the desired limits. Both specimens were 3.18 mm (0.125 in.) thick and contained starter notches. Figures 3.6-1 and 3.6-2 are data sheets identifying the sensor locations and crack data from these specimens. For Specimen XA-11, it was estimated that flaw growth would probably occur from crack A, since it had progressed beyond desired dimensions, and B and C were either minimally cracked or uncracked. As shown in Figure 3.6-3, five emissions were received during proof loading. The inset photograph is an example of the delayed oscilloscope traces showing a difference in arrival times at M_1 and M_2 of approximately 3 μs, which corresponds to a distance of approximately 18 mm (0.71 inch). The measured distance was intended to be 19 mm (0.75 inch). Similar data were taken during proof loading of Specimen XA-18 as shown in Figure 3.6-4. There the measured difference in distance of the propagating crack from M_1 and M_2 was 63.5 mm (2.50 inch) and the difference determined from the oscilloscope trace was 63 mm (2.48 inch). Specimen XA-11 was finally loaded to tensile failure with the results shown in Figure 3.6-5. No emissions were obtained until a load of 0.118 MN (26.6 kilopounds-force) was achieved. The total number of emissions recorded was 118, nearly all obtained just prior to failure.

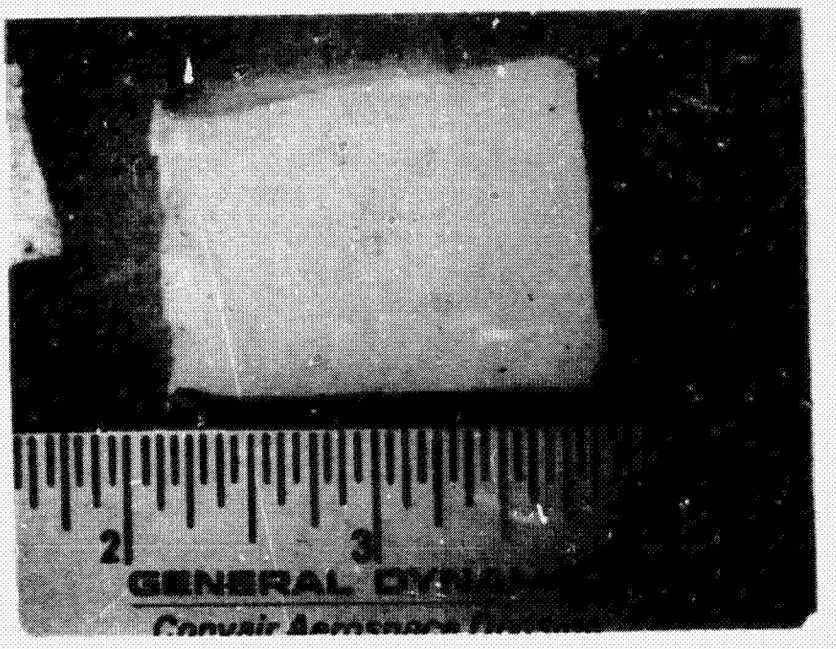

CHROMAFAX

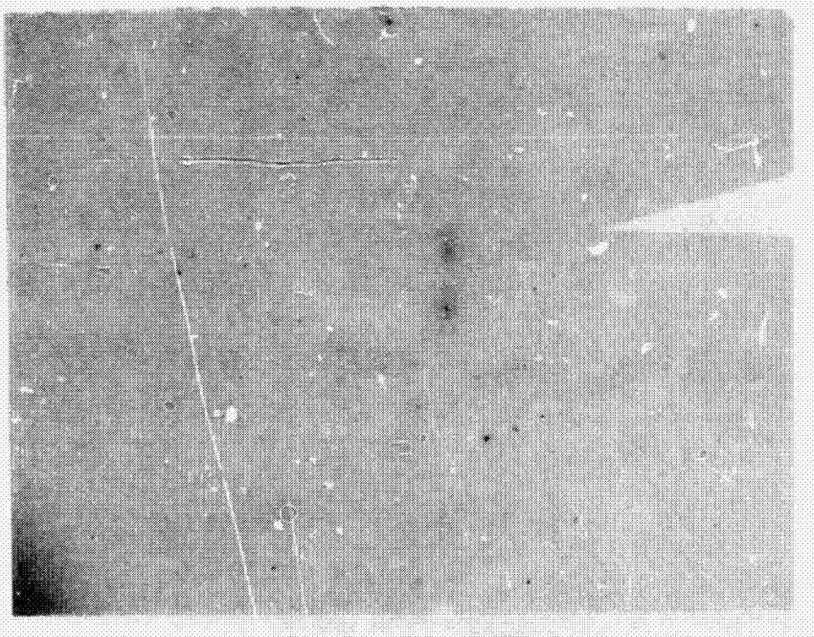

7 X

Figure 3.5-1. Typical Fatigue Crack Indication Shown by the Replication Process

NAS 9-12320
SPECIMEN DATA SHEET

IDENTIFICATION XA-11

XR
UT
PT
EC
(AE)

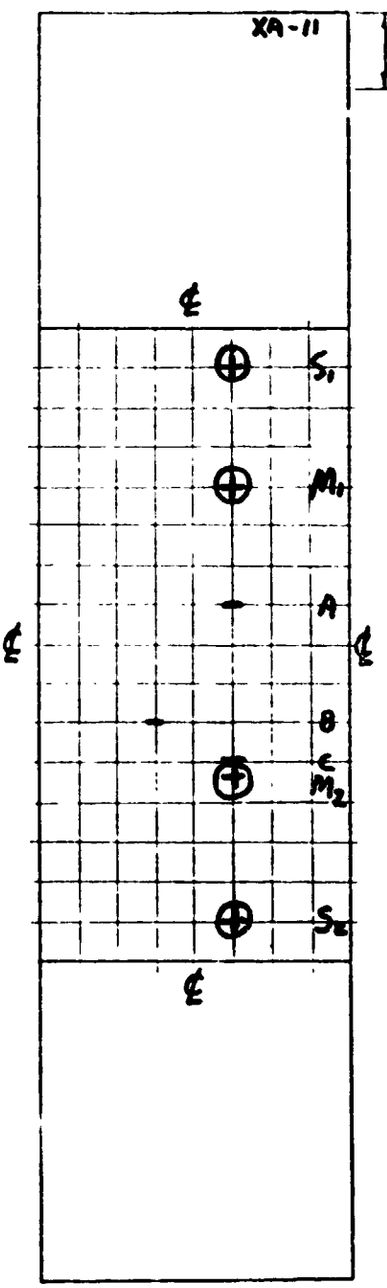

A 2nd stage fatigue crack 0.180 long
B 1st stage fatigue crack 0.080 long
C Starter notch - no fatigue cycles

$M_1 \rightarrow A \sim 1.5$ in (38.1 mm)
$M_2 \rightarrow A \sim 2.25$ in (57.1 mm)

$\Delta d \sim 0.75$ in (19.0 mm)
$\Delta T \sim 3\ \mu s$
$V_c \sim 6$ mm/μs

$V_c \Delta T = 3\ \mu s \times 6$ mm/$\mu s = 18$ mm

Crack A dimensions after failure:
$a = 0.100$ in (2.54 mm)
$2c = 0.180$ in (4.57 mm)

$\sigma_{ult} = \frac{F_{tu}}{A}$

$F_{tu} = 27,800$ lb
$A = 0.124$ in $\times$ 4.00 in $= 0.496$ in^2

$\sigma_{ult} = 56048$ lb/in^2 $= 386.45$ MN/m^2

Figure 3.6-1. Specimen XA-11 Data Sheet

NAS 9-12320
SPECIMEN DATA SHEET

IDENTIFICATION XA-18

XR
UT
PT
EC
(AE)

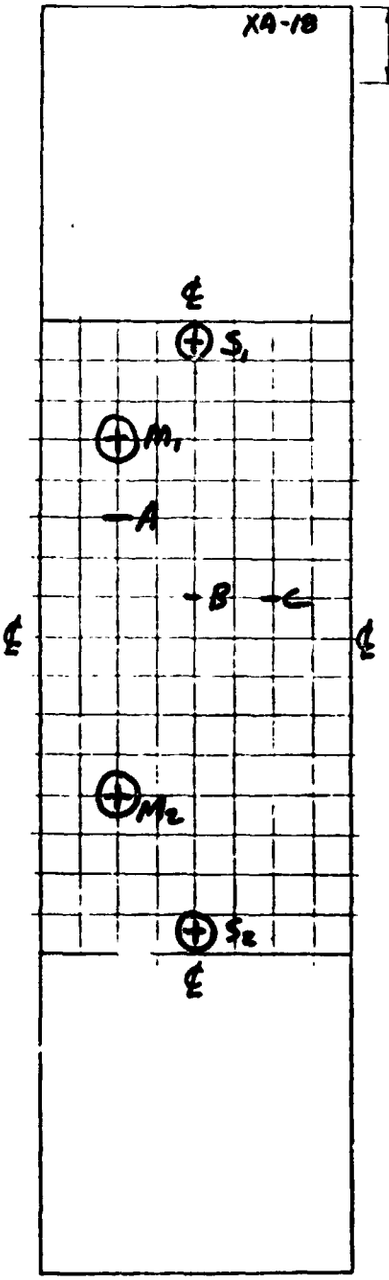

A 1st stage fatigue crack - 0.160 in long (4.07 mm)
B 1st stage fatigue crack - 0.080 in long (2.03 mm)
C 1st stage fatigue crack - 0.080 in long (2.03 mm)

$M_1 \rightarrow A \sim 1.0$ in (25.4 mm)
$M_2 \rightarrow A \sim 3.5$ in (88.9 mm)

$\Delta d \sim 2.5$ in (63.5 mm)
$\Delta T \sim 10.5\ \mu s$
$V_c \sim 6$ mm/μs

V_c [redacted] mm/$\mu s \times 10.5\ \mu s = 63$ mm

Figure 3.6-2. Specimen XA-18 Data Sheet

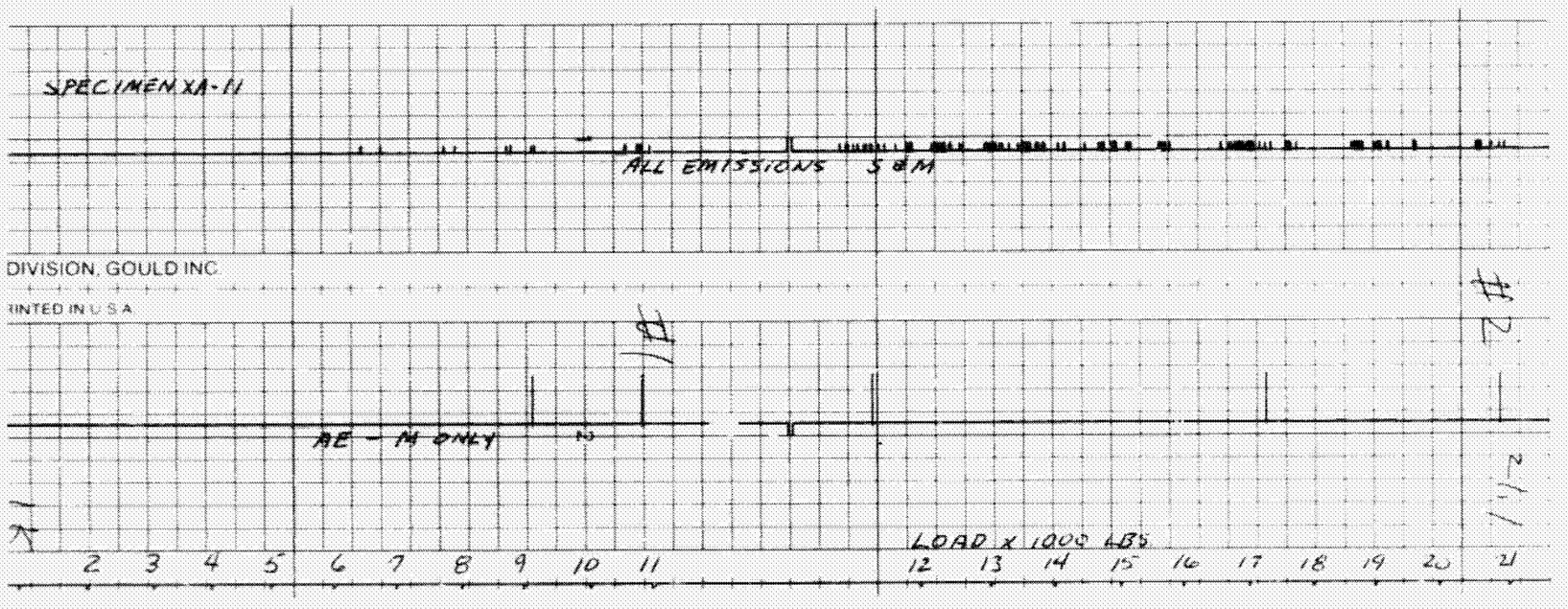

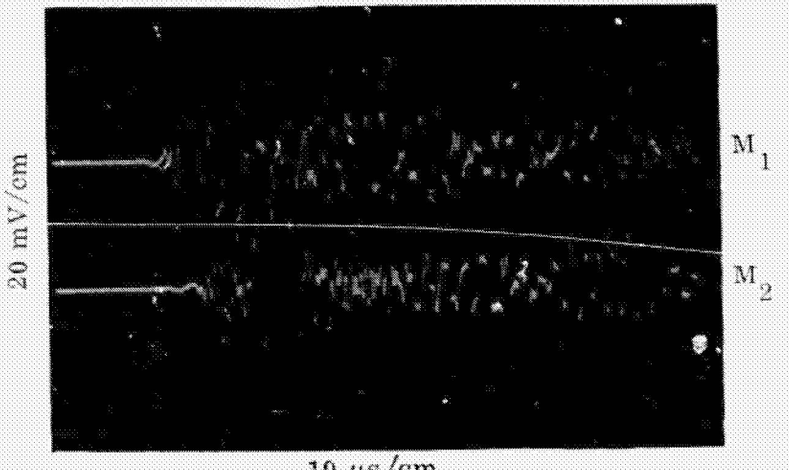

Figure 3.6-3. Acoustic Emission Data During Proof Loading of Specimen XA-11

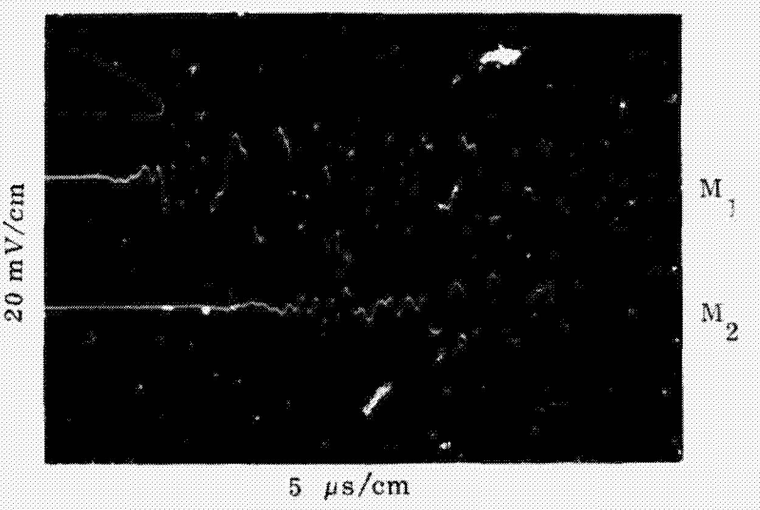

Figure 3.6-4. Acoustic Emission During Proof Loading of Specimen XA-18

This technique was adopted for the acoustic emission monitoring tasks during proof loading (see Section 4.6) and during tensile failure loading (see Section 5.2).

3.7 HOLOGRAPHIC TECHNIQUE OPTIMIZATION

The basic holographic experimental apparatus is shown in Figure 3.7-1. The beam of laser light is divided by a beam splitter into a reference beam and an object beam. Each of the beams is expanded on passing through a pinhole assembly: a 10 × microscope objective and a 25-μm pinhole spatial filter for the reference beam, and a 20 × microscope objective and a 25-μm pinhole spatial filter for the object beam. Components were selected and the pinhole assembly for the reference beam was positioned so that when the optically-filtered beam expanded after reflection from the reference mirror it fully and efficiently illuminated the 10.2 × 12.7 cm (4 × 5 in.) holographic plate with a spherical reference wave. In a similar manner, the components were selected and the pinhole assembly for the object beam was positioned so that the expanding spatially-filtered beam just fully illuminated the useful long dimension – central 20.3 cm (8 in.) – of the specimens. This efficient arrangement of reference and object beams shortened the exposure times required for recording the holograms, thus minimizing any stability problems during exposures in the holographic setup. The setup, which was located adjacent to a factory machine shop and overhead aircraft environment, is described below.

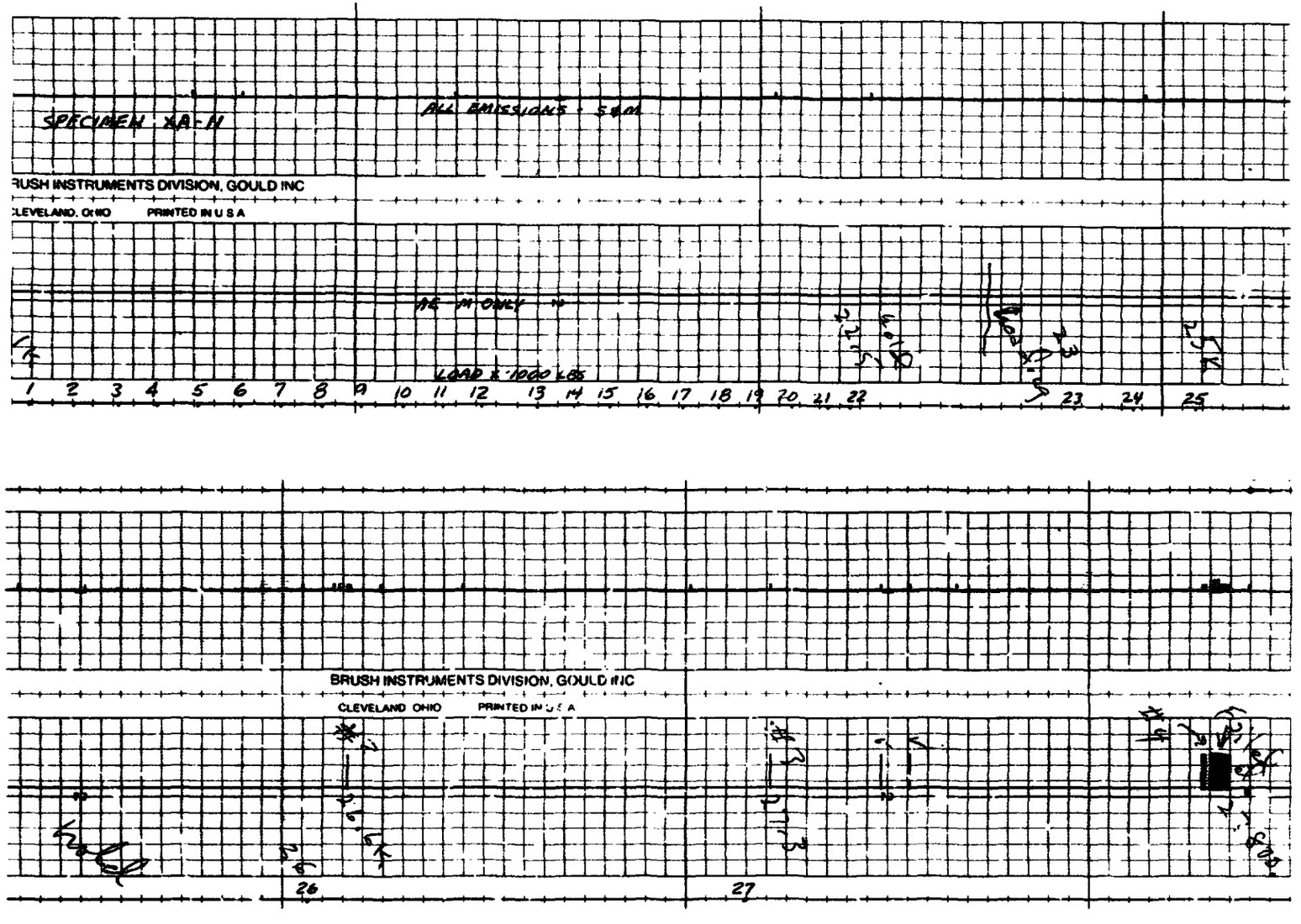

Figure 3.6-5. Acoustic Emission Data During Failure Loading of Specimen XA-11

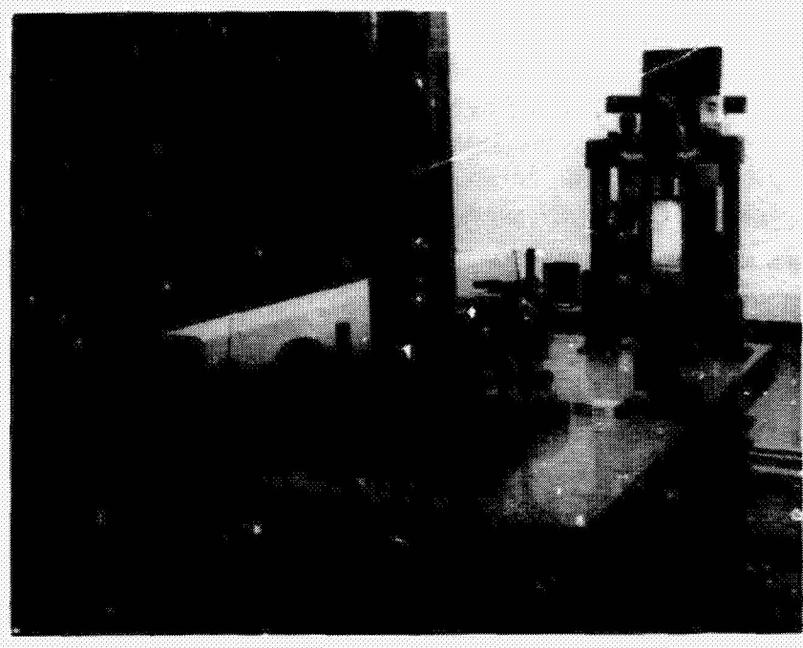

Figure 3.7-1. Holographic Interferometry Apparatus

A 50-mW He-Ne laser was used as the light source. All double-exposure holograms were recorded on Agfa-Gevaert 10E75 high-resolution holographic plates, which were subsequently developed in Kodak HRP developer.

Since holographic recording involves comparison of optical wavefronts separated in time as well as in space, the mechanical stability of the entire system is critical. The optical path lengths must remain constant to within one-quarter wavelength during exposure of the holographic plate, during the time interval between exposures in double-exposure holography, and in real-time viewing and recording. The stability requirement was met by placing massive components on a large granite slab 1.03 m × 1.52 m × 10.2 cm (4 ft × 6 ft × 4 in.) mounted 1 meter off the floor on alternate layers of common brick and 19 mm (0.75 in.) thick felt sheets. The last layer was a 2.54 cm (1 in.) thick aluminum sheet separated from the floor by air-filled tubes to isolate the apparatus from building vibrations. It did not work because of operating heavy machinery, such as the drop shear cutter in the adjoining machine shop, and because of overhead flying aircraft. However, by using shortened exposure times the probability of these "noise" events occurring during the holographic recording periods was minimized.

Several schemes of thermal, vibratory, and static mechanical loading of the original doubler-less specimens were tried. Thermal stressing over the entire surface using a hot air gun and point thermal stressing using a soldering iron led to a number of practical difficulties, including transient stress fields and lack of appropriate stress localization due to the high heat thermal conductivity of the specimens. An attempt to

use time-averaged holographic interferometry while the specimens were excited to vibratory motion also proved unsatisfactory, mostly due to insufficient loading levels. Several methods of static loading were attempted, including placing the specimens in flexure, clamping them in various ways, and bending them with a fulcrum block located behind a suspected crack site; however, none of these techniques produced sufficient differential displacement in the vicinity of the cracks to yield observable fringe anomalies.

Use of an Instron Model TM Tensile Testing apparatus on the holographic table as a sample loading device failed to give the desired result because its total load capability was too small: 890 N (200 lbf). The desired result was finally obtained using a modified Blackhawk Proto-Power Model R159 "Retracto" ram compression device, which permitted loading of the specimens up to 82.7 MN/m^2 (12,000 psi). This was accomplished by designing and constructing a lever arm arrangement attached by a dowel pin to a machined accessory fastened by bolts to the top two horizontal members of the original frame of the compression device (Figure 3.7-2). This formed the fulcrum of the lever arm. The top of the specimen was attached by three bolts to a clevis

Figure 3.7-2. Tensile Loading Device (C_1 Configuration)

accessory which was doweled into one of two available positions along the lever arm. The bottom of the specimen was attached by three bolts to another clevis accessory held in place against the bottom of the two bottom horizontal members of the original frame by two dowel pins when the specimen was put in tension. The latter was achieved by inverting the actuating piston cylinder ram attached to the top horizontal frame so that when activated, it pushed upward on the bottom side of the lever arm, thus tensile loading the specimen.

By making the specimen and piston positions interchangeable, it was possible to obtain two different loading configurations. Configuration C_1', with the specimen and piston positions located 14 cm (5 1/2 in.) and 26.7 cm (10 1/2 in.), respectively, from the fulcrum gave a load scale factor of 1.9 (Figure 3.7-2). Configuration C_2 with the specimen and piston positions located 28 cm (11 in.) and 14 cm (5 1/2 in.), respectively, from the fulcrum, gave a load scale factor of 0.5 (Figure 3.7-3). The actual total load in pounds on the specimen was equal to the product of the load scale factor and the piston gauge reading in pounds. Configuration C_1' was equivalent to configuration C_1 in load scale factor, C_1' being the mirror image of C_1.

Use of configurations C_1 and C_1' for the B (nominally 5.72 mm (0.225 in.) thick) specimens, and C_2 for the A (nominally 1.52 mm (0.060 in.) thick) specimens resulted in best control of the pressure leak in the hydraulic piston unit.

Figure 3.7-3. Tensile Loading Device (C_2 Configuration)

After a tensile specimen was loaded to an initial value of L_1 in a specific configuration, the first recording, a two-second exposure, was made on the hologram plate. The specimen was then differentially loaded by the amount ΔL to the final loading value, and a second recording, another two-second exposure, was made on the same hologram plate.

As many as five double-exposure holograms were made for some of the specimens, with the initial load value L_1 varied from a low value of 13.8 MN/m^2 (2000 psi) to a high value of 82.7 MN/m^2 (12,000 psi), to investigate the detectivity of different size cracks with initial load value. The selection of the differential load value, ΔL, at any particular L_1 value was made on the basis of obtaining interference fringe patterns of optimum spacing to best display the fringe pattern anomalies at the crack sites.

Initially, attempts were made to use the technique of real-time (live-fringe) holography to observe and subsequently photograph the fringe pattern anomalies. Unfortunately, in the first specimens inspected, the fringe patterns displayed so much parallax with respect to the specimen surface that it was not possible to photograph them with sufficient contrast for a good display of the fringe anomalies, although the visual recording was excellent. In these cases, the specimens were subjected to motions other than the desired motion in the plane of the specimen along the long dimension, which added to the complexity of the fringe pattern produced. These motions included rotation and torsion of the specimens in the tensile device during differential loading.

The real-time technique required the use of the specimens for a longer time period because the photographic recording of the "live fringes" had to be accomplished during the life-time of the real-time hologram (before its removal from the plate holder and subsequent insertion of another holographic plate for the next sample).

Since double-exposure holograms are permanent and can be reconstructed at any subsequent time, all samples were returned immediately after all double-exposures were completed. It was not necessary to first process the plates and record the reconstructions photographically. The turn-around time was important since other principal investigators associated with this program used different NDT techniques on the same specimens on a fairly rigid time schedule.

Removal of a single-exposure hologram for processing in the darkroom and re-insertion into the plateholder for viewing and recording the real-live fringes always introduces background fringes. The latter are associated with such factors as repositioning accuracy of the developed holographic plate to its exact original position, and emulsion shrinkage. In double-exposure holography, this problem does not exist since there is no plate motion or differential emulsion shrinkage between the two recordings (exposures) on any holographic plate.

Thus, the double-exposure technique was selected for recording the fringe anomalies around the fatigue cracks in this program. The fringe patterns were reconstructed on 10.2 x 12.7 cm (4 x 5 in.) Polaroid type 57 (3000 speed) film with 3-second exposure times at approximately 1/2 x magnification using a Cambo camera with a Tele-Xenar lens set at f/22 (see Figures 3.7-4 and 3.7-5).

Table 3.7-1 is a summary of the experimental results.

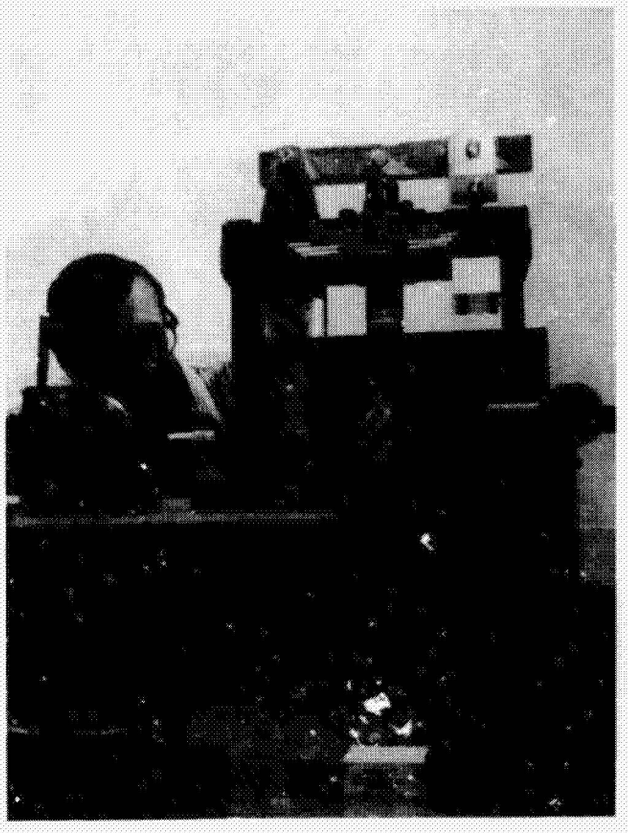

Figure 3.7-4. Camera View Through Double-Exposure Hologram of Specimen A-24 Plate 34 Focused on Sample in C_1 Configuration

1/2 SCALE

Figure 3.7-5. Polaroid Print of Reconstruction of Double-Exposure Hologram A-24 P34

Table 3.7-1. Summary of Experimental Results

Sample	L_1† kN	L_1† klb	ΔL‡ N	ΔL‡ lb	Cracks Observed	Cracks Undetected	Remarks
A-6	13.4	3	-448	-100	3_1 3_2 2_2	2_1 1	
	11.66	2.6	-448	-100	3_1 3_2	2_2 2_1 1	
A-9	11.2	2.5	-448	-100		2_1 2_2	
A-11	11.2	2.5	-896	-200	3_1 3_2 2 (barely)	1	
	11.2	2.5	-448	-100	3_1 3_2	2 1	
A-12	13.5	3.05	-336	-75	3_1 3_2	–	
	9	2.05	-448	-100	3_2 3_1 (barely)	1_1 1_2	
	4.48	1	-224	-50	3_2 (barely)	–	
A-16	5.95	1.33	-852	-190	3_1 3_2	1	
A-17	11.89	2.65	-224	-50	2_2 (barely)	2_1 1_1 1_2	
A-18	12.1	2.7	-672	-150	3_1 3_2 2_1 (barely)	2_2 1	
A-19	11.2	2.5	-448	-100	None	–	Nc flaws.
A-21	5.11	1.14	-426	-95	None	3	Fringes seen better on direct viewing.
	5.95	1.33	-852	-190	None	3	
	3.42	0.76	-1701	380	None	3	
A-22	11.64	2.6	-448	-100	3	2_1 2_2	
A-23*	6.38	1.43	-2125	-475	3	2 1_1 1_2	
A-24	10.2	2.28	-1279	-285	3_1 3_2 2 1_2	1_1	Much greater parallax. 1_1 seen better on direct viewing.
	5.11	1.14	-641	-143	3_1 3_2	1_1 1_2	
B-1	49.2	11	-3420	-760	None	–	No flaws.
B-4	51	11.4	-4260	-950	3 2 1 (barely)	–	1 seen better on direct viewing.
	10.2	2.28	-3420	-760	3 2	1	
B-6	51	11.4	-5110	-1140	3_1 3_2 2_1 2_2 1	–	1 seen better on direct viewing.
	40.9	9.12	-3420	-760	3_1 3_2 2_1 2_2 1 (Larely)	–	
	10.21	2.28	-1700	-380	3_1 3_2 2_1 2_2	1	
B-9	30.3	6.84	-4260	-950	2_1 2_2	–	
B-11	51.1	11.4	-4675	-1045	3_2 2 1	1	
	22.2	4.95	-1700	-380	3_2 2 1	1	
B-12	51.1	11.4	-17,000	-3800	3_1 3_2 2 1_2	–	Much parallax; all flaws seen on direct viewing.
B-16	49.4	11.02	-2546	-570	3_1 3_2 1 (barely)	1	
B-17*	24.2	5.42	-3420	-760	2_1 2_2	1_1 1_2	
B-18	29.8	6.65	-4260	-950	3_1 (3_2) 2_1 2_2 1 (barely)	(1)	
	9.36	2.09	-1700	-380	3_1 (3_2) 2_1 2_2	1	
B-22	30.2	6.75	-2980	-665	3 2_1 2_2	–	Much parallax; all flaws seen on direct viewing.
	10.2	2.28	-3420	-760	3 2_1 2_2		
B-23*	26	5.8	-6380	-1425	3 2 1_1 1_2	–	Much parallax. all flaws seen on direct viewing.
B-24	51.1	11.4	-4260	-950	3_1 3_2 2	1_1 1_2	
	26.8	6	-7160	-1600	3_1 3_2 2	1_2 1_2	

*Samples for subsequent acoustic emission analysis. † L_1 is highest load on sample. ‡ ΔL is differential load between double exposures.

SECTION 4

EVALUATION OF NDT METHODS

4.1 EFFECTS OF SURFACE FINISH EVALUATION

This first evaluation of specimens considered the effects of surface finish on the detectability of flaws by NDT methods. The specimens were divided into four groups, for each thickness, by surface roughness as described in Section 2.2. The NDT techniques used are included in Appendix I. Three different size flaws, as described in Section 2.1, were incorporated into each surface finish group. In all there were 120 flaws less three that were never found by any method and were later verified not to exist. Table 4.1-1 shows the data compiled during this NDT evaluation.

4.2 SURFACE ETCH

After the first evaluation, all of the specimens were subjected to a microetch for the purpose of neutralizing the surface finish and to determine if this process might enhance the detectability of the flaws with respect to any of the NDT techniques. The etching solution consisted of 5 parts HF (48%), 10 parts concentrated HCl, 10 parts HNO_3 and 75 parts H_2O. The specimens were etched in this solution for a total of 150 seconds, desmutted in concentrated HNO_3 for 5 seconds, and water cleaned. The process removes metal at the approximate rate of 0.0013 mm/s (0.0003 in/min). The etch also removed some metal smeared over crack openings left after machining the surface finish. These conditions were noted visually with the aid of a microscope. During the later stages of etching, the temperature of the solution had increased to an extent that approximately six of the thinner specimens were slightly overetched with some preferential attack on grain boundaries. The etching also had some effect on surface finish. On a sample of specimen measured, the roughest surface was reduced to approximately 3.8 μm (150 μ in.) average roughness and the finest finish increased to approximately 1.3 μm (50 μ in.).

4.3 POST-ETCH EVALUATION

4.3.1 NON-DESTRUCTIVE TESTING. Following the etch, all specimens were submitted to evaluation by the radiographic, ultrasonic, penetrant and eddy current techniques and the same specimens previously evaluated by the replication method were again evaluated. These evaluations were conducted according to the procedures outlined in the NDT instructions contained in Appendix I. The same personnel involved in the previous evaluation performed this evaluation. Specimen identification numbers were changed to avoid possible recollection of previous identifications. Table 4.3-1 summarizes the results. Comparison with the data in Table 4.1-1 reveals an apparent reduction in detectability for the penetrant method. This was most probably caused by

Table 4.1-1. Summary of Results from First NDT Evaluation

Method	A Flaw Size	Flaws Detected/Total Flaws				
		Surface Finish - Average Roughness				Totals
		0.69-0.81 μm (27-32 μin.)	1.27-1.52 μm (50-60 μin.)	3.0-3.3 μm (120-130 μin.)	5.7-5.9 μm (225-230 μin.)	
Ultrasonic	1	3/5	3/5	0/5	1/4	7/19
	2	5/5	4/4	4/4	2/5	15/18
	3	5/5	5/5	5/5	5/5	20/20
Radiography	1	0/5	0/5	0/5	0/4	0/19
	2	0/5	0/4	0/4	0/5	0/18
	3	2/5	0/5	1/5	2/5	5/20
Eddy Current	1	3/5	5/5	4/5	4/4	16/19
	2	5/5	4/4	4/4	5/5	18/18
	3	5/5	5/5	5/5	5/5	20/20
Penetrant	1	3/5	5/5	4/5	4/4	16/19
	2	5/5	4/4	4/4	5/5	18/18
	3	5/5	5/5	5/5	5/5	20/20
	B Flaw Size					
Ultrasonic	1	5/5	5/5	4/5	2/5	16/20
	2	5/5	5/5	5/5	5/5	20/20
	3	5/5	5/5	5/5	5/5	20/20
Radiography	1	0/5	0/5	0/5	0/5	0/20
	2	3/5	1/5	1/5	0/5	5/20
	3	0/5	1/5	0/5	0/5	1/20
Eddy Current	1	5/5	5/5	5/5	5/5	20/20
	2	5/5	5/5	5/5	5/5	20/20
	3	5/5	5/5	5/5	5/5	20/20
Penetrant	1	5/5	5/5	1/5	5/5	16/20
	2	5/5	5/5	5/5	5/5	20/20
	3	5/5	5/5	5/5	5/5	20/20

1. Replication was performed on six specimens. Ratios for thin specimens are: 1/3 size 1, 1/1 size 2, 4/4 size 3. Ratios for thick specimens are: 3/4 size 1, 4/5 size 2, and 3/4 size 3.

2. Five false indications were noted by radiography.

Table 4.3-1. Summary of Results from Second NDT Evaluation

Method	A Flaw Size	Flaws Detected/Total Flaws				
		Original Surface Finish Groups				Totals
		A	B	C	D	
Ultrasonic	1	2/5	3/5	0/5	1/4	6/19
	2	5/5	4/4	4/4	2/5	15/18
	3	5/5	5/5	5/5	5/5	20/20
Radiography	1	0/5	0/5	0/5	0/4	0/19
	2	0/5	0/4	0/4	0/5	0/18
	3	1/5	1/5	1/5	2/5	5/20
Eddy Current	1	3/5	4/5	4/5	3/4	14/19
	2	5/5	4/4	4/4	5/5	18/18
	3	5/5	5/5	5/5	5/5	20/20
Penetrant	1	2/5	2/5	1/5	2/4	7/19
	2	4/5	4/4	2/4	5/5	15/18
	3	5/5	5/5	5/5	5/5	20/20
	B Flaw Size					
Ultrasonic	1	5/5	4/5	4/5	2/5	15/20
	2	5/5	5/5	5/5	5/5	20/20
	3	5/5	5/5	5/5	5/5	20/20
Radiography	1	0/5	0/5	0/5	0/5	0/20
	2	3/5	1/5	1/5	0/5	5/20
	3	0/5	0/5	0/5	0/5	0/20
Eddy Current	1	5/5	5/5	5/5	5/5	20/20
	2	5/5	5/5	5/5	5/5	20/20
	3	5/5	5/5	5/5	5/5	20/20
Penetrant	1	5/5	5/5	5/5	5/5	20/20
	2	5/5	5/5	5/5	5/5	20/20
	3	5/5	5/5	5/5	5/5	20/20

1. Replication was repeated on same six specimens used in the first evaluation. Ratios for A specimens were: 1/3 size 1, 1/1 size 2, and 4/4 size 3. Ratios for B specimens were: 2/4 size 1, 2/5 size 2, and 2/4 size 3.

2. Five false indications were noted by radiography.

the type of etchant used and the condition of overetching experienced on six thin specimens. On these specimens, with the type of penetrant used, the surfaces were such that a large amount of background penetrant material remained after the washing step. This high background noise likely had a deleterious effect upon detection of the small flaws as reflected in the data reported in Table 4.3-1.

4.3.2 HOLOGRAPHY. Approximately 100 double-exposure holograms, at least one for each of the 24 specimens, were made. Table 4.3-1 presents a summary of the crack sizes observed and undetected from the Polaroid prints and from observation of the reconstructed holograms.

In most cases, no problem was experienced in photographing the reconstructed virtual image to display the anomalies in the fringe patterns around the cracks when detectable; in these cases, direct visual observation also showed sharp fringe patterns at or near the surface of the specimen, with little or no parallax between the fringe plane and specimen plane. In some cases, especially those involving specimens pulled at the higher total load values, some difficulty was experienced in photographing the fringe patterns; only portions of the fringe patterns appeared in focus at any one camera setting, as shown in Figure 4.3-1 for specimen B-12 in configuration C_1 with L_1 = 50.7 kN (11,400 lb) and ΔL = -16.9 kN (-3800 lb). Direct viewing of the reconstructed image through the hologram plate (P9) itself reveals a sharp set of fringes

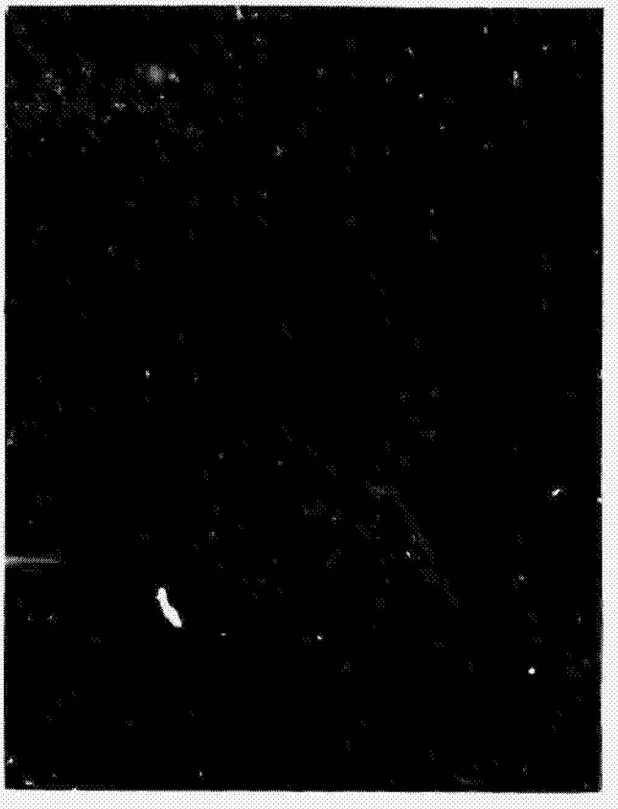

Figure 4.3-1. Reconstruction of Double-Exposure Hologram of Specimen B-12 Plate 9

of very good visibility, including pronounced fringe anomalies at the three large crack sites (3_1, 3_2, and 2) and a less-pronounced fringe anomaly at the smaller crack site (1_2). The fact that much parallax is observed between the fringe pattern and the specimen surface when the direction of observation through the hologram is changed indicates that the corresponding fringe and sample planes are far from being coincident. The fringes in this case are complicated by the torsional and rotational motion of the specimen during loading to high values of L_1 and ΔL. This explains why it is difficult to photographically record them as described above. The most perfect camera, the human eye, with its excellent depth of focus, does not experience any of these recording problems of fringes exhibiting extensive parallax with the sample plane. Most of the torsional and rotational motions could be eliminated by redesigning the loading apparatus, especially the oversize clevises.

The first general observation of the reconstructed holograms is that masking tape inadvertently left on a specimen (A-6) and subsequently baked had no effect on the fringe pattern due to the metal surface beneath it. Thus, flaws should be detectable under painted or coated surfaces as long as the coating follows the motion of the surface beneath it.

The second observation is that for any specific specimen thickness, there was a threshold load for the detectivity of the different size cracks, with the largest (size 3) cracks generally appearing first at the lowest threshold value, followed by crack size 2, and then by crack size 1 at the highest threshold value.

These load threshold values changed from specimen to specimen in a range characteristic of the variation in crack dimensions and surface preparation.

More defects were observed for the B specimens than for the A specimens at the same net tensile level.

Table 4.3-1 shows that all size 3 cracks were detected for all specimens of both thicknesses, except those of specimen A-21. The load threshold for detecting the size 3 crack in specimen A-21 was greater than 35.8 MN/m^2 (5200 psi) which corresponds to the total load value of 4650 N (1045 lb) or the crack was nonexistent.

All size 2 cracks were detected in all the B specimens. Only about one-half of the size 2 cracks in the A specimens were detected. The threshold for detection of size 2 cracks in the A specimens was between 71.7 MN/m^2 (10,400 psi) and 83.4 MN/m^2 (12,100 psi), corresponding to the total load values of 11.1 kN (2500 lb) and 12.9 kN (2900 lb), respectively.

The threshold ΔL for size 3 cracks in the B specimens was at least greater than 1780 N (400 lb). The threshold value for size 1 cracks in specimen B-23 is approximately 33.5 MN/m^2 (4860 psi) corresponding to a total load value of 19.5 kN (4375 lb),

although for specimen B-24 the two size 1 cracks could not be detected even at 85.5 MN/m^2 (12,400 psi) corresponding to a load value of 50.7 kN (11,400 lb).

The threshold value for the size 2 cracks in the B specimens was somewhere between 2.76 MN/m^2 (400 psi) and 33.5 MN/m^2 (4860 psi), probably closer to the first value.

Only one size 1 crack was detected for the A specimens: 1_2 of specimen A-24 at L_1 = 10.14 kN (2280 lb) and ΔL = 1265 N (-285 lb). Although this defect was not recorded in the corresponding Polaroid print, it was detectable on direct viewing of the corresponding reconstructed hologram using the large parallax of the fringe pattern to good advantage. This indicated a threshold value for detectivity of crack size 1_2 in specimen A-24 of approximately 60.3 MN/m^2 (8750 psi), corresponding to a total load value of 8.88 kN (1995 lb). Crack 1_2 was easier to view directly through the reconstructed hologram than crack 2, because crack size 1_2 is larger than crack size 2.

Also, cracks of a specific size were more easily detected at higher load values providing the load values were above the detectivity threshold of that particular crack size. Specimen A-12, for example, showed the ease of detectivity increased with increasing load value for both crack sizes 3_1 and 3_2. In P70, crack size 3_2 was barely discernible; in P71, 3_2 was clearly observable with 3_1 just appearing; and finally in P72 both 3_2 and 3_1 were clearly observable. Since crack size 3_2 is slightly greater than that of 3_1, this technique was sensitive in detecting small changes in crack sizes.

Attempts at observing fringe anomalies by viewing two of the samples on their reverse side proved negative. This indicated that the cracks involved were sufficiently distant from the back side that with the loading levels used this technique was not sensitive enough to record them.

4.4 EVALUATION OF MARTIN MARIETTA SPECIMENS

One hundred and eighteen specimens were received from Martin Marietta Corporation for evaluation by radiographic, ultrasonic, eddy current, and penetrant methods. The NDT techniques used were those developed during the optimization phase and described in Appendix I with the exception of the ultrasonic technique, which was altered in one respect only. Because of the different methods of producing the variable surface finishes, it was possible to scan the Martin specimens at a higher sensitivity. The difference in the surface finish was in the direction of lay. The surface lay of the Martin specimens was oriented 90 degrees from the Convair Aerospace specimens. During the ultrasonic optimization phase, some small flaw signals from specimens with coarse surface finish had to be rejected in order to also reject the noise encountered near the centerline of the specimen where the machining lay was perpendicular to the ultrasonic beam entry. In the ultrasonic evaluation of the Martin specimens, this rejection was not necessary and higher sensitivity was allowed.

The Martin specimens had flaws on both sides requiring all techniques except radiography to be performed twice for each specimen. New data recording sheets were prepared to show indications on two sides. At the start of this evaluation it was noted that several flaws found did not correlate with the master data sheets provided by Martin Marietta. Consequently a visual examination of each specimen was performed. Since the flaws were visible, a new master sheet was made up showing all flaws found with their location from specimen center line and their visual length. Figure 4.4-1 is an example. All NDT results were then entered onto these new masters. The results of the entire evaluation of the Martin specimens are shown in Table 4.4-1. A summary of those results is shown in Table 4.4-2. Figure 4.4-2 shows the grid location system used in Table 4.4-1.

NAS 9-12326

SPECIMEN DATA SHEET

MMC SPECIMENS

IDENTIFICATION M-5

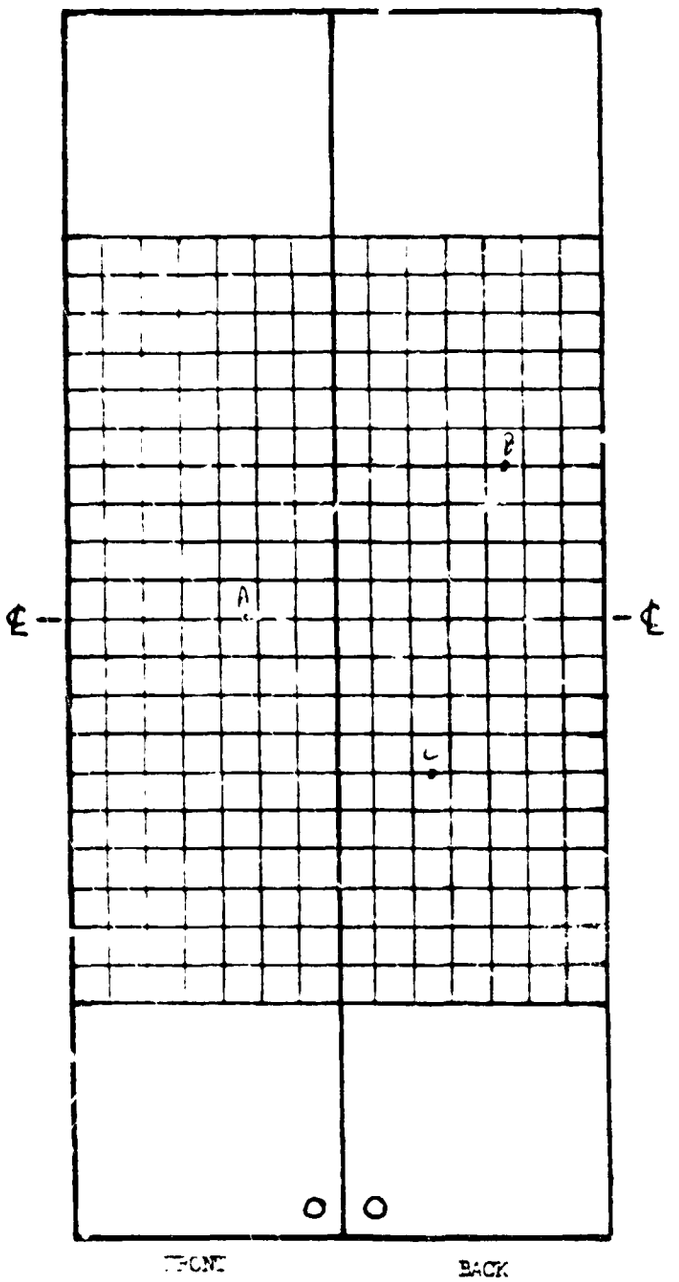

FLAW	LENGTH	CASE	METHOD P	U	X	E
A	24c		✓	✓	✓	✓
B	2c		✓	✓	✓	✓
C	2c		✓	✓	✓	✓

Figure 4.4-1. Sample of Specimen Data Sheet

Table 4.4-1. Complete Results of Martin Specimen Evaluation

Specimen No.	Flaw No.	Side	Location (2)	Length		Method (1)				Specimen No.	Flaw No.	Side	Location (2)	Length		Method (1)			
				in.	mm	P	U	X	E					in.	mm	P	U	X	E
M-1	1	F	D-4	0.265	6.73	X	X	X	X	M-16	3	B	O,P-3,4	0.250	6.35	X	X	X	X
	2	F	P-4	0.265	6.73	X	X		X	M-17	1	F	C-4	0.025	0.64	X	X		
	3	B	J-4	0.240	6.10	X	X		X		2	F	C,D-4	0.025	0.64	X	X		
M-2	1	B	C,D-5,6	0.020	0.51	X	X				3	B	F,G-6	0.035	0.89	X	X		
	2	B	I,J-2,3	0.050	1.27	X	X		X		4	B	H-2,3	0.025	0.64	X	X		
	3	B	K,L-2,3	0.080	2.03	X	X		X		5	B	N,O-3	0.065	1.65	X	X		X
	4	B	M,--	0.065	1.65	X	X		X	M-18	1	F	G-2,3	0.060	1.52	X	X		
M-3	1	F	G-4	0.080	2.03	X	X		X		2	F	H-3,4	0.040	1.14		X		
	2	F	K-4	0.060	1.52	X	X		X		3	B	F,G-6	0.035	1.89	X	X		
	3	B	I-2,3	0.080	2.03	X	X		X		4	B	H-6	0.090	2.29	X	X	X	X
	4	B	M-3	0.080	2.03	X	X		X		5	B	J-5	0.075	1.90	X	X		X
M-4	1	F	Above A-4	0.055	1.40		X			M-19	1	F	F,G-2	0.070	1.78	X	X	X	X
	2	F	Above A-3	0.065	1.65		X				2	F	I,J-3	0.070	1.78	X	X		X
	3	F	B-3,4	0.020	0.51		X				3	F	K,L-3	0.080	2.03	X	X	X	X
	4	F	M-2	0.080	2.03	X	X		X		4	F	N,O-2	0.080	2.03	X	X	X	X
	5	F	N-4,5	0.035	0.89		X				5	B	H-5	0.085	2.16	X	X	X	
	6	F	M-7	0.030	0.76		X				6	B	M-6	0.030	0.76	X	X		
	7	F	Q-7	0.015	0.38		X			M-20	1	B	I,J-5,6	0.045	1.14	X	X		X
	8	F	Q,R-7	0.015	0.38		X				2	B	L,M-5	0.085	2.16	X	X	X	X
M-5	1	F	J,K-5	0.240	6.10	X	X	X	X		3	B	M,N-3	0.030	0.76	X	X		X
	2	B	F,G-3	0.260	6.61	X	X	X	X	M-21	1	F	K,L-5	0.110	2.79	X	X	X	X
	3	B	N,O-5	0.265	6.73	X	X	X	X		2	B	Q-5	0.030	0.76	X	X		
M-6	1	F	F,G-5,6	0.150	3.81	X	X	X	X	M-22	1	F	F,G-4	0.240	6.10	X	X	X	X
	2	F	K,L-5,6	0.110	2.79	X	X	X	X		2	F	N,O-5	0.290	7.37	X	X	X	X
1 & 4 same	3	F	L,M-3	0.070	1.90	X	X		X		3	B	J,K-5	0.260	6.61	X	X	X	X
	4	B	F,G-6	0.265	6.73	X	X	X	X	M-25	1	B	F,G-5,6	0.035	0.89		X		
M-7	1	B	G-6	0.015	0.38	X	X				2	B	K-6	0.030	0.76		X		
	2	B	G-5	0.015	0.38	X	X				3	B	L,M-4	0.080	2.03	X	X	X	X
	3	B	I,J-5	0.060	1.52	X	X		X	M-26	1	B	L,M-5	0.070	1.78	X	X	X	X
	4	B	L,M-5	0.070	1.78	X	X		X	M-27	1	F	A-3,4	0.030	0.76	X	X		
	5	B	M,N-3	0.085	2.16	X	X		X		2	F	A,B-3	0.030	0.76	X	X		
M-8	1	F	J,K-5	0.340	8.64	X	X	X	X		3	F	B-3	0.040	1.14	X	X		
	2	B	F,G-5,6	0.275	6.99	X	X	X	X		4	F	B-2	0.020	0.51	X	X		
	3	B	N,O-4	0.260	6.61	X	X	X	X		5	F	C-3	0.015	0.38	X			
M-9	1	B	N,O-4,5	0.075	1.90	X	X		X		6	F	B,C-4	0.030	0.76	X	X		
M-11	1	B	F,G-4	0.025	0.64		X				7	F	D-4	0.035	0.89	X	X		
	2	B	I-4	0.065	1.65	X	X		X		8	F	K-3	0.015	0.38	X	X		
	3	B	L-4	0.070	1.78	X	X		X		9	F	N-5	0.080	2.03	X	X	X	X
	4	B	N,O-4	0.050	1.27	X	X		X		10	F	Q-4	0.015	0.38		X		
M-12	1	B	N,O-2	0.075	1.90	X	X	X	X		11	F	R-4,5	0.015	0.38		X		
M-13	1	B	L-3	0.075	1.90	X	X		X		12	B	F,G-6	0.045	1.14	X	X		X
M-14	1	B	F-4	0.070	1.78	X	X	X	X	M-28	1	F	D-3	0.015	0.38	X	X		
	2	B	N-2	0.075	1.90	X	X		X		2	F	C-4	0.045	1.14	X	X		
M-15	1	F	I-5,6	0.055	1.40	X	X	X	X		3	F	C,D-4	0.040	1.02	X	X		
	2	F	L,M-2,3	0.070	1.78	X	X		X		4	F	C,D-5	0.020	0.51	X	X		
	3	B	J-4	0.060	1.52	X	X		X		5	F	H-7	0.030	0.76	X	X		
M-16	1	B	G,H-3,4	0.255	6.48	X	X	X	X		6	F	J-3	0.050	1.27	X	X		X
	2	B	K,L-3	0.255	6.48	X	X	X	X		7	F	J-5	0.020	0.51	X	X		

Table 4.4-1. Complete Results of Martin Specimen Evaluation, Contd

Specimen No.	Flaw No.	Side	Location (2)	Length		Method (1)			
				in.	mm	P	U	X	E
M-28	8	F	I,J-6	0.020	0.51	X	X		
	9	F	J-6	0.035	0.89	X	X		
	10	F	K-5	0.030	0.76	X	X		
	11	F	L-3	0.030	0.76	X	X		
	12	F	L-5	0.045	1.14	X	X		X
	13	F	K,L-6	0.030	0.76	X	X		
	14	F	L-5	0.025	0.64	X	X		
	15	F	M-3,4	0.030	0.76	X	X		
	16	F	N,O-5,6	0.015	0.38	X	X		
	17	F	I-3,4	0.020	0.51	X	X		
	18	F	M-1	0.020	0.51	X	X		
	19	F	M-1,2	0.020	0.51	X	X		
	20	B	N,O-4	0.080	2.03	X	X		X
	21	F	L-5	0.015	0.38		X		
	22	F	L-5	0.015	0.38		X		
	23	F	K-6,7	0.015	0.38		X		
	24	F	K,L-7	0.020	0.51		X		
	25	F	K,L-7	0.020	0.51		X		
M-29	1	B	J,K-4	0.250	6.35	X	X	X	X
M-30	1	B	H-5,6	0.075	1.90	X	X		X
	2	B	I-5	0.070	1.78	X	X		X
	3	B	O-5	0.060	1.52	X	X		
M-31	1	B	F-[illegible]	0.250	6.35	X	X	X	X
	2	B	N-2	0.250	6.35	X	X		X
M-32	1	F	H,I-2	0.090	2.29	X	X		X
	2	F	M-6	0.075	1.90	X	X		X
	3	B	G,H-5,6	0.050	1.27	X	X		
	4	B	I-4	0.045	1.14	X	X		
	5	B	K,L-3	0.055	1.40	X	X		X
	6	B	M-2	0.065	1.65	X	X		X
M-33	1	F	I-5,6	0.070	1.78	X	X		X
	2	F	M-4,5	0.065	1.65	X	X		X
	3	B	F,G-3,4	0.040	1.02				X
	4	B	J,K-2,3	0.060	1.52	X	X		X
	5	B	N,O-2	0.080	2.03	X	X	X	X
M-34	1	B	E,F-5,6	0.060	1.52	X	X		X
	2	B	G-3,4	0.075	1.90	X	X	X	X
	3	B	J-2,3	0.060	1.52		X		X
	4	B	M-5,6	0.055	1.40	X	X	X	X
M-35	1	B	L-4	0.270	6.86	X	X	X	X
M-36	1	F	N,O-5	0.150	3.81	X	X	X	X
	2	B	H-2	0.050	1.27	X	X		
	3	B	I-5,6	0.070	1.78	X	X	X	X
M-39	1	F	G,H-4	0.100	2.54	X	X	X	X
	2	F	J-2	0.070	1.78	X	X		X
	3	F	K-4	0.070	1.78	X	X		X
	4	F	L,M-2,3	0.070	1.78	X	X		X

Specimen No.	Flaw No.	Side	Location (2)	Length		Method (1)			
				in.	mm	P	U	X	E
M-39	5	[illegible]	N-6	0.065	1.65	X	X		X
	6	[illegible]	O,P-4	0.100	2.54	X	X		X
M-40	1	F	J-4	0.080	2.03	X	X	X	X
	2	F	O,P-5	0.030	0.76	X	X		
	3	B	A-2	0.050	1.27	X	X		
	4	B	A,B-3	0.080	2.03	X	X		
	5	B	B-3	0.050	1.27	X	X		
	6	B	B,C-3,4	0.030	0.76	X	X		
	7	B	B-2,3	0.040	1.02	X	X		X
	8	B	C-4	0.015	0.38	X	X		
	9	B	C-3	0.035	0.89	X	X		
	10	B	C,D-4	0.020	0.51	X	X		
	11	B	D-3	0.015	0.38	X	X		
	12	B	F-2	0.050	1.27	X	X		X
	13	B	G-2	0.025	0.64	X	X		
	14	B	H-4	0.030	0.76	X	X		
	15	B	H-4	0.040	1.02	X	X		X
	16	B	H-2	0.025	0.64	X	X		
	17	B	H,I-2	0.030	0.76	X	X		
	18	B	I-2,3	0.120	3.05	X	X	X	X
	19	B	I-3	0.020	0.51	X	X		
	20	B	I-2	0.015	0.38	X	X		
	21	B	J-4	0.030	0.76	X	X		
	22	B	J-4	0.025	0.64	X	X		
	23	B	J-4	0.035	0.89	X	X		
	24	B	E-1,2	0.030	0.76		X		
	25	B	G,H-6,7	0.040	1.02		X		
	26	F	B,C-2,3	0.020	0.51		X		
M-41	1	B	F-4,5	0.090	2.29	X	X		X
	2	B	J-3	0.015	0.38				
	3	B	N-4	0.015	0.38				
M-42	1	F	H,I-2,3	0.095	2.41	X	X	X	X
	2	F	M-5,6	0.055	1.40	X	X		
	3	B	J,K-4	0.040	1.02	X	X	X	
M-43	1	B	G,H-3,4	0.265	6.73	X	X	X	X
	2	B	K,L-3	0.260	6.61	X	X	X	X
	3	B	O,P-3,4	0.245	6.22	X	X	X	X
M-44	1	F	I,J-3	0.070	1.78	X	X		X
	2	F	N-4	0.050	1.27	X	X	X	
	3	B	F,G-6	0.080	2.03	X	X		X
	4	B	K-5,6	0.030	0.76		X		
M-45	1	F	G,H-2,3	0.070	1.78	X	X		[illegible]
	2	F	L-4	0.060	1.52	X	X		X
	3	F	N-4,5	0.100	2.54	X	X		X
	4	B	F,G-3,4	0.050	1.27	X	X		
	5	B	I-4,5	0.050	1.27	X	X		
	6	B	N,O-5	0.040	1.02				

Table 4.4-1. Complete Results of Martin Specimen Evaluation, Contd

Specimen No.	Flaw No.	Side	Location (2)	Length		Method (1)			
				in.	mm	P	U	X	E
M-46	1	F	J,K-3	0.235	5.97	X	X	X	X
	2	B	F,G-5	0.260	6.61	X	X	X	X
	3	B	N,O-5	0.265	6.73	X	X	X	X
M-47	1	F	J-6	0.060	1.52	X	X		X
	2	F	M-5	0.045	1.14	X	X		X
	3	B	F,G-4	0.045	1.14		X		X
	4	B	K-3	0.085	2.16	X	X		X
	5	B	N,O-2	0.060	1.52	X	X		X
M-48	1	B	H,I-2	0.080	2.03	X	X		X
	2	B	I-5,6	0.075	1.90	X	X	X	X
	3	B	K-2,3	0.045	1.14	X	X		X
	4	B	L,M-6	0.045	1.14	X	X		X
M-49	1	B	G-3,4	0.270	6.86	X	X	X	X
	2	B	O-4,5	0.275	6.99	X	X		X
M-50	1	F	M,N-3,4	0.085	2.16	X	X		X
M-52	1	B	F,G-5,6	0.095	2.41	X	X	X	X
	2	B	H,I-2,3	0.045	1.14	X	X		
	3	B	I,J-4	0.050	1.27	X	X		
	4	B	K-2,3	0.040	1.02	X	X		
	5	B	L-5,6	0.080	2.03	X	X		X
M-53	1	B	J-3	0.030	0.76	X	X		
	2	B	L,M-6	0.075	1.90	X	X	X	X
M-54	1	F	B,C-3,4	0.100	2.54	X	X		X
	2	F	D,E-3,4	0.150	3.81	X	X	X	X
	3	F	D,E-4	0.050	1.27	X	X		
	4	B	F,G-6	0.100	2.54	X	X	X	X
	5	B	N,O-2	0.040	1.03	X	X		X
	6	F	O,A-3	0.020	0.51		X		
	7	F	A-3	0.020	0.51		X		
	8	F	B-3	0.015	0.38		X		
	9	F	C-3	0.020	0.51		X		
	10	F	D-3	0.025	0.64		X		
	11	F	F,G-2,3	0.015	0.38				
	12	F	H-2	0.020	0.51		X		
	13	F	I-3	0.025	0.64		X		
	14	F	L-2	0.060	1.52		X		X
	15	B	C,D-4	0.030	0.76		X		
	16	B	I,J-4	0.020	0.51				
M-55	1	F	M-6	0.060	1.52	X	X	X	X
	2	B	C-3	0.030	0.76	X	X		
	3	B	F,G-6	0.035	0.89	X	X		X
	4	B	G-4	0.035	0.89	X	X		
	5	B	N,O-3	0.075	1.90	X	X		X
M-56	1	F	J,K-4	0.335	8.51	X	X		X
	2	B	F,G-4	0.330	8.38	X	X		X
	3	B	N,O-4	0.300	7.62	X	X		X
M-57	1	B	G-3,4	0.315	8.00	X	X		X
M-57	2	B	J,K-2,3	0.330	8.38	X	X		X
	3	B	O-3	0.300	7.62	X	X	X	X
M-58	1	B	F-3,4	0.300	7.62	X	X	X	X
	2	B	J-2,3	0.320	8.13	X	X		X
	3	B	N-3	0.320	8.13	X	X		X
M-59	1	F	K-3	0.295	7.15	X	X		X
	2	B	G-5	0.315	8.00	X	X		X
	3	B	O-4	0.335	8.51	X	X	X	X
M-60	1	F	K-3	0.485	12.31	X	X		X
	2	B	G-5	0.510	12.95	X	X	X	X
	3	B	N,O-5	0.515	13.08	X	X	X	X
M-61	1	F	J-4	0.575	14.60	X	X	X	X
M-62	1	F	J-3	0.535	13.59	X	X	X	X
M-63	1	B	F,G-4	0.325	8.25	X	X		X
	2	B	J,K-5	0.330	8.38	X	X	X	X
	3	B	N,O-3,4	0.340	8.64	X	X	X	X
M-64	1	B	H-6	0.155	3.91	X	X		X
	2	B	J,K-2	0.115	2.92	X	X		X
M-65	1	B	J,K-5,6	0.130	3.30	X	X		X
M-66	1	F	J,K-4	0.495	12.56	X	X	X	X
	2	B	F-3	0.510	12.95	X	X	X	X
	3	B	N,O-3	0.460	11.68	X	X	X	X
M-68	1	B	F-4,5	0.035	0.89	X	X		
	2	B	G-2	0.085	2.16	X	X		X
	3	B	I-5	0.125	3.18	X	X		X
	4	B	K-6	0.065	1.65	X	X		X
	5	B	L-2	0.060	1.52		X		X
	6	B	N-5	0.035	0.89		X		
M-69	1	B	F-3	0.075	1.90	X	X		X
	2	B	H-3	0.065	1.65	X	X		X
	3	B	J-3	0.115	2.92	X	X		X
	4	B	K-6	0.090	2.29	X	X		X
	5	B	L-3	0.130	3.30	X	X		X
	6	B	M-3	0.065	1.65	X	X		X
M-70	1	F	J-4	0.105	2.67	X	X		X
	2	B	F,G-2,3	0.115	2.92	X	X		X
	3	B	N-6	0.075	1.90	X	X		X
M-71	1	B	F-4	0.505	12.82	X	X		X
	2	B	N-6	0.495	12.56	X	X	X	X
M-72	1	B	F,G-3	0.520	13.21	X	X	X	X
	2	B	J,K-3	0.560	14.22	X	X		X
	3	B	N,O-3	0.485	12.31	X	X		X
M-73	1	F	L-4	0.155	3.91	X	X		X
	2	B	G-3	0.070	1.78	X	X		X
	3	B	I-2,3	0.070	1.78	X	X		X
	4	B	M-2	0.035	0.89		X		
	5	F	J-5	0.045	1.14		X		

Table 4.4-1. Complete Results of Martin Specimen Evaluation, Contd

Specimen No.	Flaw No.	Side	Location (2)	Length		Method (1)			
				in.	mm	P	U	X	E
M-74	1	F	H-5	0.055	1.40	X	X		X
	2	F	I, J-4, 5	0.145	3.68	X	X		X
	3	F	K, L-3, 4	0.105	2.67	X	X		X
	4	F	M-3	0.130	3.30	X	X		X
	5	F	N, O-5, 6	0.495	12.56	X	X	X	X
	6	F	F, G-2, 3	0.035	0.89		X		
M-75	1	B	F-2, 3	0.320	8.13	X	X		X
	2	B	N-5, 6	0.325	8.25	X	X		X
M-76	1	B	J, K-5, 6	0.485	12.31	X	X	X	X
M-77	1	B	L-3	0.185	4.70	X	X		X
	2	B	N-3	0.050	1.27		X		
	3	F	H-5	0.018	0.46				
M-78	1	B	F-4	0.475	12.06	X	X	X	X
	2	B	N-5	0.260	6.61	X	X		X
M-79	1	B	I-5, 6	0.130	3.30	X	X		X
	2	B	L-2	0.290	7.37	X	X	X	X
M-80	1	B	F-4	0.120	3.05	X	X		X
	2	B	I-4	0.125	3.18	X	X		X
	3	B	N-3, 4	0.135	3.43	X	X		X
M-81	1	B	G-2	0.135	3.43	X	X		X
	2	B	H-5	0.090	2.29	X	X		X
	3	B	J-3	0.100	2.54	X	X		X
	4	B	N-6	0.075	1.90	X	X		X
M-84	1	B	G-4	0.080	2.03	X	X		X
	2	B	H, I-2, 3	0.135	3.43	X	X		X
	3	B	J-6	0.050	1.27	X	X		X
	4	B	K, L-6	0.105	2.67		X		X
	5	B	M-5	0.050	1.52		X		X
	6	B	O-3	0.035	0.89		X		
M-85	1	F	A, B-5	0.095	2.41	X	X		
	2	F	M-3	0.155	3.91	X	X		X
	3	B	F, G-5	0.145	3.68	X	X		X
M-86	1	B	F, G-3, 4	0.130	3.30	X	X		X
	2	B	J-5, 6	0.065	1.65	X	X		X
	3	B	J-2	0.080	2.03	X	X		X
	4	B	L-4, 5	0.095	2.41	X	X		X
	5	B	N-5	0.105	2.67	X	X		X
	6	B	A-2	0.030	0.76		X		
M-87	1	B	F, G-5, 6	0.715	18.16	X	X	X	X
	2	B	N, O-5, 6	0.560	14.22	X	X	X	X
M-88	1	B	F-23	0.310	7.87	X	X		X
	2	B	J-3	0.325	8.25	X	X		X
M-90	1	B	J, K-4	0.500	12.69	X	X	X	X
M-91	1	F	J-5, 6	0.500	12.69	X	X	X	X
M-92	1	F	F, G-4	0.300	7.62	X	X		X
	2	F	N, O-5	0.300	7.62	X	X		X
	3	B	J, K-3	0.290	7.37	X	X		X

Specimen No.	Flaw No.	Side	Location (2)	Length		Method (1)			
				in.	mm	P	U	X	E
M-93	1	F	J-4	0.485	12.31	X	X	X	X
	2	B	F-3	0.600	15.24	X	X	X	X
	3	B	N-4	0.535	13.59	X	X	X	X
M-94	1	B	G-4	0.155	3.91	X	X		X
	2	B	I-4	0.145	3.68	X	X		X
	3	B	K, L-2, 3	0.070	1.78	X	X		X
	4	B	N-4	0.100	2.54	X	X		X
M-95	1	B	F-6	0.125	3.18	X	X		X
	2	B	H-6	0.100	2.54	X	X		X
	3	B	J-4	0.100	2.52	X	X	X	X
	4	B	L-2	0.055	1.40		X		X
	5	B	M-6	0.035	0.89		X		
	6	B	N-2	0.035	0.89		X		X
M-96	1	B	F, G-6	0.395	10.03	X	X	X	X
	2	B	J, K-3	0.350	8.89	X	X		X
	3	B	N, O-5, 6	0.320	8.13	X	X		X
M-97	1	B	K-4	0.150	3.81	X	X		X
M-100	1	B	G-5, 6	0.330	8.38	X	X		X
	2	B	J, K-4, 5	0.325	8.25	X	X		X
	3	B	O-3	0.340	8.64	X	X		X
M-101	1	B	F, G-4, 5	0.050	1.27	X	X		X
	2	B	H, I-5, 6	0.090	2.29	X	X		X
	3	B	J-2, 3	0.090	2.29	X	X		X
	4	B	K, L-5, 6	0.085	2.16	X	X		X
	5	B	L, M-2	0.130	3.30	X	X		X
	6	B	N, O-5	0.070	1.78	X	X		X
M-102	1	B	H-3	0.130	3.30	X	X		X
	2	B	M-5	0.125	3.18		X		X
M-103	1	F	H, I-2, 3	0.070	1.78	X	X		X
	2	B	J, K-4	0.140	3.56	X	X		X
	3	F	L, M-5, 6	0.020	0.51		X		
M-104	1	F	J-5	0.510	12.95	X	X	X	X
	2	B	F-4	0.970	24.64	X	X	X	X
M-105	1	F	J-4	0.465	11.81	X	X	X	X
	2	B	F, G-4	0.490	12.44	X	X	X	X
	3	B	N-5	0.545	13.84	X	X	X	X
M-106	1	F	J, K-2	0.305	7.75	X	X		X
	2	B	F, G-5, 6	0.335	8.51	X	X		X
	3	B	N, O-5, 6	0.315	8.00	X	X		X
M-107	1	B	J-4	0.505	12.82	X	X	X	X
	2	B	N-2, 3	0.340	8.64	X	X		X
M-108	1	B	F-4	0.070	1.78	X	X		X
	2	B	J-6	0.085	2.16	X	X		X
	3	B	M-4	0.130	3.30	[illegible]			X
	4	B	J-2	0.060	1.52	[illegible]			X
M-109	1	F	H, I-2, 3	0.055	1.40	[illegible]	X		X
	2	B	F, G-5, 6	0.060	1.52	X	X		X

Table 4.4-1. Complete Results of Martin Specimen Evaluation, Contd

Specimen No.	Flaw No.	Side	Location (2)	Length		Method (1)				Specimen No.	Flaw No.	Side	Location (2)	Length		Method (1)			
				in.	mm	P	U	X	E					in.	mm	P	U	X	E
M-109	3	B	J,K-5,6	0.145	3.68	X	X		X	M-114	1	B	F,G-6	0.345	8.76	X	X	X	X
	4	B	N,O-5,6	0.075	1.90	X	X		X	M-116	1	B	G-6	0.125	3.18	X	X		X
	5	B	G,H-1,2	0.110	2.79		X		X		2	B	J-4	0.115	2.92	X	X		X
M-110	1	B	F,G-5	0.185	4.70	X	X		X		3	B	L-6	0.075	1.90	X	X		X
	2	B	H-3,4	0.220	5.68	X	X	X	X		4	B	O-6	0.055	1.40	X	X		X
	3	B	K,L-5,6	0.070	1.78	X	X		X		5	B	H-2	0.045	1.02		X		X
	4	B	M,N-2	0.080	2.03	X	X		X		6	B	N-2	0.045	1.14		X		X
M-111	1	B	E,F-2,3	0.095	2.41	X	X		X	M-117	1	F	D-2,3	0.105	2.67	X	X		X
	2	B	F,G-5,6	0.170	4.32	X	X		X		2	F	H,I-3	0.170	4.32	X	X		X
M-112	1	B	J,K-4	0.505	12.82	X	X	X	X		3	F	L-2,3	0.110	2.79	X	X		X
	2	B	N,O-2	0.525	13.33	X	X	X	X		4	B	F-6	0.135	3.43	X	X		X
M-113	1	B	F,G-3	0.525	13.33	X	X	X	X		5	B	N-5,6	0.070	1.78		X		X
	2	B	J,K-5,6	0.495	12.56	X	X	X	X	M-118	1	B	H-6	0.105	2.67	X	X		X
	3	B	N,O-5,6	0.505	12.82	X	X	X	X		2	B	M-4	0.135	3.43	X	X		X

(1) P = penetrant, U = ultrasonic, R = radiography and E = eddy current
(2) Determined from the grid system shown in Figure 4.4-2.

Table 4.4-2. Summary of Results from Evaluation of Martin Specimens

Method for Specimens 1 to 55	Flaw Length Interval (measured)		Flaws Found/ Total Flaws
	mm	in.	
Ultrasonic	0.38 - 1.65	0.015 - 0.065	135/142
	1.78 - 3.81	0.070 - 0.150	64/64
	5.97 - 8.64	0.235 - 0.340	28/28
Radiography	0.38 - 1.65	0.015 - 0.065	5/142
	1.78 - 3.81	0.070 - 0.150	27/64
	5.97 - 8.64	0.235 - 0.340	24/28
Eddy Current	0.38 - 1.65	0.015 - 0.065	38/142
	1.78 - 3.81	0.070 - 0.150	61/64
	5.97 - 8.64	0.235 - 0.340	28/28
Penetrant	0.38 - 1.65	0.015 - 0.065	103/142
	1.78 - 3.81	0.070 - 0.150	64/64
	5.97 - 8.64	0.235 - 0.340	28/28
Specimens 56 to 118			
Ultrasonic	0.46 - 2.41	0.018 - 0.095	53/54
	2.54 - 4.70	0.100 - 0.185	49/49
	5.68 -10.03	0.220 - 0.395	36/36
	11.68 -24.64	0.460 - 0.970	34/34
Radiography	0.46 - 2.41	0.018 - 0.095	0/54
	2.54 - 4.70	0.100 - 0.185	1/49
	5.68 -10.03	0.220 - 0.395	8/36
	11.68 -24.64	0.460 - 0.970	30/34
Eddy Current	0.46 - 2.41	0.018 - 0.95	43/54
	2.54 - 4.70	0.100 - 0.185	49/49
	5.68 -10.03	0.220 - 0.395	36/36
	11.68 -24.64	0.460 - 0.970	34/34
Penetrant	0.46 - 2.41	0.018 - 0.095	36/54
	2.54 - 4.70	0.100 - 0.185	49/49
	5.68 -10.03	0.220 - 0.395	36/36
	11.68 -24.64	0.460 - 0.970	34/34

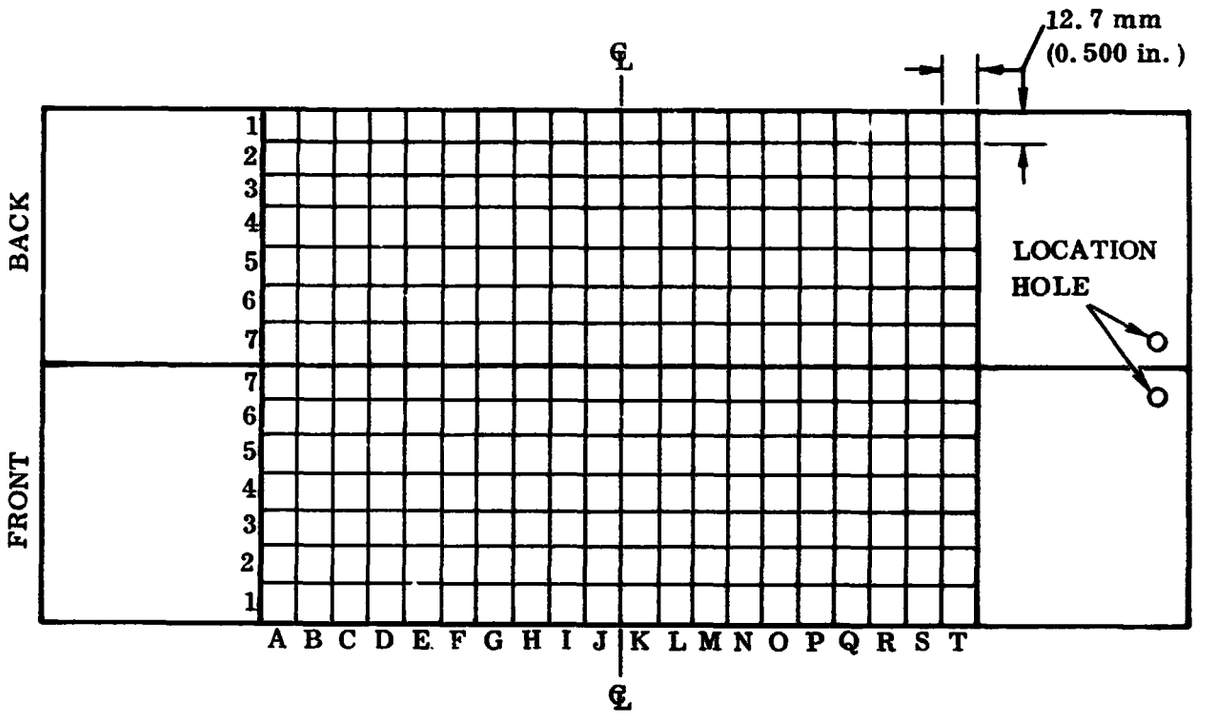

Figure 4.4-2. Grid System for Martin Specimens

4.5 PROOF TEST AND METALLOGRAPHIC EXAMINATION

All specimens were tension loaded to a stress level of 293.02 MN/m^2 (42,500 lb/in^2) prior to the final NDT evaluation. This level corresponds to 85 percent of tensile yield strength. Both prior to and following proof test, the crack width or crack opening dimensions were measured on four different flaws. The measurements were obtained from photomicrographs taken at the same locations along the cracks before and after proof testing. The surfaces were prepared by polishing and etching. Table 4.5-1 presents the results of the examination and Figure 4.5-1 shows the photomicrographs, all of which were originally magnified 500 times.

Table 4.5-1. Measurement of Crack Opening Displacement

Specimen and Crack Identification	Pre-Proof Opening (1)		Post-Proof Opening (2)		Displacement		Other Verified Crack Dimensions			
	μm	μ in.	μm	μ in.	μm	μ in.	a (mm)	a (in.)	2c (mm)	2c (in.)
A-8-2	1.02	40	1.57	62	0.56	22	0.56	0.022	2.03	0.080
A-14-3	1.60	63	17.40	685	15.80	622	1.12	0.044	8.69	0.342
B-8-2	2.79	110	7.63	300	4.83	190	2.90	0.114	13.21	0.520
B-14-3	4.06	160	8.90	350	4.83	190	2.74	0.108	13.26	0.522

(1) Average of three to five measurements made at typical locations.
(2) Measurements made at same locations as pre-proof.

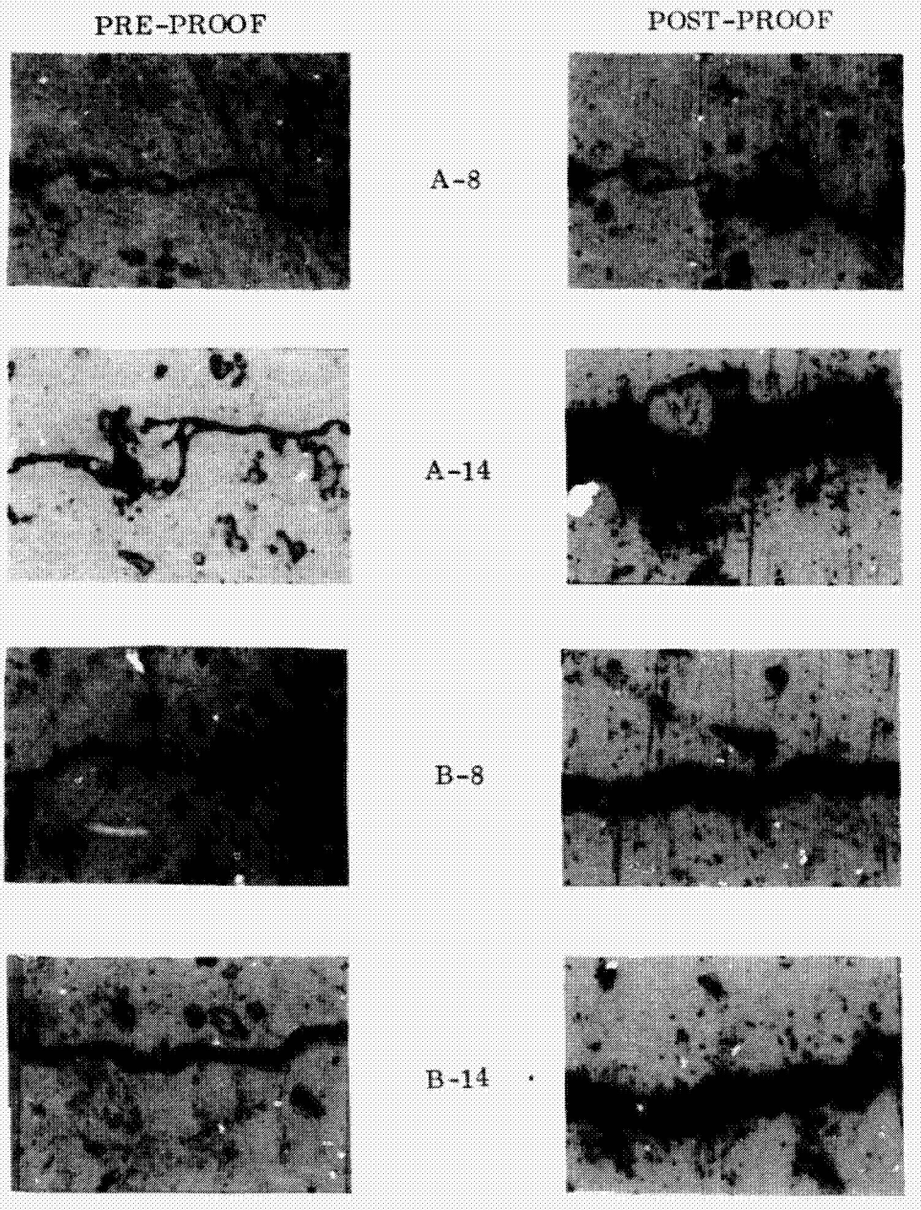

Figure 4.5-1. Photomicrographs of Crack Openings Before and After Proof Testing

4.6 ACOUSTIC EMISSION MONITORING DURING PROOF LOADING

Twelve specimens of each thickness were monitored for acoustic emissions during proof loading. The technique is described in Section 3.5. The master sensors (M1 and M2) were randomly located within the specimen test area and the slaves located as near the end doublers as possible. The sensor locations were recorded on data sheets and the specimens were proof loaded. Table 4.6-1 summarizes the results of the data and data analysis. The arrival time difference from M1 to M2 was determined from oscilloscope photos and a Δ distance was calculated from a measured velocity of 5.95 mm/μs. The Δ distance measured was determined from the sensor locations recorded on the data sheets. The error between the calculated and measured distance was determined and found to range up to 4.0 mm (0.16 in.). The errors resulted from either inaccurate measurements of velocity and Δt from the oscillographs or inaccuracies in measurement of sensor locations. In five specimens, no emissions were observed. Two of these had no flaws and the remaining three had no flaw growth during proof loading.

Table 4.6-1. Summary of Acoustic Emission Monitoring Results During Proof Loading

Specimen No.	Events Photographed	Triggered by M1	Triggered by M2	Δt μs	Δd Calculated mm	Δd Calculated in.	Δd Measured mm	Δd Measured in.	Error mm	Error in.	Crack Detected	Σ AE	Remarks
A-2	1	X		2.9	17.4	0.69	16.8	0.66	+0.6	0.02		2	
A-3	1	X		4.3	25.6	1.01	25.4	1.00	+0.2	0.01	3	2	
	2	X		4.4	26.2	1.04	25.4	1.00	+0.8	0.03	3		
A-4	1		X	5.4	32.1	1.26	33.0	1.30	-0.9	0.04	3	28	
	2		X	5.5	32.7	1.29	33.0	1.30	-0.3	0.01	3		
	3		X	5.5	32.7	1.29	33.0	1.30	-0.3	0.01	3		
	4	X		9.4	55.9	2.20	57.1	2.25	+1.2	0.05	2		
A-5	1	X		7.5	44.6	1.76	45.7	1.80	-1.1	0.04	3	14	
	2	X		7.5	44.6	1.76	45.7	1.80	-1.1	0.04	3		
A-8	1		X	3.4	20.2	0.80	20.3	0.80	-0.1	0.004	2	11	
A-10	1	X	X	0	0		0		0		3	3	
A-13	-	-	-	-	-		-		-		-	0	No flaws in specimen
A-14	-	-	-	-	-		-		-		-	0	No apparent flaw growth
A-15	1		X	8.2	48.8	1.92	50.8	2.00	-2.0	0.08	1	11	
	2		X	8.3	49.3	1.93	50.8	2.00	-1.5	0.06	1		
A-20	1	X		10.0	59.5	2.34	63.5	2.50	-4.0	0.16	2	1	
A-21	1		X	5.4	32.1	1.26	33.0	1.30	-0.9	0.04	3	1	
A-23	1	X		6.2	36.9	1.45	38.1	1.50	-1.2	0.05	3	19	
	2	X		6.1	36.6	1.43	38.1	1.50	-1.5	0.06	3		
	3	X		6.1	36.6	1.43	38.1	1.50	-1.5	0.06	3		
B-2	1	X		4.2	25.0	0.98	25.4	1.00	-0.4	0.02	1	5	
B-3	1	X		3.1	18.4	0.72	19.0	0.75	-0.6	0.03	1	86	
	2	X		3.0	17.8	0.70	19.0	0.75	-1.2	0.05	1		
	3	X		3.2	19.0	0.75	19.0	0.75	0		1		
	4	X		3.0	17.8	0.70	19.0	0.75	-1.2	0.05	1		
	5	X		2.9	17.2	0.68	19.0	0.75	-1.8	0.07	1		
B-5	-	-	-	-	-		-		-		-	0	No apparent flaw growth
B-7	-	-	-	-	-		-		-		-	0	No flaws in specimen
B-9	1		X	5.1	30.3	1.19	27.9	1.10	+2.4	0.09	2	15	
	2		X	5.2	30.9	1.22	27.9	1.10	+3.0	0.12	2		
	3		X	5.3	31.5	1.24	27.9	1.10	+3.6	0.14	2		
B-10	-	-	-	-	-		-		-		-	0	No apparent flaw growth
B-14	1		X	4.0	23.8	0.94	25.4	1.00	-1.6	0.06	3	20	
B-15	1		X	6.1	36.6	1.43	38.1	1.50	-1.5	0.06	2	14	
B-17	1	X		3.6	21.4	0.84	22.9	0.90	-1.5	0.06	1	9	
	2		X	8.0	47.6	1.87	45.8	1.80	+1.8	0.07	2_2		
	3	X		[illegible]	22.0	0.87	22.9	0.90	-0.9	0.03	2_1		
B-20	1		X	[illegible]	36.9	1.45	38.1	1.50	-1.2	0.05	2	16	
	2		X	6.0	35.7	1.40	38.1	1.50	-2.4	0.10	2		
B-21	1		X	7.5	44.6	1.76	45.7	1.80	-1.1	0.04	3	1	
B-23	1		X	8.1	48.2	1.90	50.8	2.00	-2.6	0.10	2	7	
	2	X		7.4	44.0	1.73	45.7	1.80	-1.7	0.07	3		
	3	X		7.4	44.0	1.7[illegible]	45.7	1.80	-1.7	0.07	3		
	4		X	8.2	48.8	1.92	50.8	2.00	-2.0	0.08	2		

4.7 POST-PROOF TEST EVALUATION

All 48 specimens were evaluated following proof test to study the effects on the detectability of flaws due to proof loading. The same methods and techniques used in prior evaluations and as shown in Appendix I were performed. The data resulting from this evaluation are shown in Table 4.7-1.

Table 4.7-1. Summary of Results from Third NDT Evaluation

Method	A Flaw Size	Flaws Detected/Total Flaws				Totals
		Original Surface Finish Groups				
		A	B	C	D	
Ultrasonic	1	2/5	4/5	0/5	2/4	8/19
	2	5/5	4/4	4/4	5/5	18/18
	3	5/5	5/5	5/5	5/5	20/20
Radiography	1	0/5	1/5	0/5	0/4	1/19
	2	0/5	0/4	1/4	0/5	1/18
	3	5/5	5/5	5/5	5/5	20/20
Eddy Current	1	3/5	5/5	4/5	3/4	15/19
	2	5/5	4/4	4/4	5/5	18/18
	3	5/5	5/5	5/5	5/5	20/20
Penetrant	1	2/5	3/5	0/5	3/4	8/19
	2	4/5	4/4	2/4	3/5	13/18
	3	5/5	5/5	5/5	5/5	20/20
	B Flaw Size					
Ultrasonic	1	5/5	5/5	5/5	4/5	19/20
	2	5/5	5/5	5/5	5/5	20/20
	3	5/5	5/5	5/5	5/5	20/20
Radiography	1	0/5	0/5	0/5	0/5	0/20
	2	5/5	5/5	4/5	5/5	19/20
	3	5/5	5/5	4/5	5/5	19/20
Eddy Current	1	5/5	5/5	5/5	5/5	20/20
	2	5/5	5/5	5/5	5/5	20/20
	3	5/5	5/5	5/5	5/5	20/20
Penetrant	1	5/5	5/5	5/5	5/5	20/20
	2	5/5	5/5	5/5	5/5	20/20
	3	5/5	5/5	5/5	5/5	20/20

By the replication method. 0/3 size 1, 0/1 size 2, and 4/4 size 3 flaws were detected on the thin specimens; 4/4 size 1, 5/5 size 2, and 4/4 size 3 flaws were detected on the thicker specimens. In this evaluation no false indications were noted.

SECTION 5

CORRELATION OF DATA

5.1 FRACTURE SURFACE ANALYSIS

The specimens were failed through all known crack sites by saw cutting near the crack tips and bending to failure. The exposed fracture surface of each crack was photographed at carefully controlled magnifications of 5× or 10×, depending upon the size of the crack. A polarizer was used to enhance the contrast between the fatigue crack and the surrounding fracture surface. Measurements of the crack sizes were made from photographs; area determinations were made using a planimeter. Examples of the photographs are shown in Figure 5.1-1.

5.2 ACOUSTIC EMISSION MONITORING DURING FAILURE LOADING

During tensile loading to failure, the specimens that had been monitored during proof loading were again monitored. The techniques used were as described in Section 3.6 and the monitoring data taken during proof loading are shown in Section 4.6. Table 5.2-1 presents a summary of the acoustic emission data and the failure loads. Figure 5.2-1 shows the acoustic emission counts as a function of stress for Specimens A-8, B-8, and B-5. These specimens were chosen because A-8 and B-8 contained single flaws and produced typical data. In Specimen B-5, failure was forced through crack 2_1 by reducing the net section adjacent to 2_1.

The data collected during this task were not particularly conclusive. It had been hoped that there would be more correlation between flaw size, growth rate, and emission counts. Much more amplification than the 40 dB available would have been required to improve correlation.

5.3 DATA ANALYSIS

During the evaluations, the assumption that the desired flaw sizes had been obtained was a necessary one and the data were grouped accordingly. However, post-mortem flaw size measurement showed the extent of variability from the desired sizes and suggested different grouping of flaws for analysis purposes. Table 5.3-1 summarizes the variations obtained versus those desired.

$\overline{a}$ and $\overline{2c}$ are the average flaw sizes; R_a and R_{2c} are the ranges of a and 2c. As shown in the table, the averages of a and 2c are nearly those desired for size 1 flaws in A specimens and reasonably close for size 3 flaws in A specimens and size 3 flaws

A-12-1$_1$

B-16-1

A-18-2$_2$

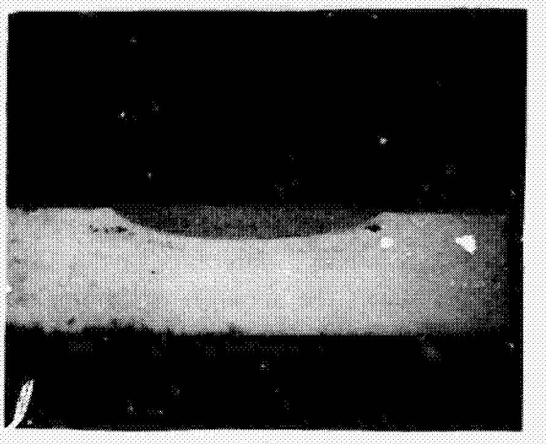

B-5-2$_1$

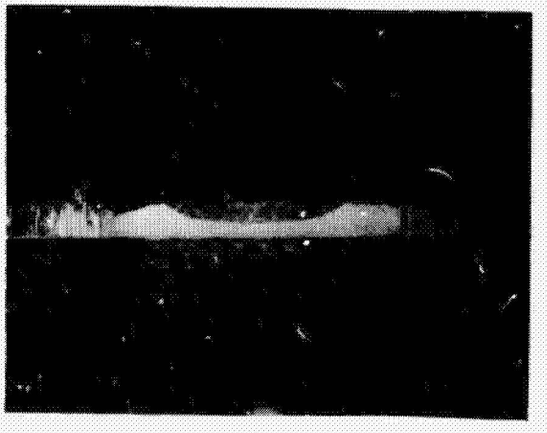

A-16-3$_1$

B-18-3$_2$

Figure 5.1-1. Typical Photomacrographs of Fatigue Crack Fracture Surfaces

Table 5.2-1. Acoustic Emission and Failure Stress Data

Specimen No.	Crack Failure	Net Stress at Failure		Monitor Sensitivity		ΣAE	Remarks
		MN/m^2	lbf/in^2	Master mV	Slave mV	(counts)	
A-2	-	-	-	40	10	-	Failed at grip
A-3	3	411.02	59,613	40	10	139	
A-4	3	338.51	49,097	40	10	16	
A-5	3	423.15	61,372	40	10	9	
A-8	2	334.97	48,584	40	10	18	
A-10	3	411.23	59,644	30	10	2	
A-13	-	-	-	-	-	-	No flaws
A-14	3	378.85	54,948	30	10	6	
A-15	1	374.87	54,370	30	10	16	
A-20	2	417.99	60,625	30	10	10	
A-21	3	405.97	58,881	30	10	6	
A-23	3	397.01	57,582	30	10	11	
B-2	1	392.44	56,918	30	10	53	
B-3	3	365.74	53,046	30	10	92	
B-5	2_1	419.00	60,771	30	10	35	
B-7	-	-	-	-	-	-	No flaws
B-8	2	379.95	55,107	30	10	85	
B-10	3	387.35	56,180	30	10	61	
B-14	3	406.61	58,974	30	10	250	
B-15	2	427.17	61,956	30	10	22	
B-17	2_1	388.82	56,393	30	10	42	
B-20	2	398.45	57,790	30	10	14	
B-21	3	389.88	56,548	30	10	26	
B-23	3	424.48	61,565	30	10	50	

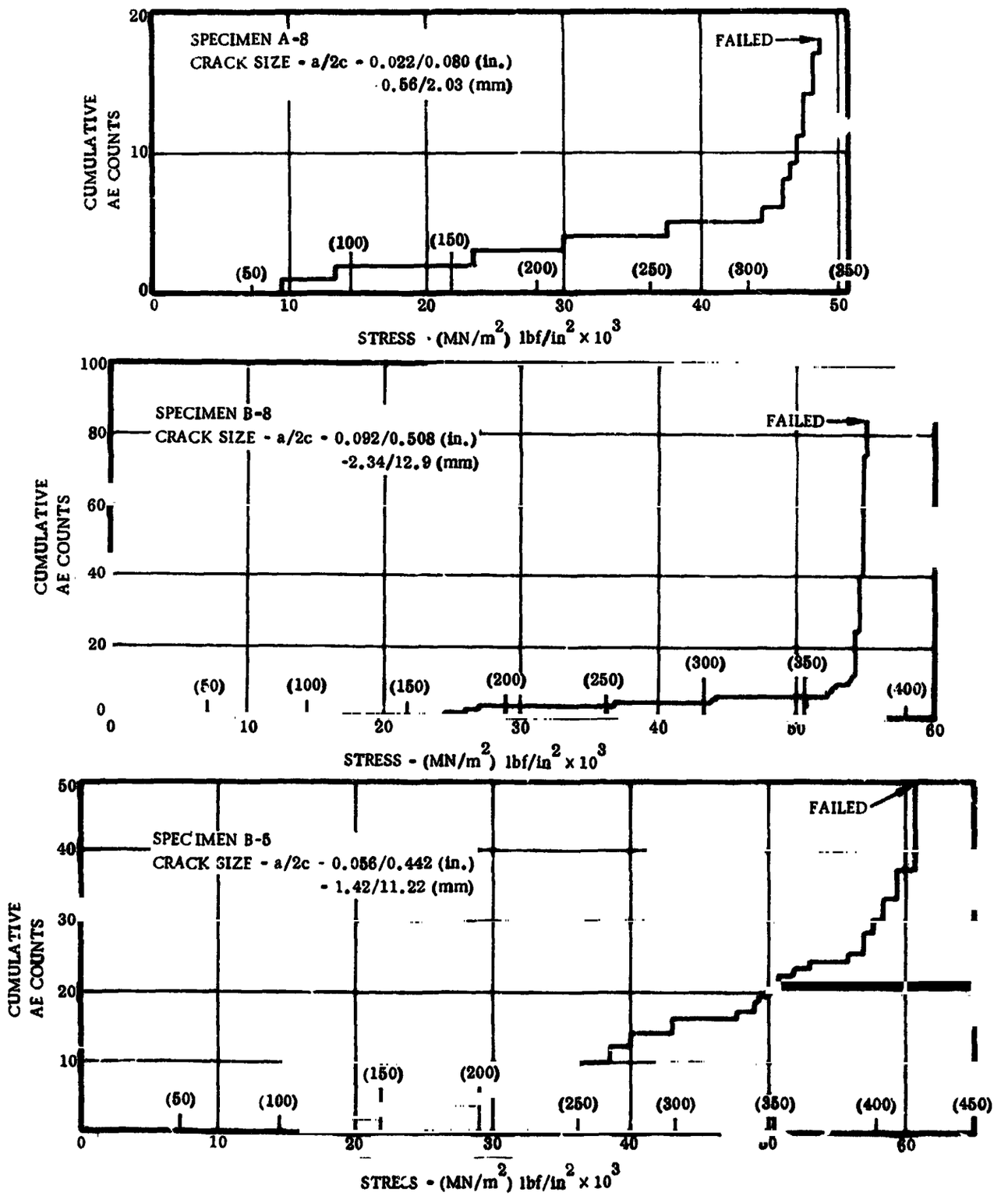

Figure 5.2-1. Acoustic Emission Data

Table 5.3-1. Average and Desired Dimensions

Flaw Size	Desired Geometry				Attained Geometry							
	a		2c		$\bar{a}$		R_a		$\overline{2c}$		R_{2c}	
	in.	mm	in.	mm	in.	mm	in.	mm	in.	mm	in.	mm
A-1	0.015	0.38	0.060	1.52	0.016	0.41	0.005	0.13	0.063	1.60	0.022	0.56
							0.029	0.74			0.104	2.64
A-2	0.030	0.76	0.060	1.52	0.026	0.66	0.019	0.48	0.091	2.31	0.069	1.75
							0.040	1.02			0.129	3.28
A-3	0.030	0.76	0.300	7.62	0.040	1.02	0.012	0.30	0.336	8.54	0.197	5.00
							0.054	1.37			0.384	9.75
B-1	0.056	1.42	0.113	2.88	0.044	1.12	0.027	0.69	0.137	3.48	0.109	2.77
							0.064	1.63			0.190	4.83
B-2	0.045	1.14	0.450	11.42	0.102	2.59	0.054	1.37	0.472	12.00	0.426	10.82
							0.144	3.66			0.520	13.21
B-3	0.113	2.88	0.450	11.42	0.101	2.56	0.088	2.24	0.521	13.23	0.498	12.65
							0.112	2.84			0.550	13.97

in B specimens. The A-2 flaws were of appropriate depth but longer than desired. B-1 flaws were longer but more shallow, and B-2 flaws were substantially deeper than desired.

Within a given thickness, when flaw size parameters were ordered from small to large, a reasonable continuum was apparent. A number of statistical tests were applied to the data to evaluate the effects of surface finish, etching, and proof testing. The results of those tests are summarized in Appendix II.

In the statistical test for assessing the effect of surface finish on the detectability of flaws, sample sizes were small and, in one case, human variables possibly accounted for unexpected results. It had been a purpose of the experimental design to minimize human factors. To this end, the personnel selected to perform the evaluations were only those that would be classified as skilled and experienced. In addition, the same persons who performed tests during the first evaluation also did the testing during subsequent evaluations. It was hoped, therefore, that learning variations and human operational inconsistencies would be suppressed, thereby permitting more reliance on the small-sample statistics. Generally, the statistical results tend to show that this ideal

was successful, except in one instance. The chi-square value obtained from analysis of the penetrant tests on the thick specimens showed significance. This implies that the surface finish did have some effect. The difficult rationalization is that the surface finish of the thin specimens did not produce similar significance. However, upon investigation of the data, it can be seen that the undetected flaws producing the unexpected statistic were in one group of specimens with a nominal surface finish of 3.2 μm (125 μm) average roughness. Upon reexamination of remnants from these specimens, the surface finish was found to have some peculiar characteristics. It is possible that one slightly dull cutter produced some very small tears that did not affect the overall roughness measurement, but did cause sites for residual penetrant entrapment. One log book entry during the original evaluation notes difficulty in interpretation because of excessive background noise. A further contributing factor is the slight over-etching of some of the thin specimens (see Section 4.2). This condition caused a noticeable effect on the washability of the penetrant materials used. The increased background noise undoubtedly reduced the reliability of interpretation as the statistical tests show.

The statistical tests clearly indicate that the detection capability of the nondestructive tests improved following proof test. These and other effects are more clearly shown in Figures 5.3-1 through 5.3-6. Figures 5.3-7 through 5.3-12 show the data combined from all three evaluations.

All data concerning final measured flaw sizes and the outcome of the evaluations are presented in Table 5.3-2.

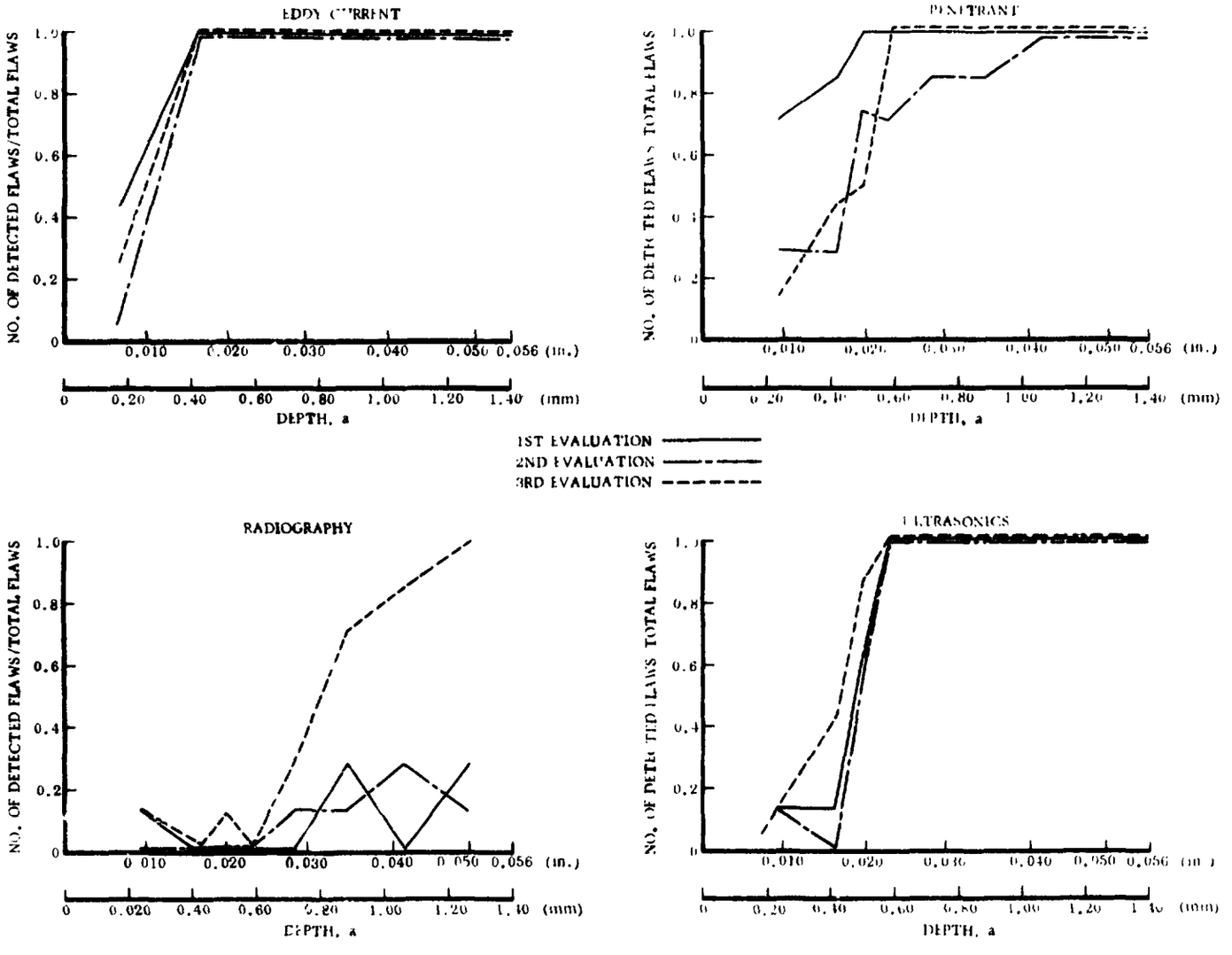

Figure 5.3-1. Proportion as a Function of Depth in Thin Specimens

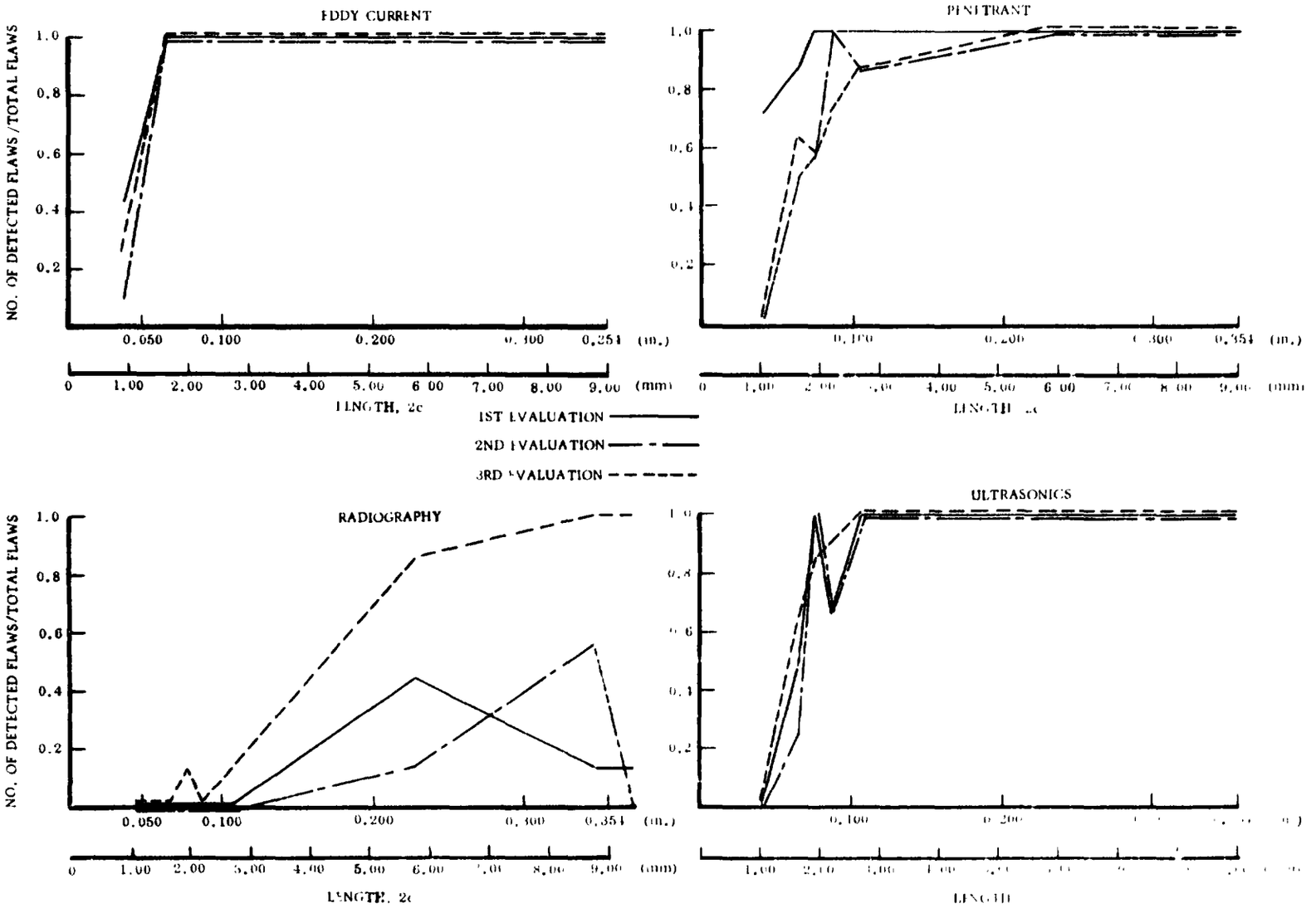

Figure 5.3-2. Proportion as a Function of Length in Thin Specimens

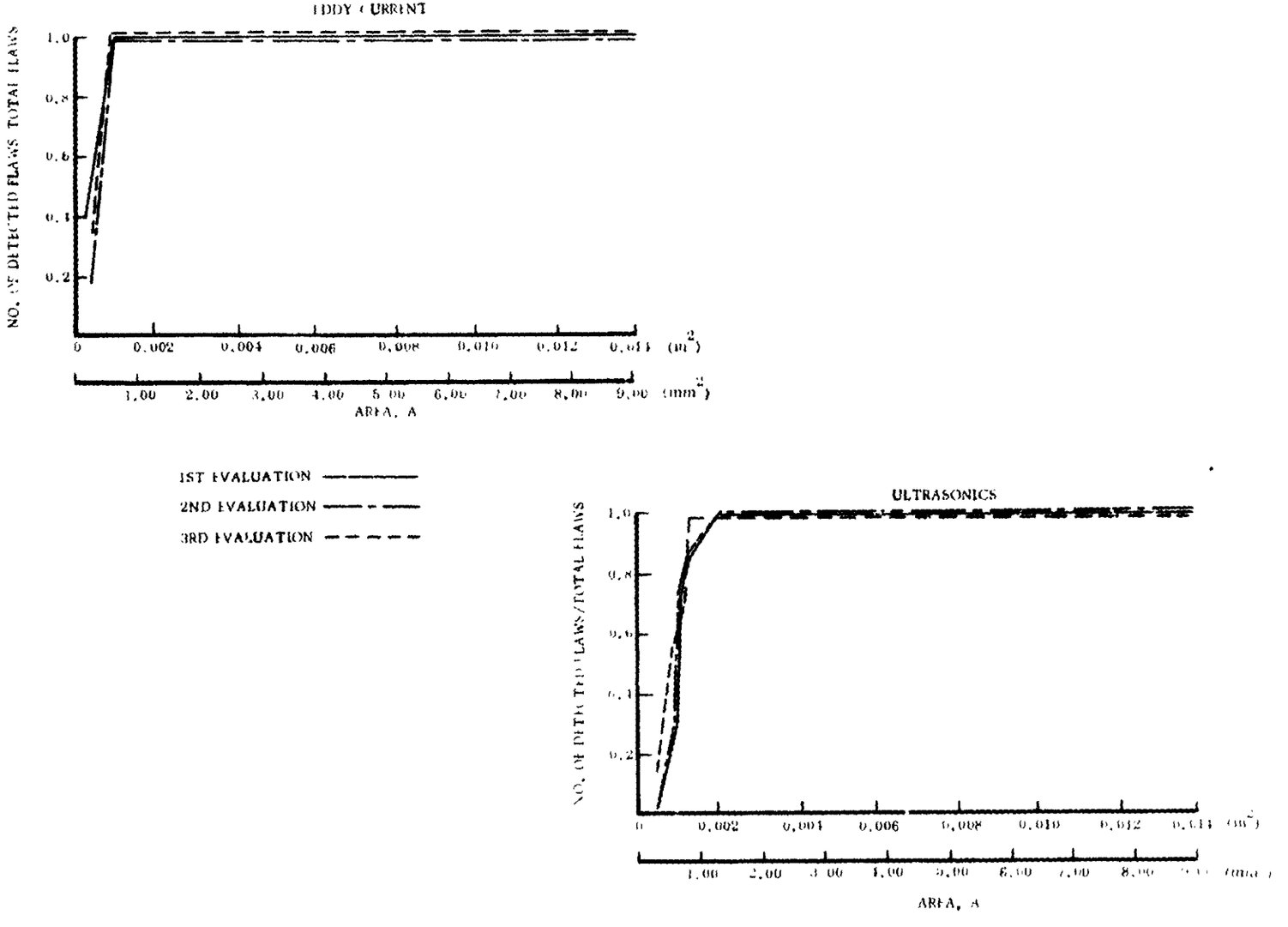

Figure 5.3-3. Proportion as a Function of Area in Thin Specimens

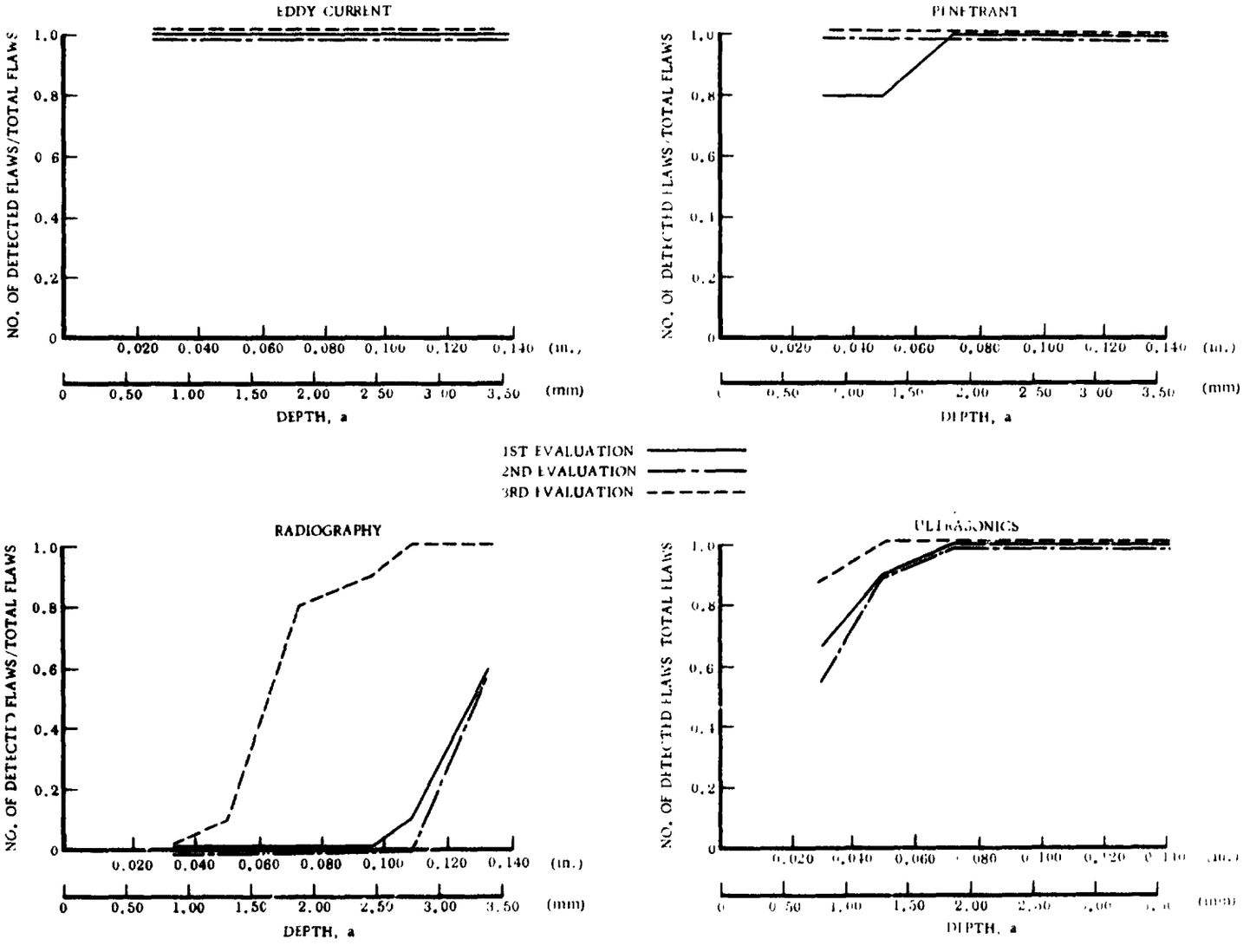

Figure 5.3-4. Proportion as a Function of Depth in Thick Specimens

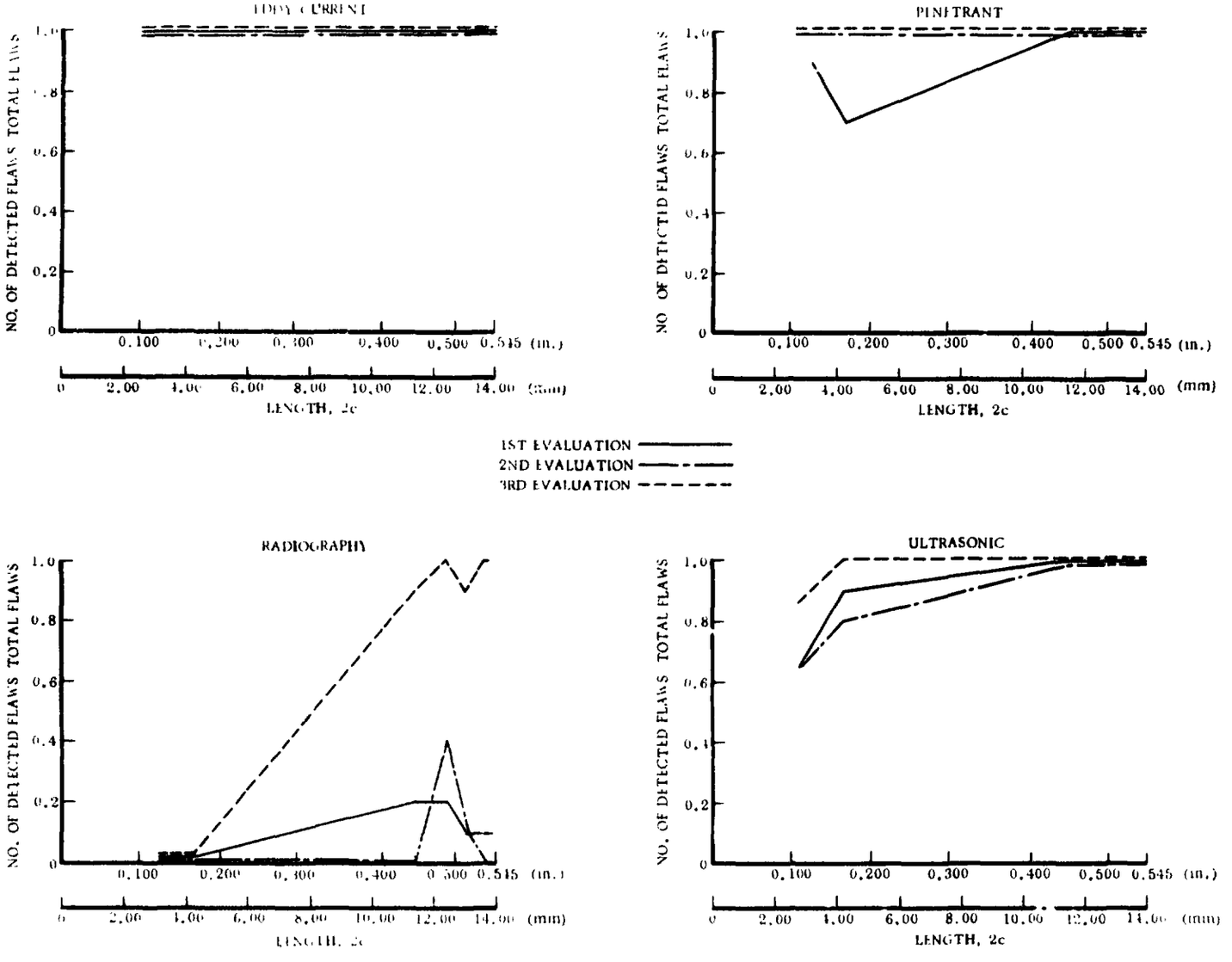

Figure 5.3-5. Proportion as a Function of Length in Thick Specimens

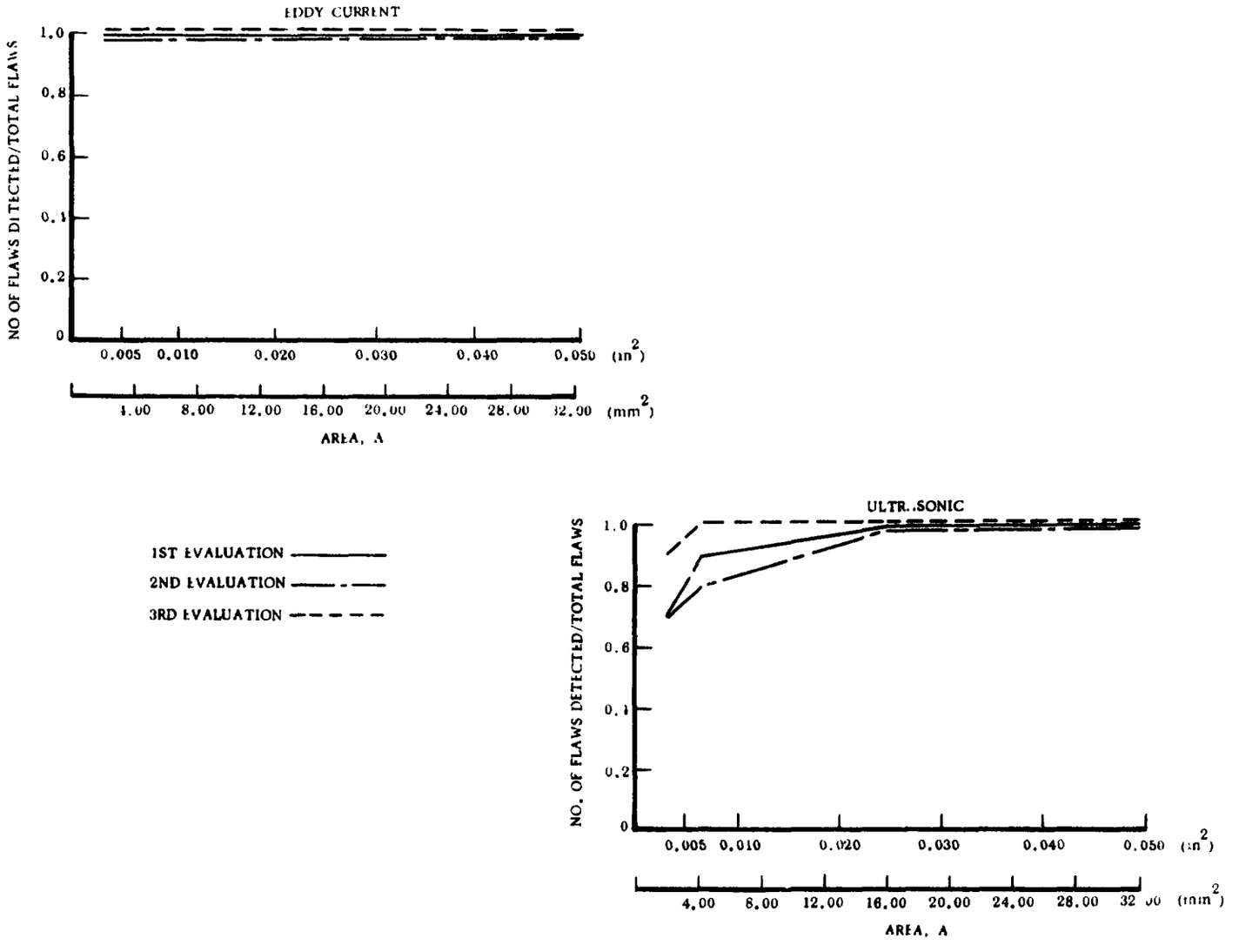

Figure 5.3-6. Proportion as a Function of Area in Thick Specimens

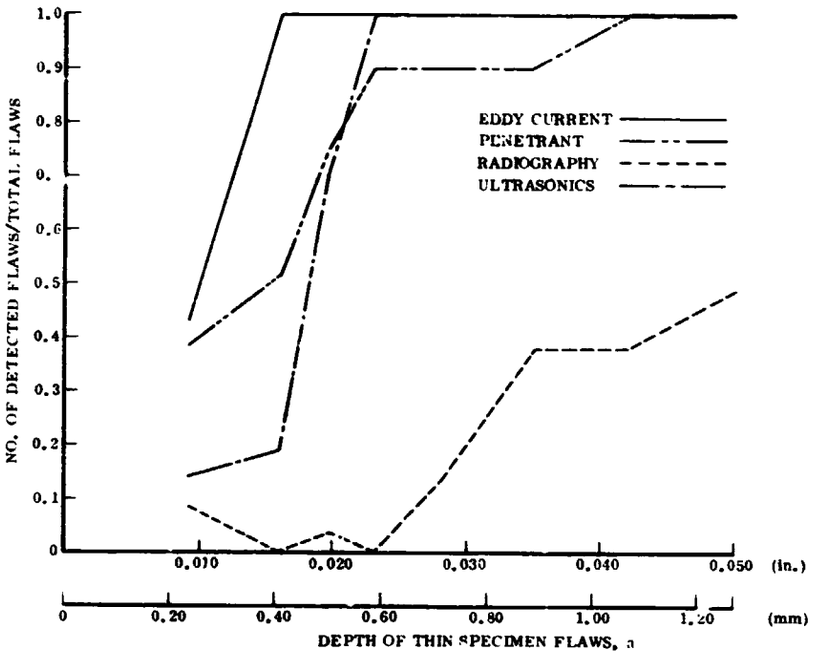

Figure 5.3-7. Proportion as a Function of Depth in Thin Specimens, Combined Data

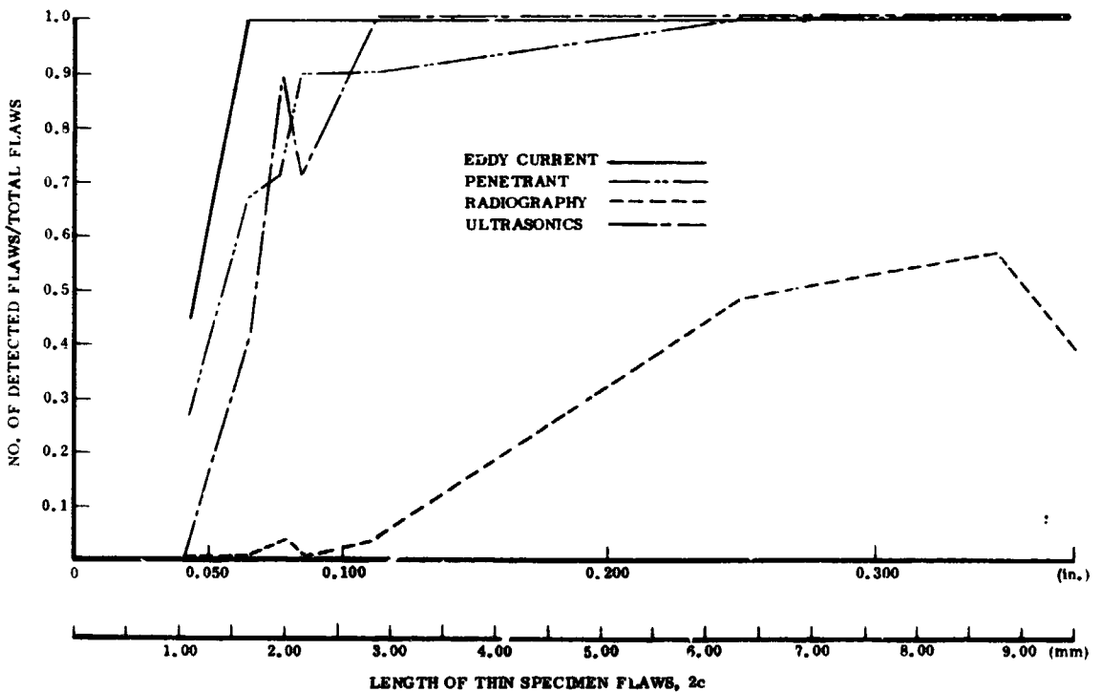

Figure 5.3-8. Proportion as a Function of Length in Thin Specimens, Combined Data

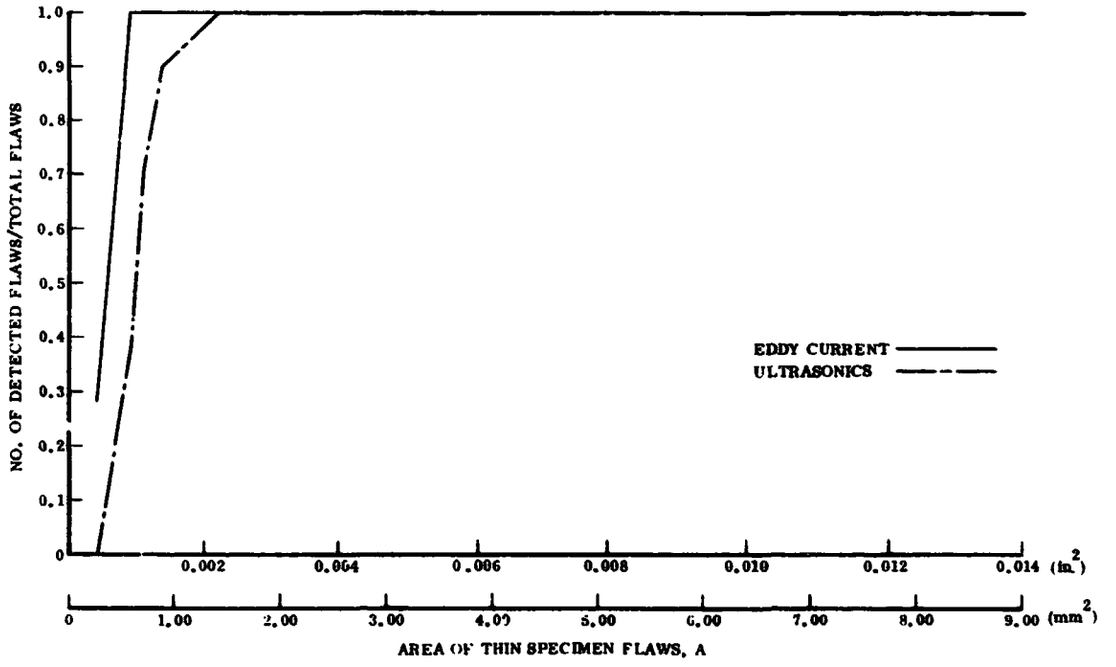

Figure 5.3-9. Proportion as a Function of Area in Thin Specimens, Combined Data

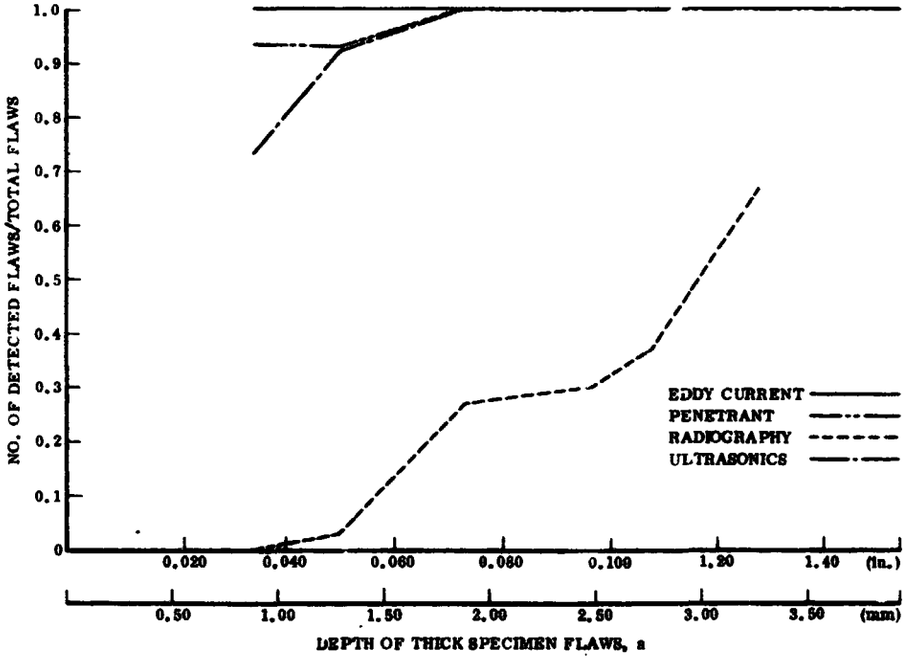

Figure 5.3-10. Proportion as a Function of Depth in Thick Specimens, Combined Data

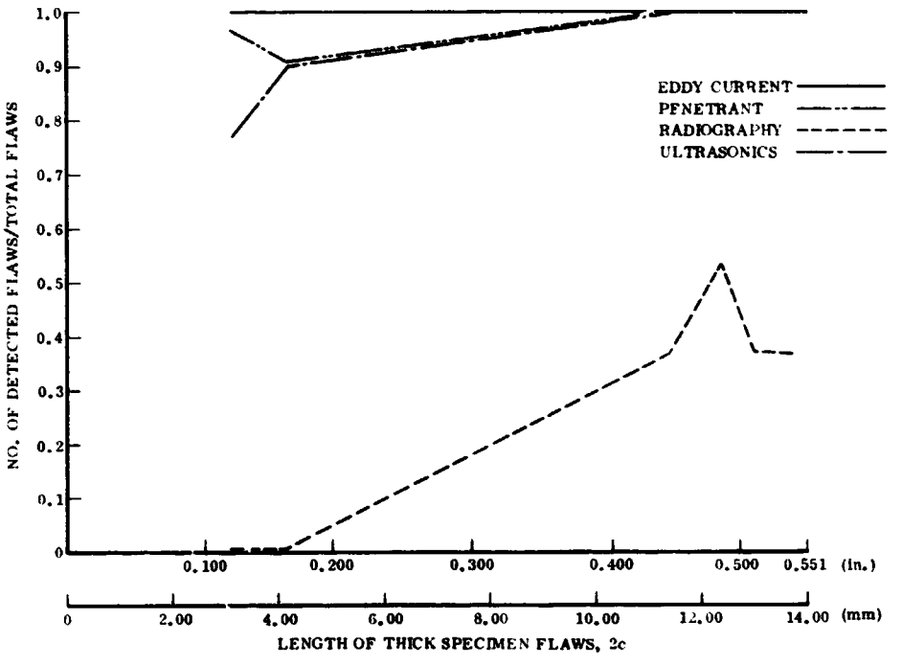

Figure 5.3-11. Proportion as a Function of Length in Thick Specimens, Combined Data

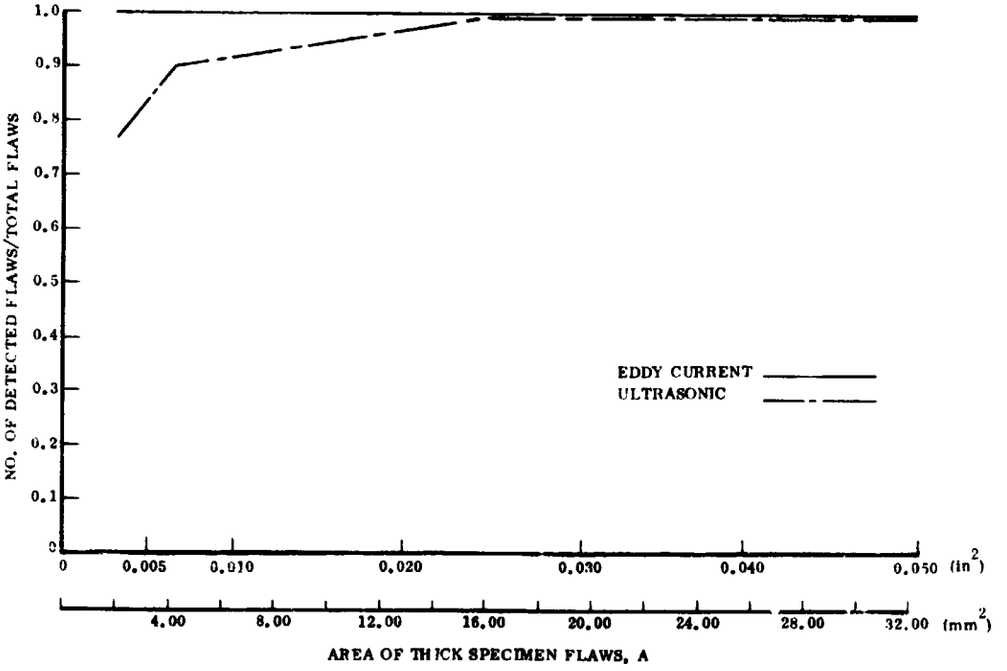

Figure 5.3-12. Proportion as a Function of Area in Thick Specimens, Combined Data

Table 5.3 -2. Master Data Tabulation

Flaw	a (in.)	a (mm)	2c (in.)	2c (mm)	Area (in.)	Area (mm)	a/2c	a/t	1st Evaluation E	P	X	U	2nd Evaluation E	P	X	U	3rd Evaluation E	P	X	U
A-2-1	0.016	0.41	0.068	1.72	0.0008	0.52	0.235	0.278	X	X		X	X	X			X	X		X
A-3-1	0.005	0.13	0.027	0.69	0.0002	0.13	0.185	0.084												
A-3-3	0.036	0.91	0.318	8.06	0.0082	5.93	0.113	0.642	X	X	X	X	X	X		X	X	X	X	X
A-4-1	0.007	0.18	0.022	0.56	0.0003	0.19	0.316	0.118												
A-4-2	0.034	0.86	0.111	2.82	0.0029	1.87	0.306	0.539	X	X		X	X	X		X	X	X		X
A-4-3	0.032	0.81	0.340	8.64	0.0120	7.74	0.094	0.500	X	X		X	X	X	X	X	X	X	X	X
A-5-1	0.021	0.53	0.075	1.91	0.0012	0.77	0.280	0.300	X	X		X	X	X		X	X			X
A-5-2_1	0.027	0.69	0.094	2.39	0.0014	0.90	0.287	0.435	X	X		X	X	X		X	X	X		X
A-5-2_2	0.034	0.61	0.085	2.16	0.0015	0.97	0.282	0.375	X	X		X	X	X		X	X	X		X
A-5-3	0.046	1.17	0.384	9.75	0.0104	6.71	0.119	0.719	X	X		X	X	X		X	X	X	X	X
A-6-1	0.024	0.61	0.067	1.70	0.0010	0.65	0.358	0.380	X	X		X	X			X	X	X		X
A-6-2_1	0.019	0.48	0.081	2.06	0.0012	0.77	0.234	0.292	X	X		X	X			X	X			X
A-6-2_2	0.040	1.02	0.129	3.28	0.0037	2.39	0.310	0.415	X	X		X	X	X		X	X	X		X
A-6-3_1	0.048	1.22	0.370	9.40	0.0185	9.80	0.129	0.727	X	X	X	X	X	X		X	X	X	X	X
A-6-3_2	0.046	1.17	0.370	9.40	0.0108	6.97	0.124	0.676	X	X		X	X	X		X	X	X	X	X
A-8-2	0.022	0.56	0.080	2.03	0.0014	0.90	0.275	0.407	X	X		X	X	X		X	X	X		X
A-9-2	0.024	0.61	0.090	2.29	0.0017	0.16	0.266	0.400	X	X		X	X	X		X	X	X		X
A-9-2_2	0.022	0.56	0.073	1.85	0.0010	0.65	0.127	0.379	X	X		X	X	X		X	X	X		X
A-10-1_1	0.021	0.53	0.078	1.98	0.0012	0.77	0.269	0.350	X	X		X	X	X		X	X	X	X	X
A-10-1_2	0.023	0.58	0.075	1.91	0.0016	1.03	0.306	0.353	X	X		X	X			X	X	X		X
A-10-3	0.046	1.17	0.362	9.19	0.0716	7.46	0.127	0.741	X	X		X	X	X		X	X	X	X	X
A-11-1	0.029	0.74	0.086	2.18	0.0026	1.35	0.337	0.488	X	X		X	X	X		X	X	X		X
A-11-2	0.036	0.91	0.096	2.49	0.0027	1.74	0.367	0.563	X	X		X	X	X		X	X	X		X
A-11-3_1	0.044	1.12	0.362	9.19	0.0160	10.38	0.121	0.637	X	X		X	X	X		X	X	X	X	X
A-11-3_2	0.042	1.07	0.352	8.94	0.0112	7.22	0.119	0.606	X	X		X	X	X	X	X	X	X	X	X
A-12-1_1	0.015	0.38	0.069	1.75	0.0008	0.52	0.217	0.277	X	X			X				X			X
A-12-1_2	0.013	0.33	0.062	1.57	0.0007	0.45	0.209	0.216	X	X							X			X
A-12-2	no flaw produced																			
A-12-3_1	0.036	0.86	0.296	7.52	0.0048	2.97	0.087	0.446	X	X		X	X	X		X	X	X	X	X
A-12-3_2	0.036	0.91	0.340	8.64	0.0080	5.16	0.105	0.500	X	X		X	X	X		X	X	X	X	X
A-14-3	0.044	1.12	0.342	8.69	0.0100	6.45	0.128	0.698	X	X		X	X	X		X	X	X	X	X
A-15-1	0.015	0.38	0.059	1.50	0.0010	0.65	0.254	0.272	X	X			X				X			
A-15-2	no flaw produced																			
A-16-1	0.007	0.18	0.034	0.86	0.0002	0.13	0.205	0.125		X										
A-16-3_1	0.036	0.91	0.290	7.37	0.0080	5.16	0.124	0.600	X	X	X	X	X	X	X	X	X	X	X	X
A-16-3_2	0.034	0.86	0.286	7.32	0.0046	2.97	0.117	0.557	X	X		X	X	X		X	X	X	X	X
A-17-1_1	0.013	0.33	0.064	1.63	0.0005	0.32	0.204	0.206	X	X			X	X			X			
A-17-1_2	0.017	0.43	0.065	1.65	0.0010	0.65	0.261	0.265	X				X				X			
A-17-2_1	0.022	0.56	0.069	1.76	0.0012	0.77	0.317	0.353	X	X		X	X	X		X	X	X		X
A-17-2_2	0.025	0.64	0.096	2.44	0.0015	0.97	0.260	0.400	X	X		X	X	X		X	X	X		X
A-18-1	0.014	0.36	0.055	1.40	0.0010	0.65	0.254	0.232	X	X			X				X			
A-18-2_1	0.036	0.91	0.123	3.12	0.0032	2.06	0.292	0.571	X	X		X	X			X	X		X	X
A-18-2_2	0.026	0.66	0.081	2.06	0.0017	1.10	0.320	0.412	X	X		X	X			X	X			X
A-18-3_1	0.044	1.12	0.326	8.28	0.0112	7.22	0.134	0.676	X	X		X	X	X		X	X	X	X	X
A-18-3_2	0.046	1.17	0.372	9.45	0.0124	8.00	0.123	0.707	X	X		X	X	X		X	X	X	X	X
A-20-2	0.019	0.48	0.085	2.16	0.0011	0.71	0.223	0.351	X	X			X	X			X			X
A-21-1	no flaw produced																			
A-21-3	0.012	0.30	0.197	5.00	0.0015	0.97	0.060	0.250	X	X	X	X	X	X		X	X	X	X	X
A-22-2_1	0.021	0.53	0.069	1.75	0.0011	0.71	0.304	0.323	X	X		X	X	X		X	X	X		X
A-22-2_2	0.029	0.74	0.085	2.16	0.0017	1.10	0.341	0.460	X	X		X	X	X		X	X	X		X
A-22-3	0.054	1.37	0.356	9.04	0.0176	11.35	0.151	0.870	X	X	X	X	X	X	X	X	X	X	X	X
A-23-1_1	0.018	0.46	0.069	1.75	0.0010	0.65	0.260	0.315	X	X			X				X	X		
A-23-1_2	0.008	0.20	0.048	1.22	0.0006	0.39	0.166	0.123	X	X										
A-23-2	0.020	0.51	0.089	2.26	0.0013	0.84	0.224	0.327	X	X			X	X			X	X		X
A-23-3	0.046	1.17	0.372	9.45	0.0128	8.26	0.123	0.621	X	X		X	X	X		X	X	X	X	X
A-24-1_1	0.014	0.36	0.064	1.63	0.0007	0.45	0.218	0.245	X	X			X	X			X	X		X
A-24-1_2	0.021	0.53	0.104	2.64	0.0016	1.03	0.201	0.386	X	X		X	X	X		X	X	X		X
A-24-2	0.021	0.53	0.084	2.13	0.0010	0.65	0.250	0.362	X	X			X	X			X			X
A-24-3_1	0.040	1.02	0.334	8.48	0.0096	6.19	0.119	0.606	X	X		X	X	X		X	X	X	X	X
A-24-3_2	0.042	1.07	0.352	8.94	0.0112	7.22	0.119	0.666	X	X		X	X	X	X	X	X	X	X	X
B-2-1	0.063	1.35	0.145	3.68	0.0084	3.48	0.365	0.238	X	X		X	X	X		X	X	X		X
B-3-1	0.052	1.32	0.144	3.66	0.0055	3.54	0.368	0.236	X	X		X	X	X		X	X	X		X
B-3-3	0.106	2.69	0.526	13.36	0.0380	24.51	0.201	0.481	X	X		X	X	X		X	X	X	X	X
B-4-1	0.030	0.76	0.116	2.96	0.0023	1.48	0.258	0.135	X	X		X	X	X		X	X	X		X
B-4-2	0.128	3.25	0.478	12.14	0.0480	30.96	0.267	0.592	X	X		X	X	X	X	X	X	X	X	X
B-4-3	0.094	2.39	0.510	12.95	0.0352	22.70	0.184	0.425	X	X		X	X	X		X	X	X	X	X
B-5-1	0.036	0.89	0.121	3.07	0.0029	1.87	0.28.	0.167	X	X		X	X	X		X	X	X		X
B-5-2_1	0.056	1.42	0.442	11.23	0.0168	10.84	0.128	0.269	X	X		X	X	X		X	X	X	X	X
B-5-2_2	0.136	3.45	0.482	12.24	0.0488	31.96	0.282	0.618	X	X	X	X	X	X	X	X	X	X	X	X
B-5-3	0.092	2.34	0.506	12.85	0.0320	20.64	0.181	0.412	X	X		X	X	X		X	X	X	X	X
B-6-1	0.034	0.86	0.124	3.15	0.0030	1.94	0.274	0.153	X	X		X	X	X		X	X	X		X
B-6-2_1	0.128	3.25	0.474	12.04	0.0472	30.44	0.270	0.587	X	X	X	X	X	X		X	X	X	X	X
B-6-2_2	0.130	3.30	0.492	12.50	0.0486	31.99	0.264	0.580	X	X	X	X	X	X	X	X	X	X	X	X
B-6-3_1	0.092	2.34	0.524	13.31	0.0352	22.70	0.175	0.408	X	X		X	X	X		X	X	X	X	X
B-6-3_2	0.092	2.34	0.508	12.90	0.0356	22.96	0.181	0.410	X	X		X	X	X		X	X	X	X	X
B-8-2	0.114	2.90	0.520	13.21	0.0464	29.93	0.219	0.473	X	X	X	X	X	X	X	X	X	X	X	X
B-9-2_1	0.080	2.03	0.478	12.14	0.0296	19.09	0.167	0.344	X	X		X	X	X		X	X	X	X	X
B-9-2_2	0.064	1.63	0.460	11.68	0.0244	15.74	0.139	0.284	X	X		X	X	X		X	X	X	X	X
B-10-1_1	0.048	1.22	0.137	3.48	0.0046	3.10	0.350	0.216	X	X		X	X	X		X	X	X		X
B-10-1_2	0.045	1.14	0.128	3.43	0.0039	2.52	0.333	0.202	X	X		X	X	X		X	X	X		X
B-10-3	0.110	2.79	0.550	13.97	0.0500	32.25	0.200	0.497	X	X	X	X	X	X		X	X	X	X	X
B-11-1	0.050	1.27	0.144	3.66	0.0052	3.35	0.347	0.226	X	X		X	X	X		X	X	X		X
B-11-2	0.118	2.95	0.496	12.60	0.0532	21.61	0.239	0.517	X	X		X	X	X		X	X	X	X	X
B-11-3_1	0.104	2.64	0.512	13.00	0.0428	27.60	0.203	0.484	X	X		X	X	X		X	X	X	X	X
B-11-3_2	0.108	2.74	0.530	13.46	0.0452	29.15	0.203	0.480	X	X		X	X	X		X	X	X	X	X

Table 5.3-2. Master Data Tabulation, Contd

Flaw	a (in.)	a (mm)	2c (in.)	2c (mm)	Area (in.)	Area (mm)	a/2c	a/t	1st Evaluation E	P	X	U	2nd Evaluation E	P	X	U	3rd Evaluation E	P	X	U
B-12-1_1	0.038	0.97	0.124	3.15	0.0037	2.39	0.306	0.171	X	X		X	X	X		X				X
B-12-1_2	0.043	1.09	0.143	3.63	0.0046	2.97	0.300	0.193	X	X		X	X	X			X	X		X
B-12-2	0.126	3.20	0.478	12.14	0.0468	30.19	0.263	0.560	X	X		X	X	X		X	X	X	X	X
B-12-3_1	0.106	2.69	0.530	13.46	0.0388	25.03	0.200	0.452	X	X		X	X	X		X	X	X	X	X
B-12-3_2	0.108	2.74	0.534	13.56	0.0452	29.15	0.202	0.482	X	X		X	X	X		X	X	X	X	X
B-14-3	0.108	2.74	0.522	13.26	0.0500	32.25	0.206	0.457	X	X		X	X	X		X	X	X	X	X
B-15-1	0.05[illegible]	1.37	0.149	3.78	0.0054	3.48	0.362	0.243	X			X	X	X		X	X	X		X
B-15-2	0.144	3.66	0.490	12.45	0.0532	34.41	0.293	0.654	X	X	X	X	X	X	X	X	X	X	X	X
B-16-1	0.053	1.35	0.140	3.56	0.0059	3.81	0.378	0.238	X			X	X	X		X	X	X		X
B-16-3_1	0.106	2.69	0.520	13.21	0.0428	27.60	0.203	0.443	X	X		X	X	X		X	X	X	X	X
B-16-3_2	0.106	2.69	0.534	13.56	0.0436	28.12	0.198	0.452	X	X		X	X	X		X	X	X	X	X
B-17-1_1	0.043	1.09	0.143	3.63	0.0038	2.45	0.300	0.193	X			X	X	X		X	X	X		X
B-17-1_2	0.033	0.84	0.123	3.12	0.0029	1.87	0.268	0.148	X	X		X	X	X		X	X	X		X
B-17-2	0.114	2.90	0.474	12.04	0.0372	23.99	0.240	0.518	X	X		X	X	X		X	X	X	X	X
B-17-2_2	0.054	1.37	0.426	10.82	0.0164	10.58	0.126	0.244	X	X		X	X	X		X	X	X		X
B-18-1	0.037	0.94	0.134	3.40	0.0034	2.19	0.276	0.166	X				X	X			X	X		X
B-18-2_1	0.090	2.29	0.458	11.63	0.0316	20.38	0.196	0.412	X	X		X	X	[illegible]		X	X	X	X	X
B-18-2_2	0.084	2.13	0.458	11.63	0.0304	19.61	0.183	0.373	X	X		X	X	X		X	X	X	X	X
B-18-3_1	0.088	2.24	0.498	12.65	0.0332	21.41	0.176	0.400	X	X		X	X	X		X	X	X	X	X
B-18-3_2	0.094	2.39	0.512	13.00	0.0364	23.48	0.183	0.421	X	X		X	X	X		X	X	X		X
B-20-2	0.086	2.18	0.478	12.14	0.0308	19.87	0.179	0.358	X	X		X	X	X		X	X	X	X	X
B-21-1	0.055	1.40	0.144	3.66	0.0058	3.61	0.381	0.247	X	X			X	X			X	X		X
B-21-3	0.112	2.84	0.538	13.67	0.0496	31.99	0.208	0.496	X	X		X	X	X		X	X	X	X	X
B-22-2_1	0.096	2.44	0.466	11.84	0.0348	22.45	0.206	0.428	X	X		X	X	X		X	X	X	X	X
B-22-2_2	0.080	2.03	0.444	11.28	0.0284	20.90	0.180	0.352	X	X		X	X	X		X	X	X	X	X
B-22-3	0.094	2.39	0.506	12.85	0.0360	23.22	0.185	0.429	X	X		X	X	X		X	X	X	X	X
B-23-1_1	0.058	1.47	0.157	3.99	0.0065	4.19	0.369	0.261	X	X		X	X	X		X	X	X		X
B-23-1_2	0.064	1.63	0.190	4.83	0.0086	5.55	0.336	0.286	X	X		X	?	X		X	X	X		X
B-23-2	0.[illegible]	2.49	0.470	11.94	0.0344	22.19	0.208	0.426	X	X		[illegible]	X	X		X	X	X	X	X
B-23-3	0.110	2.79	0.534	13.56	0.0440	28.38	0.206	0.460	X	X		X	X	X		X	X	X	X	X
B-24-1_1	0.027	0.69	0.109	2.77	0.0024	1.55	0.247	0.121	X	X			X	X			X	X		
B-24-1_2	0.031	0.79	0.118	3.00	0.0029	1.87	0.262	0.139	X	X			X	X			X	X		X
B-24-2	0.124	3.15	0.472	11.99	0.0436	28.12	0.262	0.563	X	X		X	X	X		X	X	X	X	X
B-24-3$_1$	0.090	2.29	0.512	13.00	0.0368	23.74	0.175	0.400	X	X		X	X	X		X	X	[illegible]	X	X
B-24-3_2	0.094	2.39	0.504	12.80	0.0388	25.03	0.186	0.419	X	X		X	X	X		X	X	X	X	X

SECTION 6

CONCLUSIONS AND RECOMMENDATIONS

Of the NDT methods evaluated, eddy current, ultrasonic, and penetrant methods provided the highest reliability and greatest sensitivity for detection of the fatigue cracks present. Holographic interferometry results were encouraging, but the requirement for loading and the precision necessary limit the present practical applications. Acoustic emission monitoring has greater application than was demonstrated in this program. Equipment developments and applications of acoustic emission monitoring are progressing very rapidly.

The data support the assumption that flaw detectability is enhanced after large loads have been applied. The effects of etching were not as had been expected, and lead to the conclusion that the etching process, if it is to be used, must be carefully controlled.

Although the differences in detection capability between eddy current and ultrasonic methods are slight, when all aspects of practical application are considered the conclusions favor eddy current. Each method uses probe fields of essentially equal size. The limitations in probe manipulation are largely mechanical and essentially equal. The major advantages of eddy current are that no intermediate coupling is required between probe and test surface and, more important, probe scanning orientation with respect to flaw orientation is less significant than with ultrasound. Considering these factors and imagining the effects of engineering improvements that could be made in applying eddy current test methods, it is not difficult to arrive at the conclusion that development of eddy current systems would be favored if it is necessary to inspect large areas for fatigue cracks.

It is apparent that even though precautions were taken to suppress the human factors, further reduction of human influence in both application and interpretation would improve the reliability of NDT. For the reliable inspection of large critical components, the major thrust should be in system developments that eliminate or minimize human manipulation and judgement. Building systems around off-the-shelf commercial equipment would provide improvement; tailoring equipment to specific applications and integrating it into automatic systems would surely yield greater improvement.

In order to obtain higher reliability from NDT and to narrow the scope of methods that should be studied as candidates for system integration, the following recommendations should be pursued:

a. A study should be directed toward methods of artificially producing flaws that simulate natural flaws under a variety of processing conditions. Welding flaws are perhaps the most critical from a structural viewpoint and the most difficult to simulate with an adequate degree of control. It should be recognized that even in relatively simple cases, such as in this program, specimen preparation costs represent an extremely significant proportion of the total cost. Independent development of flawed specimens would provide greater return from the NDT methods studies.

b. On the basis of data generated from this and parallel NASA programs, specimen flaw size requirements in future programs should be narrowed to those that produce statistically significant numbers of sizes in the near-threshold detectibility regions.

c. The data from this program and the parallel NASA programs should be analyzed in combination and the results presented to fracture control designers as soon as possible.

d. A study should be made of the optimization and application of the most promising NDT methods for detection of welding defects and other critical structural defects. The study should emphasize the elimination (or, at least, standardization) of human elements and provide demonstration of the feasibility of systems integration.

SECTION 7

REFERENCES

1. C. S. Noritake, F. D. Walsh, and E. C. Roberts, "Polarized Light Brings out Details of Fracture Zones," Metal Progress, February 1971.

2. Berryman, L., Nondestructive Test Program for S-IC Tank Weldments," CR-69501, Contract NAS 8-5608, August 1963.

3. Yee, B.C.W., et al, Evaluation and Optimization of NDT Techniques for Flaw Detection in D6 ac Steel, Report FZM-5795, Convair Aerospace Division of General Dynamics, August 15, 1972.

APPENDIX I

PROCEDURES

NDT INSTRUCTION

EDDY CURRENT CRACK DETECTION ON 2219-T87 ALUMINUM

SHEET SPECIMENS

1.0 SCOPE

This nondestructive test instruction establishes the procedures to be used in detecting fatigue cracks in 2219-T87 aluminum sheet specimens for Contract NAS 9-12326 by the eddy current method of nondestructive testing.

2.0 RESPONSIBILITY

Only personnel qualified by the Program Manager shall perform testing on the specimens produced in Contract NAS 9-12326. It is required that these personnel shall have basic knowledge of the eddy current test method but do not routinely perform eddy current testing on production parts. It is further required that these personnel do not know the number or location of the cracks during or after these tests.

3.0 EQUIPMENT REQUIREMENTS

3.1 Eddy current instrument (as specified by the Program Manager)

3.2 Scanning fixture

3.3 Strip chart recorder (as specified by the Program Manager)

3.4 Nonconductive shim (paper or nonconductive plastic 0.076 mm (0.003 in) thick)

3.5 Probe coil (as specified by the Program Manager)

4.0 PROCEDURE

4.1 Mount the specimen to be tested in the test fixture and clamp in place.

4.2 Connect the probe coil to the COIL jack on the front of the eddy current instrument.

4.3 Mount the spring-loaded probe coil on the test fixture such that the outer guide shoe is in light contact with the test specimen and the spring load clamp permits between 1 mm (0.04 in.) and 2 mm (0.08 in.) of spring travel.

4.4 With the coil in contact with the specimen, energize the eddy current instrument and set the controls as follows:

FREQUENCY — Switch position 8

FINE FREQUENCY — 3.4 turns counter-clockwise from the clockwise stop

GAIN — Maximum clockwise

BALANCE — Turn the control until the meter reading is on-scale

4.5 Alternately insert the shim between the probe coil and the test specimen surface and remove it. Adjust the FINE FREQUENCY control slightly until the meter reading remains constant when the shim is in place or removed.

4.6 Connect the recorder input cable to the output jacks on the side of the eddy current instrument and energize the recorder. Set the recorder sensitivity at 1 mV/division. Select the paper drive speed at 1 mm/s.

4.7 Carefully adjust the BALANCE control until the meter reads 0 and start the recorder. Set the POSITION control on the recorder to locate the pen along the lower axis of the strip chart. Adjust the BALANCE control until the meter reads 100 μA and record for 15 to 20 seconds. Reset the BALANCE control at 200, 300, 400, and 500 μA, recording each interval. Refer to Figure 1. If the recording of each level is greater than $\pm$ 1 mm (0.04 in.) from that shown in Figure 1, adjust the variable SENSITIVITY control to reproduce the recording in Figure 1. Reset the meter reading to 0.

4.8 Advance or retard the micrometer slide on the test fixture until the probe coil is within 6.3 mm (0.25 in.) from either edge of the test specimen.

4.9 With the recorder running at 1 mm/s, manually move the longitudinal slide to either end stop.

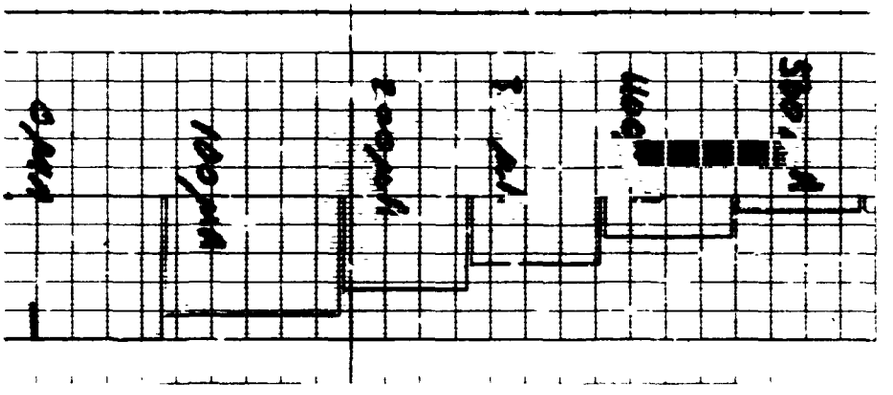

Figure 1. Calibration Control Strip for Eddy Current Test

4.10 Rotate the micrometer slide as follows:

For the A specimens: 1.91 mm (0.075 in.) - 3 full turns

For the B specimens: 2.54 mm (0.100 in.) - 4 full turns

4.11 Manually move the longitudinal slide to the opposite end stop.

4.12 Repeat 4.10 and 4.11, observing the recording while moving the probe coil. A crack indication will appear as a very sharp spike on the recording ranging in amplitude from a few millimeters to full scale. When a spike is observed, carefully position the coil over the location that produced the spike and mark the specimen with an ink mark along the left edge of the probe coil housing.

4.13 Proceed, repeating steps 4.10, 4.11 and 4.12. Mark each crack found only once.

4.14 When the specimen has been completely scanned, reposition the probe coil to match the ink marks produced in 4.12. Observe the recorder for a maximum as the longitudinal slide is moved slowly back and forth in the vicinity of the crack. Rotate the micrometer until the recorder again reads 0.

4.15 On the Specimen Data Sheet, arbitrarily identify the crack being located and record the location of the probe coil centerline from the transverse centerline of the specimen. By convention, locations to the right of (below) the transverse specimen centerline are positive (+) and locations to the left of (above) that centerline are minus (-). Enter the distance from the probe coil centerline to the specimen centerline in inches on the Specimen Data Sheet. Also record the micrometer measurement on the same crack. The micrometer reads 0 when the probe coil is centered over the outer side of the specimen. Move the micrometer slide along the length of the crack until the recorder returns to 0 and record the micrometer measurement. Subtract the two micrometer measurements and divide by 2 in order to locate the approximate center of the crack. Locate the center of the crack on the scaled grid of the Data Sheet and record the crack identification letter. See Figure 2 for an example. Also record specimen identification number and evaluation number in the spaces provided.

4.16 Proceed in the same manner for each crack detected.

4.17 Remove the test specimen, replace with another and repeat this procedure until all specimens have been scanned.

NAS 9-12326
SPECIMEN DATA SHEET

IDENTIFICATION A-3

XR
UT
PT
EC E-3

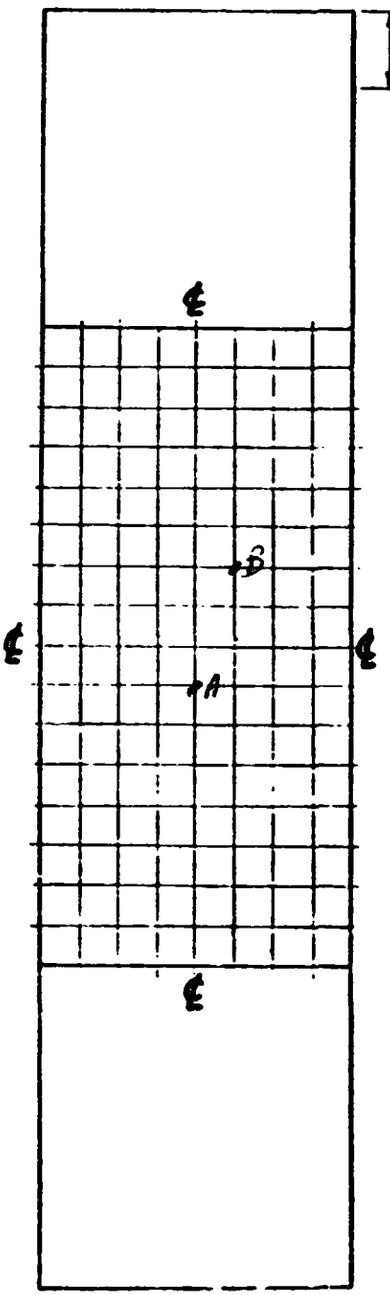

	A	B
Ref	.500	1.000
Start	2.155	1.660
End	1.730	1.200
	3.435	2.860
Middle	1.968	1.436
Length	.435	.460

Figure 2. Specimen Data Sheet

NDT INSTRUCTION

CHROMAFAX REPLICATION PROCESS FOR CRACK DETECTION ON

2219-T87 ALUMINUM SHEET SPECIMENS

1.0 SCOPE

This nondestructive test instruction establishes the procedures to be used in detecting fatigue cracks in 2219-T87 aluminum sheet specimens for Contract NAS 9-12326 by the Chromafax replication method of nondestructive testing.

2.0 RESPONSIBILITY

Only personnel qualified by the Program Manager shall perform testing on the specimens produced in Contract NAS 9-12326. It is required that these personnel shall have basic knowledge of the replication test method but do not routinely perform replication testing on production parts. It is further required that these personnel do not know the number or location of the cracks during or after these tests.

3.0 EQUIPMENT AND MATERIAL REQUIREMENTS

3.1 Dichloromethane (Cl_2CH_2)

3.2 Ultrasonic cleaner

3.3 Chromafax penetrant (General Dynamics proprietary material - furnished by Program Manager)

3.4 Silicone potting compound RTV-8111 per MIL-S-23586 (Wep), Type I, Class I, Grades B and A.

3.5 RTV silicone rubber curing catalyst (dibutyl tin delamate)

3.6 Masking tape, clean brush, clean rags

4.0 PROCEDURE

4.1 Preclean specimens by immersion in dichloromethane in an ultrasonic cleaner for ten minutes.

4.2 Remove specimens from cleaner and allow to dry.

4.3 Apply the Chromafax penetrant by brushing over the surface area to be tested. Periodically rebrush if necessary to keep the surface wetted.

4.4 After 60 minutes, remove excess dye by washing with water at room temperature. Wetted rags may be used to aid the removal of excess dye.

4.5 Dry the specimen by wiping with dry, clean rags.

4.6 Apply masking tape or other suitable material to clean the area that is to be inspected.

4.7 Apply a thin film of aerosol spray penetrant developer per MIL-I-23135 and MIL-I-6866.

4.8 After 20 minutes development time, apply the RTV catalyzed with 1.5 drops of dibutyl tin dilamate per gram of RTV.

4.9 Pour enough RTV over the surface to assure a replicate at least 2 mm (0.08 in.) thick.

4.10 After 3 hours cure time, or when the rubber is tack-free, remove the dams and strip off the replicate.

4.11 Carefully examine the surface of the replicate for indications of fatigue cracks. Record the locations of indications on the gridded portion of the Specimen Data Sheets and a measure of their length. Remember that the replicate surface is a mirror image of the specimen surface.

4.12 Post-clean the specimens as in 4.1.

NDT INSTRUCTION

ULTRASONIC CRACK DETECTION ON 2219-T87

ALUMINUM SHEET SPECIMENS

1.0 SCOPE

This nondestructive test instruction establishes the procedures to be used in detecting fatigue cracks in 2219-T87 aluminum sheet specimens for Contract NAS 9-12326 by the ultrasonic method of nondestructive testing.

2.0 RESPONSIBILITY

Only personnel qualified by the Program Manager shall perform testing on the specimens produced in Contract NAS 9-12326. It is required that these personnel shall have basic knowledge of the ultrasonic test method but do not routinely perform ultrasonic testing on production parts. It is further required that these personnel do not know the number or location of the cracks during or after these tests.

3.0 EQUIPMENT REQUIREMENTS

3.1 Ultrasonic instrument.

3.2 Immersion tank, scanning bridge, and facsimile recorder.

3.3 Ultrasonic transducer, 10 MHz, 12.7 mm (0.5 in.) diameter, lithium sulfate, 44.5 mm (1.75 in.) focus.

3.4 Reference standard specimens (Convair A-6, A-24, B-6, B-23; MMC 28C, 68C).

4.0 PROCEDURE

4.1 The specimens shall be segregated into two groups: those having surface roughness greater than and less than 1.6 μm (63 μin.) average roughness.

4.2 Select the reference standard specimen(s) appropriate for the thickness and surface roughness of the group of specimens to be tested. Position the standard specimen(s) on the support table in the immersion tank with the long axis parallel with the long axis of the tank.

4.3 Adjust the manipulator to indicate -0.53 rad (-30.5°) in the plane of the long axis and 0.0 rad (0°) in the plane of the short axis.

4.4 Position the transducer to provide a water path along the centerline of the transducer from the face of the transducer to the surface of the reference specimen of 44.5 mm (1.75 in.).

4.5 Adjust the ultrasonic instrument controls as follows:

FREQUENCY	— 5 MHz
PULSE LENGTH	— Maximum
REJECT	— 12:00
GAIN	— 3.5 × 1
TEST SWITCH	— Normal
SWEEP CONTROLS	— As required to obtain specimen edge reflection

4.6 Manually scan the specimen test area until a flaw indication is obtained. Position the sweep gate to accept the flaw indication signal. Adjust the gain to provide a signal of 25.4 mm (1.0 in.) amplitude. Adjust the flaw alarm level to trigger above this amplitude. Reset the gain to 3.5 × 1.

4.7 Set the scan limits to scan the full width of the specimen(s). Adjust the scan speed to approximately 45.7 cm/s (18 in/s) and the index interval at 0.64 mm (0.025 in.).

4.8 Produce a trial recording of one or more flaws of the reference standard specimen. Compare the flaw indications with those of Figure 1, 2, or 3 as appropriate. Repeat as required at different gain levels to reproduce the reference standard recordings.

4.9 Replace the reference standard specimen with the defect specimens. Four specimens of like surface finish and thickness can be scanned at one time.

4.10 Scan the specimens from end to end assuring that some fiduciary (specimen edge, holes, doubler) is also recorded.

4.11 On the Specimen Data Sheet, record the location of flaw indications as shown on the C-scan recordings with reference to the specimen centerlines.

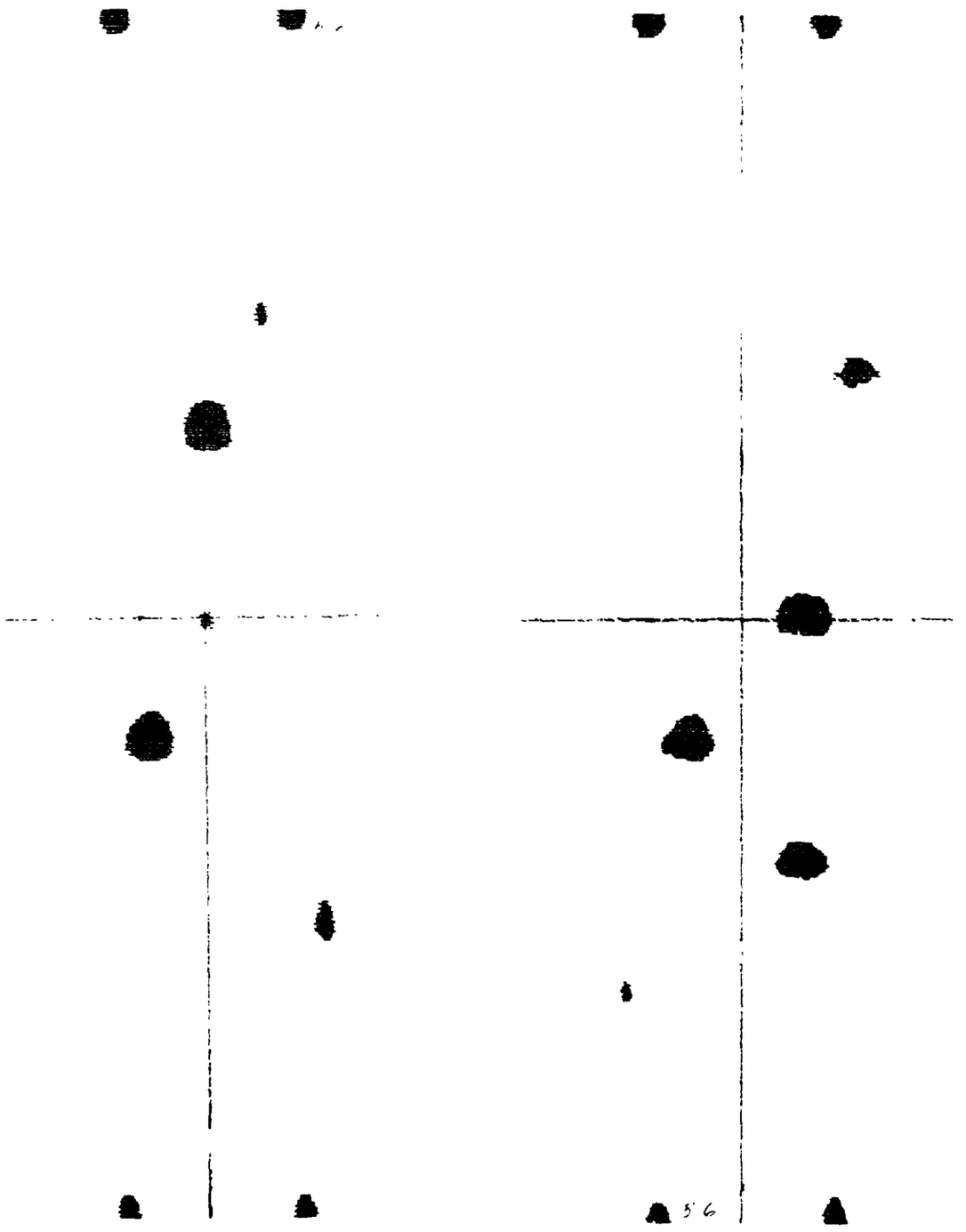

Figure 1. Ultrasonic Reference Recordings for Convair Specimens. Fine Surface Finish, Thin Specimen Standard A-6, Left; Fine Surface Finish, Thick Specimen Standard B-6, Right

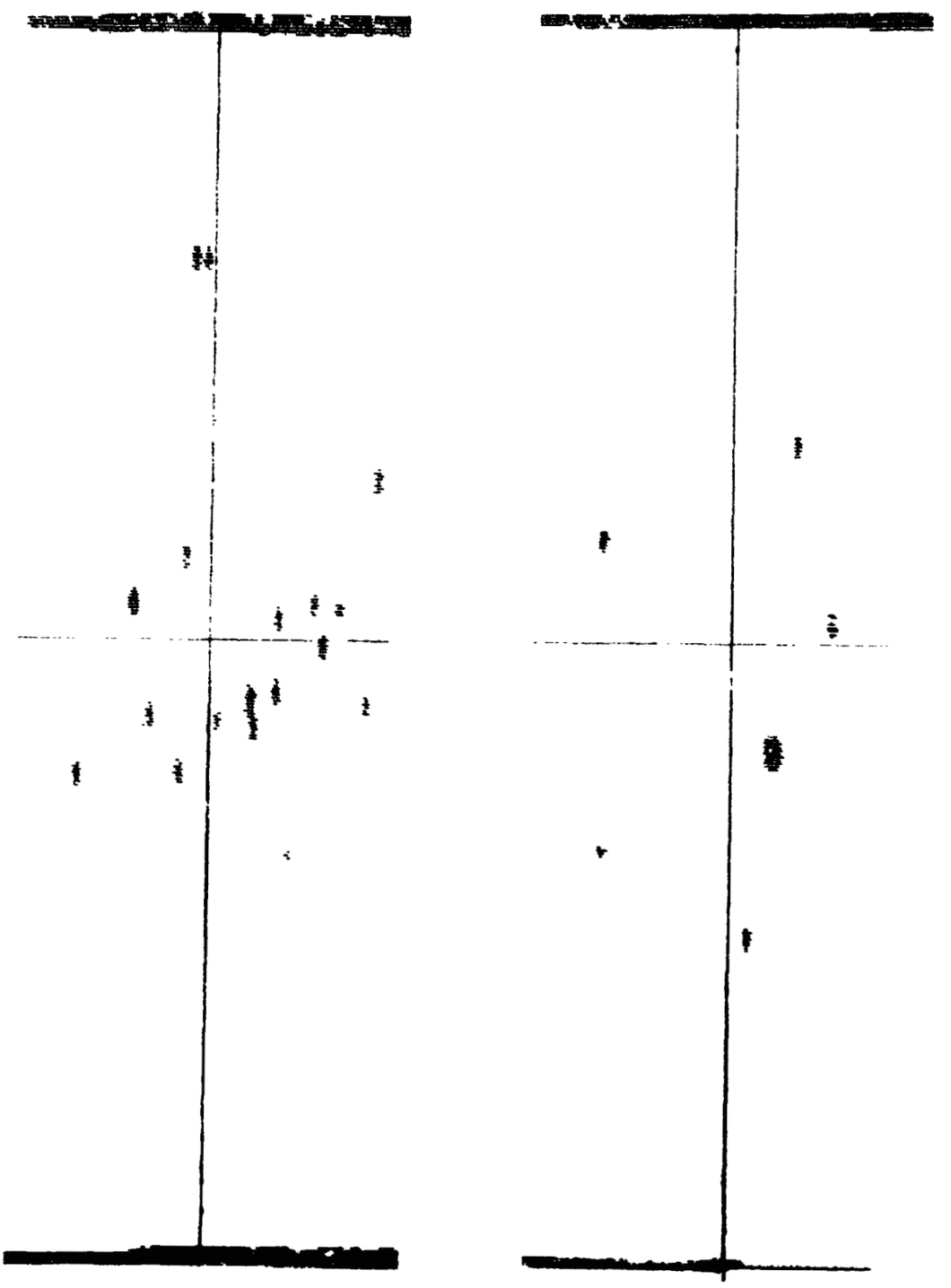

Figure 2. Ultrasonic Reference Recordings for Martin-Marietta Specimens. Thi
Specimen Standard 28C, Left; Thick Specimen Standard 68C, Right

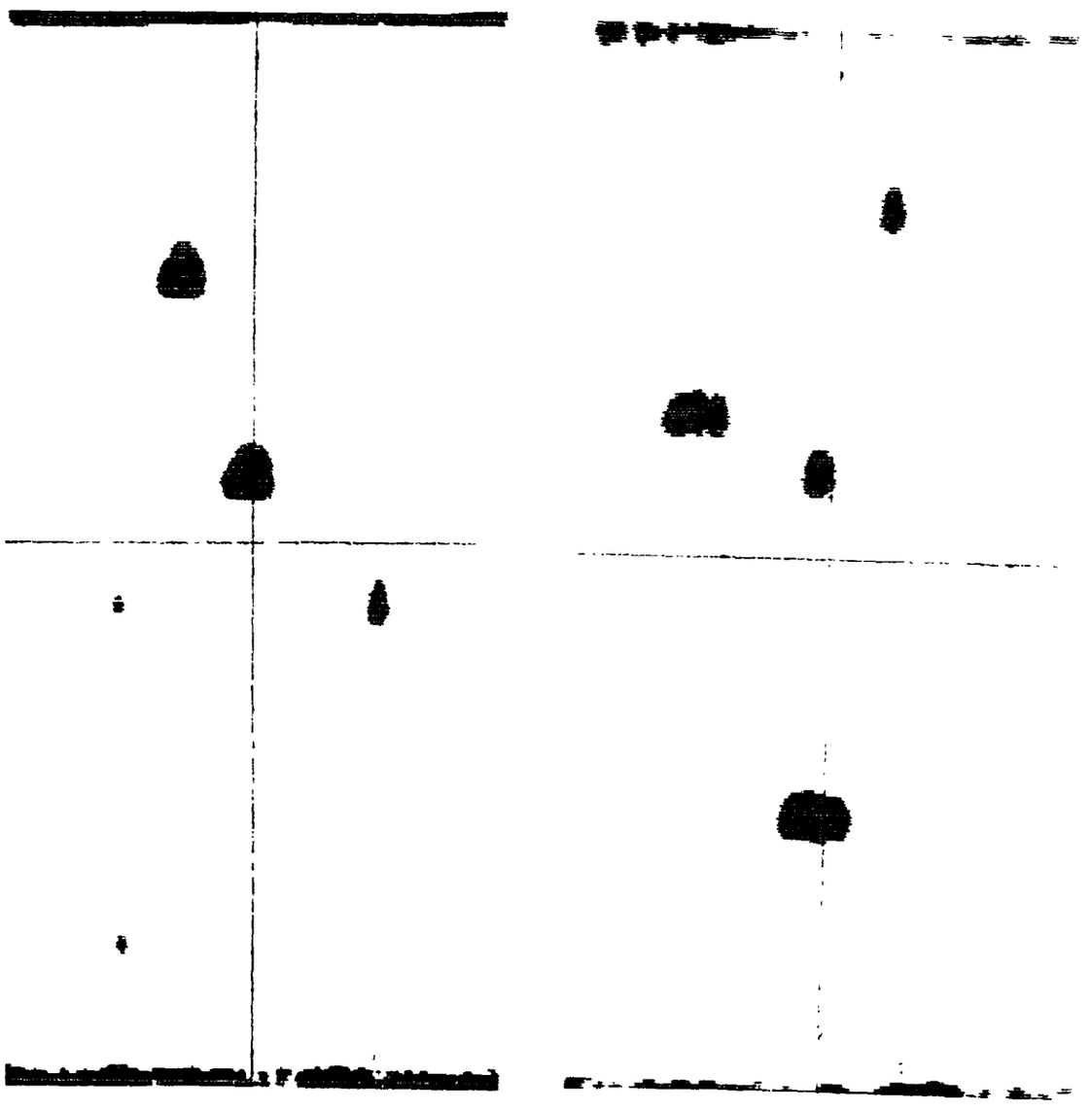

Figure 3. Ultrasonic Reference Recordings for Convair Specimens. Coarse Surface Finish, Thin Specimen Standard A-24, Left; Coarse Surface Finish, Thick Specimen Standard B-23, Right

NDT INSTRUCTION

PENETRANT CRACK DETECTION ON 2219-T87 ALUMINUM

SHEET SPECIMENS

1.0 SCOPE

This nondestructive test instruction establishes the proced. to be used in detecting fatigue cracks in 2219-T87 aluminum sheet specimens for Contract NAS 9-12326 by the fluorescent penetrant method of nondestructive testing.

2.0 RESPONSIBILITY

Only personnel qualified by the Program Manager shall perform testing on the specimens produced in Contract NAS 9-12326. It is required that these personnel shall have basic knowledge of the penetrant test method but do not routinely perform penetrant testing on production parts. It is further required that these personnel do not know the number or location of the cracks during or after these tests.

3.0 EQUIPMENT REQUIREMENTS

3.1 Water washable fluorescent penetrant. equivalent to Group VII sensitivity; reference MIL-I-25135C (ASG), Amendment 4 (material as specified by Program Manager).

3.2 Brush applicator (as required).

3.3 Nonaqueous solvent spray developer, reference MIL-I-25135C (material as specified by Program Manager).

3.4 Air assist, hydrowash pressure-spray system with 3-way valve permitting use of penetrant removers; 1:19/1:500 remover, water ratio capability; water consumption approximately 0.2 to 0.4 liter/second (3-6 gallons/minute) at 0.276 MN/m^2 (40 psi).

3.5 The black light used for fluorescent penetrant inspection shall be a 100 watt mercury lamp, or equivalent, with suitable filter in the 3200 to 4000 . trom unit wavelength range. The intensity of the black light shall be not less than 1350 lumens/square meter (125 foot candles) when measured 0.38 meter from the light source.

3.6 Ultrasonic cleaner; dichloromethane (Cl_2CH_2) solvent.

4.0 PROCEDURE

4.1 Clean specimens prior to the application of penetrant utilizing vapor degreasing and/or ultrasonic cleaning in dichloromethane (Cl_2CH_2) solvent. Where liquid solvent is employed, it shall be periodically sampled to assure clear, contamination free material.

4.2 Set air and water pressure regulators (hydrowash) to 0.276 MN/m^2 (40 psi) each.

.3 Turn on black light.

4.4 Apply penetrant to surface of specimen by brushing; apply sufficient quantity of penetrant to produce puddle over entire surface; allow penetrant to dwell for 600 seconds.

4.5 Following dwell period, remove penetrant by hydrowash. Wash specimen for a period of 90 seconds.

NOTE

During wash, periodically examine specimen under black light to assure uniform removal of penetrant (background). Allow full 90 seconds of cumulative wash time.

4.6 Following wash, remove excess penetrant by blowing (compressed air); allow specimen to air dry at ambient temperature.

4.7 Apply thin layer of nonaqueous solvent suspendable developer to surface of dried specimen; allow 600 seconds development time.

4.8 Following development, view specimen under black light; note the location and size of crack-like defects.

4.9 Record the location and size of defects on the traveler record.

4.10 Repeat operations 4.4 through 4.9 until all specimens have been examined.

NDT INSTRUCTION

RADIOGRAPHIC INSPECTION OF 2219-T87 ALUMINUM

SHEET SPECIMENS

1.0 SCOPE

This nondestructive test instruction establishes the procedures to be used in detecting fatigue cracks in 2219-T87 aluminum sheet specimens for Contract NAS 9-12326 by the X-ray method of nondestructive testing.

2.0 RESPONSIBILITY

Only personnel qualified by the Program Manager shall perform testing on the specimens produced in Contract NAS 9-12326. It is required that these personnel shall have basic knowledge in radiographic testing but do not routinely perform radiography on production parts. It is further required that these personnel do not know the number or location of the cracks during or after these tests.

3.0 EQUIPMENT REQUIREMENTS

3.1 X-ray machine: 0-110 keV beryllium window tube X-ray machine.

3.2 Film: Single emulsion, fine grain X-ray film.

3.3 Film processor/developer: Minimum 19 liter (5 gallon) hand processing tank with nitrogen burst or continuous bleed agitation; high contrast developer.

3.4 Penetrameter: Aluminum wires (as specified by Program Manager).

3.5 Viewing apparatus: High intensity film view with variable illumination suitable for distinguishing detail in radiographs of up to 3.5 H&D units optical density (background). A viewing facility shall be available which will exclude background light of sufficient intensity to produce reflection on the radiograph.

3.6 Film dryer: Forced air dryer with heater (140°F, 588°K).

3.7 Cassettes: Paper

3.8 Back-up material: Lead sheet, minimum thickness 0.051 cm (0.020 inch).

3.9 Viewer magnifier: Optical magnifier, graduated pocket comparator type, 7.0 × magnification.

4.0 PROCEDURE

4.1 Center the loaded film cassette beneath specimen and centerline of X-ray beam.

4.2 Adjust the distance between the radiation source and film to 1.2 m (48 inches).

4.3 Set exposure controls for 32 keV incident energy (max) for 0.153 cm (0.060 inch) specimens, 47 keV for 0.572 cm (0.225 inch) specimens.

4.4 Set exposure cutoff for 150 milliampere minutes (film density 2.5 ± 0.2 H&D units).

4.5 Complete exposure.

4.6 Remove specimen from exposure area.

4.7 Develop X-ray film 360 +5, -0 seconds; temperature of developer should be 70°F (294°K).

4.8 Remove film from developer; drain excess developer from film surface.

4.9 Place film in stop bath for 10 seconds; remove film.

4.10 Place developed radiograph in fixer solution for 360 + 30, -0 seconds; film should be agitated during first 30 seconds of fixation.

4.11 Remove radiograph from fixing solution; wash film in running water for 1200 seconds (ambient temperature).

4.12 Place washed film in wetting agent solution for 30 seconds (agitate continuously).

4.13 Remove radiograph. Dry radiograph using heated forced air or ambient still air dry technique.

5.0 INTERPRETATION OF RADIOGRAPHS

5.1 Place developed radiograph on film viewer.

5.2 Turn on illuminator and adjust for optimum light transmission (background); darken room to exclude background light of sufficient intensity to produce reflection on surface of radiograph.

5.3 Using grid (ruled overlay) and comparator, scan radiograph along its length indexing in increments of about 1 cm (0.39 in.) vertically, until entire radiograph has been examined. Mark the boundaries of the defects with grease pencil.

5.4 Measure the length of visible defects using graduations of the comparator.

5.5 Record the location and size of all detects on the traveler work sheet.

APPENDIX II

STATISTICAL TEST RESULTS

The data compiled from the three evaluations were analyzed to answer the following questions.

I. For each NDT method and test specimen thickness, does the surface finish affect the method's ability to detect flaws?

II. Is there a difference in ability of each NDT method for each thickness to detect flaws after the specimens are etched to reduce surface finish variability?

III. Does the NDT method's ability to detect flaws change from before and after proof test?

Question I Analysis. For each NDT method and test specimen thickness, a χ^2-test was utilized for independence of surface finish and number of flaws detected. A table such as the following was constructed for each of the eight total method/surface finish combinations.

Surface Finish	No. Flaws Detected	No. Flaws Not Detected	Total
1	X_{11}	X_{12}	$T_{1.}$
2	X_{21}	X_{22}	$T_{2.}$
3	X_{31}	X_{32}	$T_{3.}$
4	X_{41}	X_{42}	$T_{4.}$
Total	$T_{.1}$	$X_{.2}$	$T_{..}$

Then

$$\chi^2_{(r-1)(c-1)} = \sum_{i=1}^{r}\sum_{j=1}^{c} \frac{(X_{ij} - T_{i.}\ T_{.j}/n)^2}{T_{i.}\ T_{.j}/n}$$

was computed, where

r = number of rows

c = number of columns

n = $T_{..}$

X_{ij} = observation (No. in this cell)

$T_{i.}$ or $T_{.j}$ = appropriate total

$T_{..}$ = grand total

This calculated value was then compared to the table value to determine if the surface finish is significant or not. The following table summarizes the results.

			Table Value at or Level of			
	Method	Computed χ^2 Value	0.10	0.05	0.01	Results
Thin	Ultrasonic	4.962	6.25	7.81	11.34	No effect
	Radiography	2.712	6.25	7.81	11.34	No effect
	Eddy Current	3.549	6.25	7.81	11.34	No effect
	Penetrant	3.549	6.25	7.81	11.34	No effect
Thick	Ultrasonics	4.430	6.25	7.81	11.34	No effect
	Radiography	3.705	6.25	7 81	11.34	No effect
	Eddy Current	0	6.25	7.81	11.34	No effect
	Penetrant	12.857	6.25	7.81	11.34	Significant

Question II Analysis. For the two thicknesses of specimens, a nonparametric test called the "McNemur test for significance of changes" was used to determine if after etching there is a change in the overall detection of flaws. For each of the two cases a four-cell table is developed, such as

	After Etch	
Before Etch	As Bad or Worse	As Good or Better
Good	A	B
Bad	C	D

The appropriate test is $\chi^2_{(1)} = \frac{[(A - D)-1]^2}{A+D}$ or in the case of 1/2 (A-D) being very small, an equivalent test is based on the binomial, with N = A+D and $\chi^2_{(1)}$ = the minimum of A or D, and testing P = Q = 1/2 against the two sided alternation P ≠ 1/2. Results of this test for thin specimens is $\chi^2_{(1)} = 4.00$ while the probability of achieving this value if both methods are equivalent is approximately 0.04. This resulting change is a degradation of detectability. For the thick specimens the second analysis was used and a high probability of no difference (0.375) was determined leaving the conclusion of no significant difference due to the etching process on the thick specimens.

Question III Analysis. The same tests described in II were used. The $\chi^2_{(1)}$ value for thin specimens is 4.90 and the probability of getting this value if there were no change is 0.025. The $\chi^2_{(1)}$ value for thin specimens is 4.90 and the probability of getting this value if there were no change is 0.025. The $\chi^2_{(1)}$ value for thick specimens is 5.14 and the probability of getting this value if there were no change is 0.02. Therefore we conclude that proof test has a significant effect on the detectability of flaws by these NDT methods.